In-Situ Stress Analysis of Southwest Saskatchewan

A Thesis

Submitted to the College of Graduate Studies and Research

In Partial Fulfillment of the Requirements

For the

Degree of Master of Science

In the

Department of Civil and Geological Engineering

University of Saskatchewan, Saskatoon, SK, Canada

By

Osman Hamid

PERMISSION TO USE

In presenting this thesis in partial fulfillment of the requirements for a degree of Master of Science from the University of Saskatchewan, I agree that the Libraries of this University may make it freely available for inspection. I further agree that permission for copying of this thesis in any manner, in whole or in part, for scholarly purposes may be granted by the professor or professors who supervised my thesis work or, in their absence, by the Head of the Department or the Dean of the College in which my thesis work was done. It is understood that any copying or publication or use of this thesis or parts thereof for financial gain shall not be allowed without my written permission. It is also understood that due recognition shall be given to me and to the University of Saskatchewan in any scholarly use which may be made of any material in my thesis.

Head of the Department of Civil and Geological Engineering
University of Saskatchewan
Engineering Building
57 Campus Drive
Saskatoon, Saskatchewan
Canada S7N 5A9

Osman Hamid
February 20, 2008

ABSTRACT

Scenarios developed by the National Energy Board of Canada predict that Canadian unconventional gas production, including coalbed methane (CBM), may be required to meet Canadian energy demands by the year 2008, and could constitute up to 65% of supply by 2025. Although there has been considerable CBM exploration and development in Alberta in recent years, there has been relatively limited activity in Saskatchewan.

The in-situ stress regime can have a strong influence on coal bed methane (CBM) production, coal permeability, hydraulic fracturing pressure, and borehole stability while drilling horizontal wells. A limited number of stress regime analyses have been conducted previously on a regional scale, for the entire Western Canada Sedimentary Basin (WCSB), but none has been conducted with a focus on Saskatchewan. The primary objective of this study was to investigate in-situ stress magnitudes and orientations in southwestern Saskatchewan. The secondary objective was to quantify the influence of in-situ stresses on operational practices that would be used to exploit CBM targets.

Analysis of vertical stress magnitudes and gradients were conducted using bulk density data compiled for 257 wells in southwest Saskatchewan. Vertical stress magnitudes calculated at the base of the Belly River Formation in the region where its CBM potential is greatest were found to be in the 6 to 12 MPa range. Vertical stress magnitudes at the top of the Mannville Group in the region where its CBM potential is greatest were found to be in the 12 to 18 MPa range. Data available for interpretation of minimum horizontal stress magnitudes were considerably more limited. A technique was developed to estimate these magnitudes using fracture stimulation data, which were available for the Viking Formation and Mannville Groups. Using this technique, minimum horizontal stress magnitudes at the top of the Mannville Group in the region of greatest interest were estimated to be 10 to 14 MPa. The results of these analyses suggest that depth is a dominant controlling factor for minimum horizontal stress magnitude, but that pore pressures (sub-normal pressures cause lower stresses) and lithology (shaley rocks, and perhaps coals, have higher stresses) also have notable effects. Insufficient data were obtained for direct estimation of minimum horizontal stresses in the Belly River

Formation. Minimum horizontal stress magnitudes in this formation might be quite close to vertical stress magnitudes.

Borehole breakouts were analyzed to interpret the orientation of maximum horizontal stress (σ_{Hmax}) in the study area. The mean orientation of the mean borehole breakouts gives a 137º with a circular standard deviation of 12º, which parallels the minimum horizontal stress in the study area with a notable inflection overlying the Swift Current platform. The data is portrayed in a trajectory map. The trajectories indicated on the map can be used for predicting the orientation of induced hydraulic fractures, and the likely orientation of face cleats in coals. Knowledge of the orientations of these features is essential to effective development of CBM resources.

Based on the stress and pore pressure data presented in this thesis, it is anticipated that minimum effective stresses in the Belly River coals will typically be a few MPa, and up to 10 MPa in the Mannville coals. A very rough estimate of permeabilities based on the data compiled for various Canadian coals suggests that permeabilities could be in the 0.01 to 10 millidarcy range for the former, and 0.01 to 1 millidarcy range for the latter.

Borehole stability analyses were conducted for both the Belly River Formation and the Mannville Group. The results suggest that horizontal drilling of the Mannville coals should be feasible, without the need for high-density drilling muds. Given that the Belly River coals occur in numerous thin seams, they are most likely to be developed using vertical wells. Borehole instability is not likely to be a major problem in these vertical wells.

Recommendations are provided for laboratory investigation of coal permeabilities and mechanical properties, field testing for minimum horizontal stress magnitudes in coal seams and adjacent strata, and additional analysis of existing fracture stimulation, log and core data for strata not analyzed in this project.

ACKNOWLEDGEMENT

To accomplish any kind of success, one person's capabilities alone are not enough. There are several factors that contribute towards achieving one's goals and objectives. Some of these factors include inspiration, guidance, motivation, and encouragement. While working towards completion of this thesis, several individuals have made valuable and significant contributions. I would like to express my sincere gratitude to all of those individuals. It would not be possible to name each individual, but I would like to mention some of them.

Professor Hawkes, my supervisor, who from the beginning, through my work and until the end provided guidance, support, valuable advice and constant encouragement. I feel honoured to have had such a great adviser. Thanks Chris.

Professor Milne, my thesis committee member, always provided me with inspiration and built a strong desire in me to work hard to succeed. I've learned a lot from Doug, my first rock mechanics instructor. Thanks Doug for your support.

Professor Sharma, my thesis committee member, provided support, feedback and help that has proved to be very valuable.

Several organizations and individuals have made significant contributions, and I would like to thank them:

- The Petroleum Technology Research Centre, of Regina, provided financial support for this project, which was crucial for its success.
- BJ Service Company of Canada provided valuable hydraulic fracturing data that was used for interpretation of horizontal stress magnitude. Special thanks to Robert Hawkes and Keri Yule for their support.
- Craig Lamb, Chief Geoscientist with Husky Energy, provided me with motivation, guidance and data that were valuable to the project.
- Nexen Inc. and EnCana Corp. were also supportive and provided data for my thesis.
- Advanced Geotechnology, a Weatherford company based in Calgary, gave me a great opportunity to use their software to interpret horizontal stress magnitudes and orientations.

- Melinda Yurkowski and Bob Troyer of Saskatchewan Industry and Resources (Geological Services / Well Information) for their advice and assistance in accessing public well data.

Finally, I thank my family for their support over the years. I hope this work will make a contribution in expanding the existing knowledge of the Petroleum industry and that means so much to me.

TABLE OF CONTENTS

Page

PERMISSION TO USE i

ABSTRACT ii

ACKNOWLEDGEMENT iv

LIST OF TABLES viii

LIST OF FIGURES ix

1. INTRODUCTION 1

1.1 Background 1
1.1.1 General 1
1.1.2 Western Canada 1
1.2 Objectives 2
1.3 Scope 3
1.4 Structure of the Thesis 3

2. IN-SITU STRESS REGIME AND GEOLOGICAL SETTING 5

2.1 In-Situ Stresses 5
2.2 Coal-Bearing Strata of Southwest Saskatchewan 7
2.2.1 General Structure and Stratigraphy 7
2.2.2 Belly River Coals 9
2.2.3 Mannville Group Coals 12
2.2.4 Viking Formation 14
2.3 Effects of In-situ Stresses on Borehole Stability in Coal Beds 14
2.4 Effects of In-situ Stress on Coal Permeability 17

3. METHODOLOGY 21

3.1 Vertical Stress Magnitude 21
3.1.1 Introduction 21
3.1.2 Data Compilation and Quality Control 22
3.1.3 Estimation of Near-Surface Bulk Densities 23
3.2 Minimum Horizontal Stress Magnitude 25
3.2.1 Background 25
3.2.2 Tests Used for Estimating Minimum Horizontal Stress: 26
3.2.3 Hydraulic Fracture Treatments for Well Stimulation 28
3.2.4 Hydraulic Fracturing Data Compiled for the Project 28
3.2.5 Post-Fracture Shut-in Pressure Analysis 31
3.3 Maximum Horizontal Stress Magnitude 35
3.4 Horizontal Stress Orientations 37

4. RESULTS AND DISCUSSION 39

4.1 Vertical Stress Magnitude 39
4.1.1 Selection of Geological Reference Surfaces 39
4.1.2 Vertical Stress – Top of Lea Park Formation 40

4.1.3 Vertical Stress – Top of Viking Formation 44
4.1.4 Vertical Stress – Top of Mannville Group 44
4.2 Minimum Horizontal Stress Magnitude 49
4.2.1 Minimum Horizontal Stress – Top of Viking Formation 49
4.2.2 Minimum Horizontal Stress – Top of Mannville Group 52
4.2.3 Minimum Horizontal Stress – Belly River Formation 54
4.2.4 Pore Pressure Effects 57
4.2.5 Measurement in Coal 60
4.3 Maximum Horizontal Stress Magnitude 61
4.4 Horizontal Stress Orientations 62

5 PRACTICAL IMPLICATIONS OF STRESS REGIME ON COALBED METHANE DEVELOPMENT 68

5.1 Coal Permeability 68
5.2 Hydraulic Fracturing 71
5.3 Borehole Stability 72
5.3.1 Modelling Approach 72
5.3.2 Mannville Coals 73
5.3.3 Belly River Coals 78

6. CONCLUSIONS AND RECOMMENDATIONS 79

6.1 Conclusions 79
6.2 Recommendations 81

7. REFERENCES 83

APPENDIX A: Vertical Stress Data A-1

APPENDIX B: Minimum Horizontal Stress Data B-1

APPENDIX C: A Literature Review of Coal Mechanical Properties C-1

APPENDIX D: Borehole Stability Analyses for Belly River Coals D-1

LIST OF TABLES

Page

Table 3.1: Ratio of caliper diameter to bit size for wells used for vertical stress calculations. 23

Table 3.2: Average bulk density corrections for wells used for vertical stress calculations, expressed as a percentage of average bulk density. 23

Table 3.3: Data fields in the database of Viking Formation fracture treatments. 30

Table 3.4: Ratio of fracture close pressure (*FCP*) to instantaneous shut-in pressure (*ISIP*) interpreted from fracture stimulation data for ten Viking and two Mannville wells. 35

Table 4.1: Minimum horizontal stresses interpreted from fracture stimulation treatments and a mini-frac test in the Milk River Formation. 57

Table 4.2: Orientation of horizontal stresses in southwest Saskatchewan. 63

Table 5.1: Input parameters for borehole stability modelling- Mannville coal. 75

Table A.1: Well ID, glacial till bottom, till density and surface to bedrock. A-4

Table A.2: Summary of vertical in-situ stress calculation for the study area. A-5

Table A.3: Assumed data, average density corrections and average caliper/drill bit ratio used for vertical in-situ stress calculations. A-9

Table B.1: Magnitude of minimum horizontal stress at the perforated zone- Viking Formation (estimated as 0.90× ISIP). B-1

Table B.2: Magnitudes and gradients of minimum horizontal stress and pore pressure at the top of the Mannville Group. σ_{Hmin} was estimated by a simple gradient model, using relevant Viking Formation data. B-3

Table C.1: Hoek-Brown parameters for Moura DU coal. C-6

Table D.1: Input parameters for borehole stability modelling - Belly River coal. D-2

LIST OF FIGURES

Page

Figure 1.1: Map of southwest Saskatchewan showing the study area location, basement tectonic features (after Christopher et al., 1971) and limits of Belly River and Mannville Group coals (after Saskatchewan Geological Survey, 2005). 4

Figure 2.1: Principal in-situ stress components acting on a point in the subsurface (after Bell et al., 1994). 5

Figure 2.2: Stress regimes and horizontal stress orientations interpreted for the Western Canada Sedimentary Basin (after Bell et al., 1994) 7

Figure 2.3: Upper Mesozoic and Cenozoic Stratigraphy of southern Saskatchewan, showing coal-bearing strata (after Saskatchewan Geological Survey, 2005). 8

Figure 2.4: Total net coal thickness of Belly River coal seams; contour interval 1 m (after Frank, 2005). 10

Figure 2.5: Thickness of overburden overlying the uppermost Belly River coal seam; contour interval 50 m (after Frank, 2005). 11

Figure 2.6: Gamma ray (GR), bulk density, compressive wave transit time (AC) and Caliper (CAX) logs for a Belly River section containing coal. well101/14-15-005-27W3-00. 12

Figure 2.7: Depth (from ground surface) to the top of the Mannville Group. Basement tectonic features (after Christopher et al., 1971) are: (1) Battle Creek Anticline, (2) Val-Marie Arch, (3) Ponteix Syncline, (4) Swift Current Arch, and (5) Sweetgrass-North Battle Arch. 13

Figure 2.8: Depth (from ground surface) to the top of the Viking Formation. Basement tectonic features (after Christopher et al., 1971) are: (1) Battle Creek Anticline, (2) Val-Marie Arch, (3) Ponteix Syncline, (4) Swift Current Arch, and (5) Sweetgrass-North Battle Arch. 15

Figure 2.9: Stability problems during drilling (after Fjaer, et al., 1992). 16

Figure 2.10: A photo of coal, showing face and butt cleats (after Ma, 2004). 18

Figure 2.11: Comparison of permeability versus minimum effective stress in the Black Warrior Basin, U.S.A and the Sydney Basin, Australia (Sparks et al., 1995). [Note: A permeability of 1 millidarcy (mD) is equivalent to a hydraulic conductivity of 10^{-6}cm/s, when water is the pore fluid.] 19

Figure 2.12: Relationship between in-situ stress and coalbed methane production (after Sparks et al., 1995). 20

Figure 2.13: Permeabilities measured for coal seams in the Western Canada Sedimentary Basin plotted against depth. (Data compiled from Gentzis,

2004; Saskatchewan permeability data added from a public-domain well test report provided to the author by Saskatchewan Industry and Resources). 20

Figure 3.1: Sample bulk density dataset used for vertical stress calculation, including linear extrapolation of shallow bedrock densities, and estimated thickness and bulk density of glacial deposits. UWI 141/10-01-024-26W3-00. 24

Figure 3.2: Typical pressure-time record for a micro- or mini-frac test. Fracture initiation pressure and fracture breakdown pressure may occur at the same point, especially in the case of a solids-free injection fluid. 27

Figure 3.3: Schematic plot of mini-frac pressure decline data showing various flow regimes on log-log scale (after Hannan and Nzekwu, 1992). 32

Figure 3.4: Post shut-in pressure decline data for a fracture stimulation treatment in the Viking Formation, well 12-07-025-17W3. 34

Figure 3.5: Shut-in pressure versus square root of time for a fracture stimulation treatment in the Viking Formation, well 12-07-025-17W3. 34

Figure 3.6: Orientation of a borehole breakout in a vertical well indicates the direction of the minimum horizontal stress. 38

Figure 4.1: Vertical stress magnitude at the top of the Lea Park Formation in southwest Saskatchewan. Basement tectonic features (after Christopher et al., 1971) are: (1) Battle Creek Anticline, (2) Val-Marie Arch, (3) Ponteix Syncline, (4) Swift Current Arch, and (5) Sweetgrass-North Battle Arch. 41

Figure 4.2: Depth (from ground surface) to the top of the Lea Park Formation. Basement tectonic features (after Christopher et al., 1971) are: (1) Battle Creek Anticline, (2) Val-Marie Arch, (3) Ponteix Syncline, (4) Swift Current Arch, and (5) Sweetgrass-North Battle Arch. 42

Figure 4.3: Vertical stress gradient at the top of the Lea Park Formation in southwest Saskatchewan. Basement tectonic features (after Christopher et al., 1971) are: (1) Battle Creek Anticline, (2) Val-Marie Arch, (3) Ponteix Syncline, (4) Swift Current Arch, and (5) Sweetgrass-North Battle Arch. 43

Figure 4.4: Vertical stress magnitude at the top of the Viking Formation in southwest Saskatchewan. Basement tectonic features (after Christopher et al., 1971) are: (1) Battle Creek Anticline, (2) Val-Marie Arch, (3) Ponteix Syncline, (4) Swift Current Arch, and (5) Sweetgrass-North Battle Arch. 45

Figure 4.5: Vertical stress gradient at the top of the Viking Formation in southwest Saskatchewan. Basement tectonic features (after Christopher et al., 1971) are: (1) Battle Creek Anticline, (2) Val-Marie Arch, (3) Ponteix Syncline, (4) Swift Current Arch, and (5) Sweetgrass-North Battle Arch. 46

Figure 4.6: Vertical stress magnitude at the top of the Mannville Group. Basement tectonic features (after Christopher et al., 1971) are: (1) Battle Creek Anticline, (2) Val-Marie Arch, (3) Ponteix Syncline, (4) Swift Current Arch, and (5) Sweetgrass-North Battle Arch. 47

Figure 4.7: Vertical stress gradient at the top of the Mannville Group. Basement tectonic features (after Christopher et al., 1971) are: (1) Battle Creek Anticline, (2) Val-Marie Arch, (3) Ponteix Syncline, (4) Swift Current Arch, and (5) Sweetgrass-North Battle Arch. 48

Figure 4.8: Minimum horizontal stress magnitude in the Viking Formation, southwest Saskatchewan. Basement tectonic features (after Christopher et al., 1971) are: (1) Battle Creek Anticline, (2) Val-Marie Arch, (3) Ponteix Syncline, (4) Swift Current Arch, and (5) Sweetgrass-North Battle Arch. 50

Figure 4.9: Minimum horizontal stress gradient in the Viking Formation, southwest Saskatchewan. Basement tectonic features (after Christopher et al., 1971) are: (1) Battle Creek Anticline, (2) Val-Marie Arch, (3) Ponteix Syncline, (4) Swift Current Arch, and (5) Sweetgrass-North Battle Arch. 51

Figure 4.10: Graphical representation of the simple gradient model that was used to estimate the minimum horizontal stress magnitude at the top of the Mannville Group in the study area, using magnitudes interpreted for the Viking Formation. 53

Figure 4.11: Minimum horizontal stress magnitude at the top of the Mannville Group, southwest Saskatchewan. Basement tectonic features (after Christopher et al., 1971) are: (1) Battle Creek Anticline, (2) Val-Marie Arch, (3) Ponteix Syncline, (4) Swift Current Arch, and (5) Sweetgrass-North Battle Arch. 55

Figure 4.12: Minimum horizontal stress gradient in the top of Mannville Group, southwest Saskatchewan. Basement tectonic features (after Christopher et al., 1971) are: (1) Battle Creek Anticline, (2) Val-Marie Arch, (3) Ponteix Syncline, (4) Swift Current Arch, and (5) Sweetgrass-North Battle Arch. 56

Figure 4.13: Pore pressure at the top of the Mannville Group in southwest Saskatchewan (converted from potentiometric surface data presented by Christopher, 2003). Basement tectonic features (after Christopher et al., 1971) are: (1) Battle Creek Anticline, (2) Val-Marie Arch, (3) Ponteix Syncline, (4) Swift Current Arch, and (5) Sweetgrass-North Battle Arch. 58

Figure 4.14: Pore pressure gradient at the top of the Mannville Group in southwest Saskatchewan (converted from potentiometric surface data presented by Christopher, 2003). Basement tectonic features (after Christopher et al., 1971) are: (1) Battle Creek Anticline, (2) Val-Marie Arch, (3) Ponteix Syncline, (4) Swift Current Arch, and (5) Sweetgrass-North Battle Arch. 59

Figure 4.15: Relationship between pore pressure, minimum horizontal stress and vertical stress in the Mannville Group, southwest Saskatchewan. 61

Figure 4.16: Well locations having data that were used for interpretation of horizontal stress orientations. Basement tectonic features (after Christopher et al., 1971) are: (1) Battle Creek Anticline, (2) Val-Marie Arch, (3) Ponteix Syncline, (4) Swift Current Arch, and (5) Sweetgrass-North Battle Arch. 64

Figure 4.17: Roseplot of borehole breakout data for the seven wells analyzed in this project. 65

Figure 4.18: Roseplot of borehole breakout data from all wells in the study area, including six wells reported by Bell et al. (1994). 65

Figure 4.19: Horizontal stress trajectories in southwest Saskatchewan determined from borehole breakouts. The blue lines represent the orientation of the minimum horizontal stress. Continuous trajectory lines were taken from Bell et al. (1994). Short trajectory lines show local orientations interpreted in this project. 66

Figure 4.20: Frequency distribution diagrams of natural fracture strike directions in late Cretaceous to late Pleistocene strata in Saskatchewan (after Stauffer and Gendzwill, 1987) 67

Figure 5.1: Combined effective stress and permeability measurements made in coal seams in four basins in Australia (from Enever et al., 1998). 69

Figure 5.2: Value of the effective minimum horizontal stress (σ_{Hmin}-P_o) at the top of Mannville Group of southwest Saskatchewan plotted against depth. 69

Figure 5.3: Permeability measurements made in coal seams in BC, Alberta and Saskatchewan, plotted against estimated effective horizontal stress (BC and Alberta data from Gentzis, 2004; Saskatchewan data obtained from SIR). 70

Figure 5.4 Cross-sectional view of a yielded borehole (McLellan and Hawkes, 2001). 73

Figure 5.5: Gamma ray, sonic transit time, dual-arm caliper (CAX, CAY), and density log reading through Mannville coal and adjacent strata for FCE MARENGO S A3-14-28-27. 74

Figure 5.6: Cross-sectional view of rock yielding around a horizontal well for base-case conditions in the Mannville coal, predicted using Phase2. The contours show strength factor, which is the ratio of shear strength to applied shear stress. 76

Figure 5.7: Sensitivity of borehole yielding to unconfined compressive strength (UCS) for a horizontal well in the Mannville coal at 900 m depth. UCS for the base case is 10.8 MPa. 77

Figure 5.8: Sensitivity of borehole yielding to well trajectory for a horizontal well in the Mannville coal at 900 m depth. The base case trajectory is parallel to σ_{Hmin}. 78

Figure A.1: Southwest Saskatchewan glacial till thickness (m). A-2

Figure A.2: Southwest Saskatchewan glacial till density (kg/m^3). A-3

Figure C.1: Relationship between Young's modulus and Poisson's ratio for coal: (data for Cretaceous and Pennsylvanian coal from Jones, et al. 1988, Western Canadian coal parameters from Kaiser and Maloney 1982) C-2

Figure C.2: Mohr-Coulomb failure envelope fit to peak multistage triaxial strength test for coal (data complied from Foroughi, et. al. 1999). C-4

Figure C.3: Hoek-Brown failure envelope fit to peak multistage triaxial strength test for coal (data complied from Foroughi, et. al. 1999). C-4

Figure C.4: Effect of angle of weakness plane inclination ($\beta°$) on unconfined compressive strength (UCS) (data complied from Foroughi, et. al. 1999).....C-5

Figure C.5: Effect of angle of weakness plane inclination ($\beta°$) on peak cohesion (C_P) (data complied from Foroughi, et. al. 1999). C-5

Figure D.1: Gamma ray (GR), sonic transit time (AC), dual-arm caliper (CAX, CAY), and density log readings through Belly River coals and adjacent strata, TEXACO EDGELL 1-4-10-22W3. ..... D-2

Figure D.2: Cross-sectional view of rock yielding around a vertical well for base-case conditions in Belly River coal, predicted using Phase2..... D-3

Figure D.3: Sensitivity of borehole yielding to UCS for a vertical well in Belly River coal at a vertical depth of 436 m. UCS for the base case is 4.2 MPa. D-4

Figure D.4: Sensitivity of borehole yielding to maximum horizontal stress (σ_{Hmax}) magnitude for a vertical well in Belly River coal at a vertical depth of 436 m. σ_{Hmax} for the base case is 10.2 MPa. D-4

1. INTRODUCTION

1.1 Background

1.1.1 General

From exploration to abandonment, geomechanics affects most of the technical aspects of the life of a hydrocarbon reservoir. Understanding the in-situ stress state of the subsurface is the key to solving many geomechanical problems such as wellbore instability, drilling mud weight window, planning and management of casing design, open hole completion stability, solids production, reservoir stimulation, subsidence and compaction of the reservoir and induced seismicity.

The exploration for coalbed methane is focused mainly in the regions of relatively higher permeability and where successful applications of appropriate stimulation techniques have been made. Both of these issues are critically impacted by the in-situ stress field existing in coal seams. Many researchers have reported a strong relationship between effective stress, more specifically the magnitude of minimum principal in-situ stress minus relevant pore pressure ($\sigma_3 - \alpha P_o$), and permeability of coals (e.g., Seidle et al., 1992; Enever et al., 1994, Bustin, 1997; Palmer and Mansoori, 1998; and Kwon et al., 2004). The low levels of effective stress may provide the rock with improved permeability in pore and conductive fracture systems and a decrease in cementation (BJ Service Canada and Rakhit Petroleum Consultant, 2006).

1.1.2 Western Canada

In the energy production scenarios envisioned by the National Energy Board of Canada (2003), "unconventional" and frontier gas production will be required to meet Canadian demand by the year 2008, and could constitute up to 65% of supply by 2025. Reservoirs classified as unconventional include coalbed methane (CBM) and gas shales.

The former is the focus of this project, although the results are also likely to prove useful in the development of gas shales in Saskatchewan.

There has been considerable CBM exploration and development in Alberta in recent years, particularly in the Horseshoe Canyon Formation, Mannville Group and Belly River Formation. The Mannville and Belly River coals extend into southwest Saskatchewan. Some preliminary work has been done on the CBM potential of Mannville Group coals in Saskatchewan (Bend and Frank, 2004), and at least one operator latter has recently conducted well tests and obtained cores for gas content measurements in the Belly River Formation. However, CBM activity has otherwise been relatively limited in this province.

The potential exists for CBM to become a significant resource for Saskatchewan. However, in order to streamline the development process, and improve the odds of success for early CBM projects in the province, various aspects of the coal deposits – including in-situ stress state - must be characterized. For example, detailed mapping of vertical and minimum horizontal stress magnitudes in coal-bearing formations has been conducted in Alberta (Bachu and Michael, 2002), and the results of this work have served as a useful tool in site selection and operations design in that province. Although stress characterization has previously been conducted at the regional scale for the Western Canada Sedimentary Basin (Bell et al., 1994), there has not yet been a study focused solely on coal-bearing strata in Saskatchewan.

1.2 Objectives

The main objective of this research was to characterize the principal in-situ stresses in coal-bearing strata in southwest Saskatchewan, more specifically in the Belly River Formation and the Mannville Group. Secondary objectives were: (a) to develop procedures for estimating minimum horizontal stresses from data that are widely available in many oil and gas fields; (b) to assess the factors controlling stresses in the study area; and (c) to conduct a preliminary assessment of the practical implications of the interpreted stresses on future CBM development activities.

1.3 Scope

The study area, shown in Figure 1.1, is roughly defined by a polygon with vertices at township 1 - range 1 west of the third meridian (i.e., T1-R1W3, T22-R1W3, T47-R30W3, and T1-R30W3). This area was chosen because it contains the principal coal areas in both the Belly River Formation and the Mannville Group. Only stresses within (or near) the latter stratigraphic units were considered in this work.

No new data were collected during this research; no new field or laboratory tests were conducted. The focus was on methods for extracting measurements and estimates of in-situ stresses from existing data.

1.4 Structure of the Thesis

Chapter 2 of this thesis provides a review of literature that is pertinent to this project, including the geology of the coal-bearing strata of interest in this project, previous investigations of in-situ stresses in the Western Canada Sedimentary Basin, and the effects of in-situ stresses on borehole stability and permeability in coals. Chapter 3 describes the procedures used to interpret vertical stress magnitudes and horizontal stress magnitudes and orientations. Chapter 4 describes and discusses the results obtained for vertical and horizontal stresses. Chapter 5 discusses the practical effects of these stresses on CBM development; specifically with respect to coal permeability, hydraulic fracturing and borehole stability. Chapter 6 provides conclusions and recommendations derived from this work.

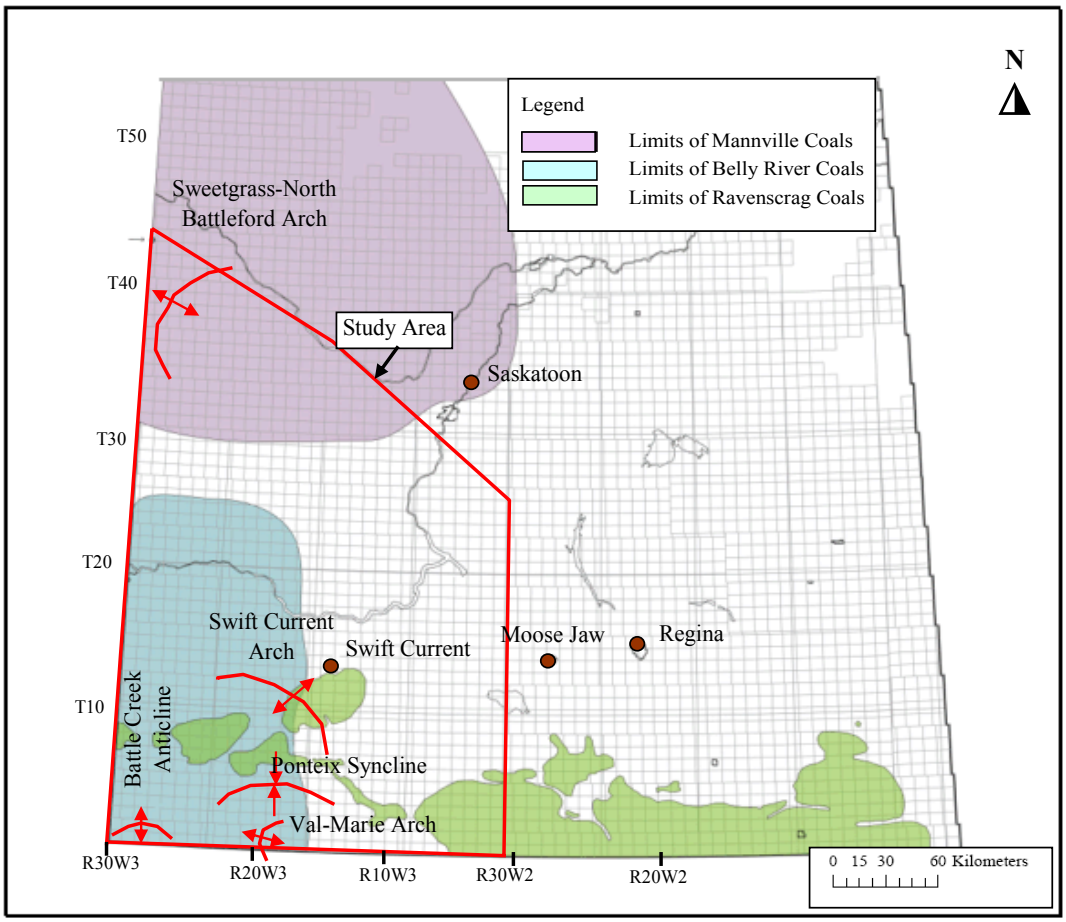

Figure 1.1: Map of southwest Saskatchewan showing the study area location, basement tectonic features (after Christopher et al., 1971) and limits of Belly River and Mannville Group coals (after Saskatchewan Geological Survey, 2005).

2. IN-SITU STRESS REGIME AND GEOLOGICAL SETTING

2.1 In-Situ Stresses

In sedimentary basins with relatively flat-lying rock strata and limited ground surface relief, it is reasonable to assume that the vertical stress at any point within these strata is due simply to the weight of the overburden. Further, there are no shear stresses acting in the vertical direction in such a setting, hence the vertical stress is a principal stress component. Due to the orthogonal nature of principal stresses, the other two principal stresses lie in the horizontal plane, and are oriented at right angles to one another. As such, the in-situ stress state at any point may be fully defined by specifying the magnitudes of the vertical stress (σ_V), the maximum horizontal stress (σ_{Hmax}) and the minimum horizontal stress (σ_{Hmin}), as well as the orientation of either one of the horizontal stresses. These stress components are illustrated in Figure 2.1.

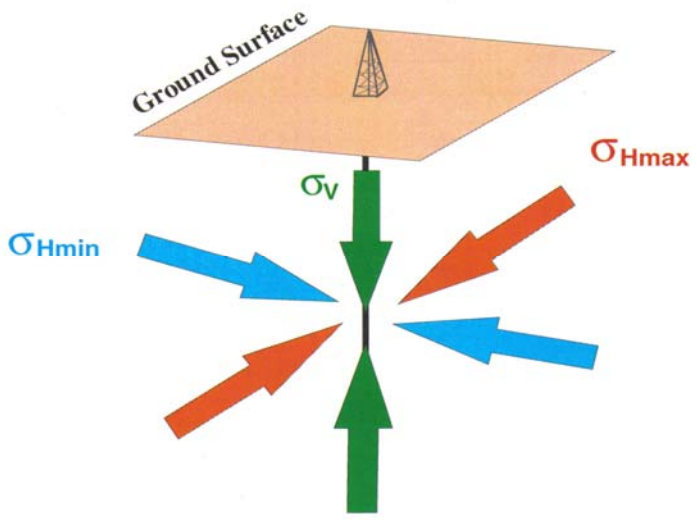

Figure 2.1: Principal in-situ stress components acting on a point in the subsurface (after Bell et al., 1994).

The above-noted conditions are assumed to be valid for the Western Canada Sedimentary Basin (WCSB) in Saskatchewan; hence, the work presented in this thesis will focus on vertical and horizontal stress magnitudes and orientations. Throughout the thesis, compressive stress magnitudes will be considered positive, and tensile stresses will be considered negative.

Regional-scale work by Bell et al. (1994) on in-situ stresses in the WCSB has established the general trend of horizontal stress orientations in western Canada, and identified the stress regimes believed to exist across the basin. The results of this work are shown in Figure 2.2. These regional-scale results indicate that:

- Southwest Saskatchewan lies in a strike-slip fault regime, meaning that the vertical stress magnitude is intermediate between the maximum and minimum horizontal stresses, and
- The maximum horizontal stress in southwest Saskatchewan trends roughly northeast-southwest.

These regional-scale results, however, provide very limited information on stress magnitudes in southwest Saskatchewan. Further, very little information exists on stress magnitudes specifically within coal beds in the WCSB; only one subsurface well measurement (Woodland and Bell, 1989) and one set of mine measurements (Kaiser et al., 1982) exist. On the other hand, fracture (i.e., cleat system) axes, which may be an indicator of principal-stress orientations, have been documented in many shallow coal mines (Campbell, 1979). To augment the database on the stress regime of the coal-bearing upper Cretaceous–Tertiary strata in Western Canadian Sedimentary Basin, Bell, (2003) interpreted stress magnitudes from well logs and from records of microfrac and minifrac tests, from leak-off tests, and from commercial hydraulic fracture treatments measured in oil and gas reservoirs in Alberta. Unfortunately, no similar work has yet been done in Saskatchewan.

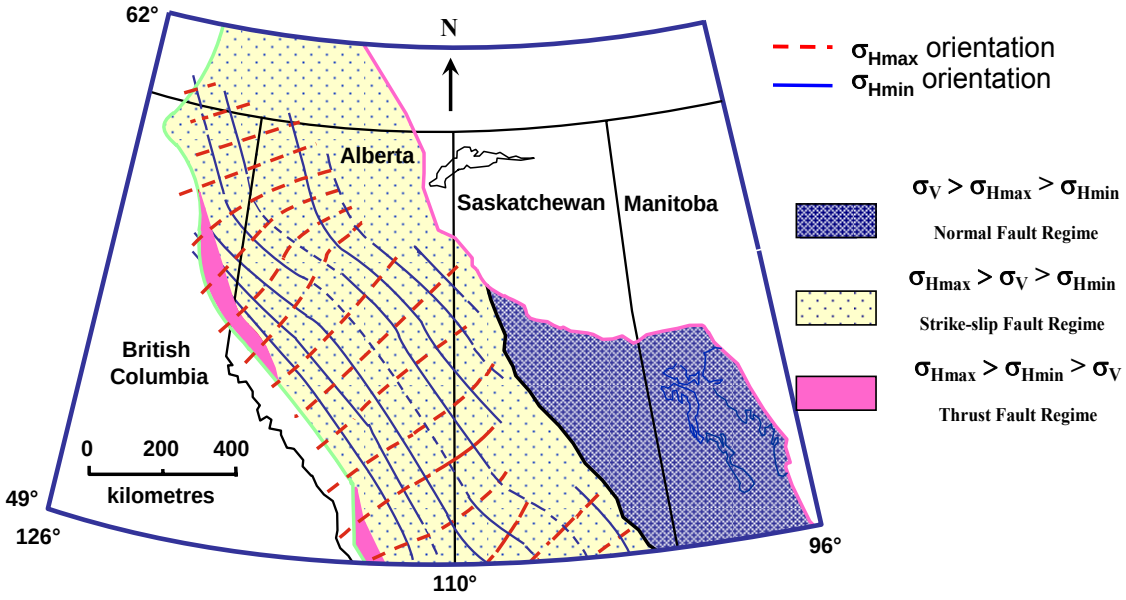

Figure 2.2: Stress regimes and horizontal stress orientations interpreted for the Western Canada Sedimentary Basin (after Bell et al., 1994)

2.2 Coal-Bearing Strata of Southwest Saskatchewan

2.2.1 General Structure and Stratigraphy

The sedimentary strata of the Western Canada Sedimentary Basin rest upon Precambrian-age basement rocks and, in general, dip up to 10m/km in a predominantly southwesterly direction (Christopher et al., 1971). Tectonic processes in the basement led to the formation of major arches and troughs (Porter et al., 1982). Figure 1.1 shows the major features present in the study area. They are relevant to this project because it is likely that they exert some control on in-situ stresses in the area.

Figure 2.3 shows a stratigraphic column for southern Saskatchewan, including the three main coal-bearing units; i.e.:

- Ravenscrag Formation (Tertiary),
- Belly River Formation (Upper Cretaceous), and
- Mannville Group (Lower Cretaceous).

The Mannville and Belly River coals are deemed to have the highest potential for production of coalbed methane. Their rank ranges from sub-bituminous A to sub-bituminous C (Saskatchewan Geological Survey, 2005). The coals of the Ravenscrag Formation are not known to be of immediate interest as a coalbed methane resource, hence they were not considered in this project.

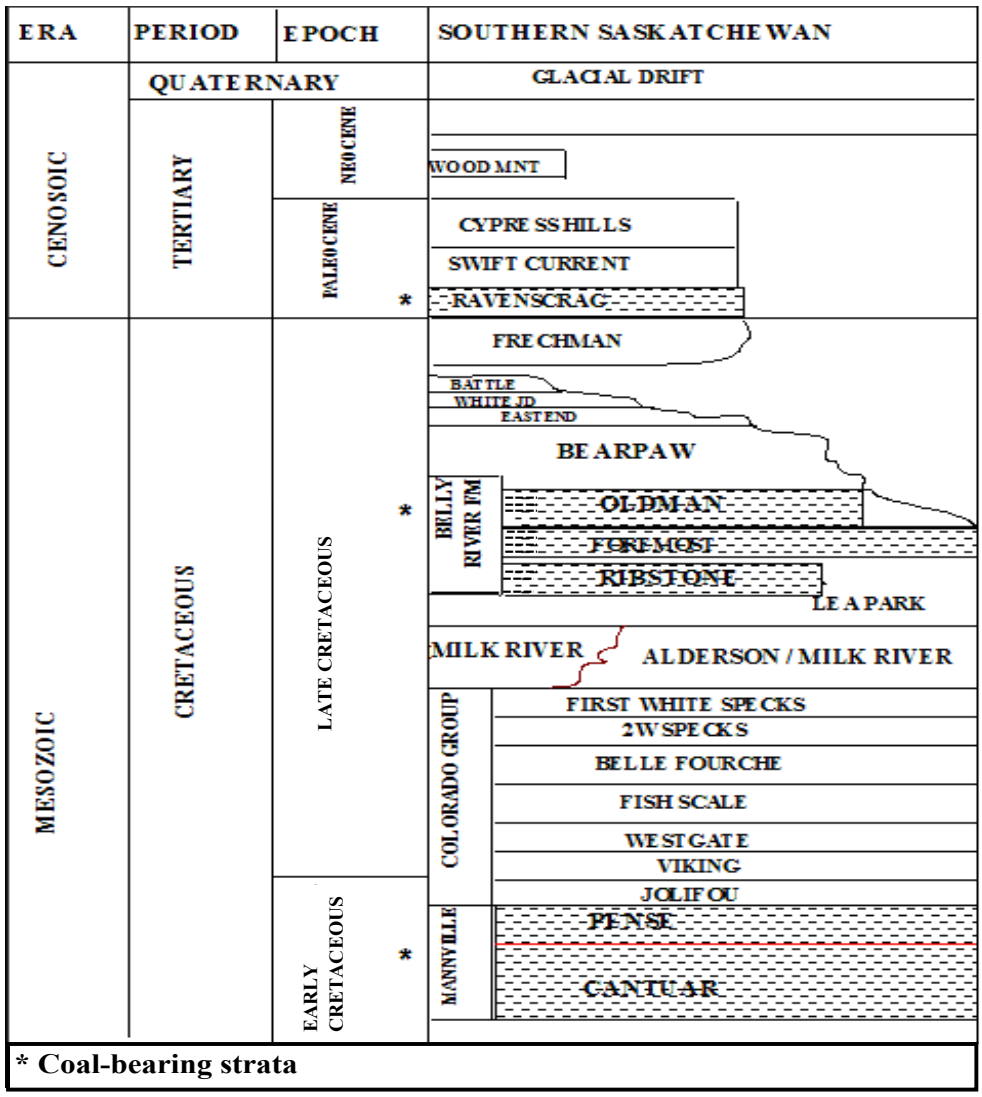

Figure 2.3: Upper Mesozoic and Cenozoic Stratigraphy of southern Saskatchewan, showing coal-bearing strata (after Saskatchewan Geological Survey, 2005).

2.2.2 Belly River Coals

The Belly River Group is a largely nonmarine succession overlain by the marine Bearpaw Formation and underlain by the marine Lea Park Formation. The deposition of this group is interpreted to represent the fourth of the five cycles of foreland basin deposition that occurred during the formation of the Western Canada Sedimentary Basin (Leckie and Smith, 1993).

The Belly River Formation is one of the main coal-bearing units in Saskatchewan. In the study area, the Belly River Formation contains numerous coal seams that have potential for production of coalbed methane. In fact, some of the Belly River coals have already been exploited in Alberta and, to a lesser extent, in southwest Saskatchewan. The coal seams are primarily concentrated in the upper part of the formation, and are most prevalent in an area lying south of township 15 and west of range 20W3, as shown in Figure 2.4. The zone of greatest net coal thickness is characterized by an increase in the number of seams, rather than simply an increase in the thickness of individual seams. Within the main coal-bearing area, up to 17 coal seams are present, ranging in thickness from 0.1 to 3.3 m (Frank, 2005). Coals in this group are deepest, at around 550 m, along an east-west trend within T7, 8 and 9, as shown in Figure 2.5.

Figure 2.6 shows geophysical logs for a coal-bearing section of the Belly River Formation. The coals are identified by lower density values. The figure also shows extensive borehole enlargement in the coals and adjacent strata.

It should be noted that the Belly River coals may extend further north and southwest than shown in Figures 2.4 and 2.5. If present, these coals lie at depths less than the surface casing depths used for wells in these areas, hence they have not been logged.

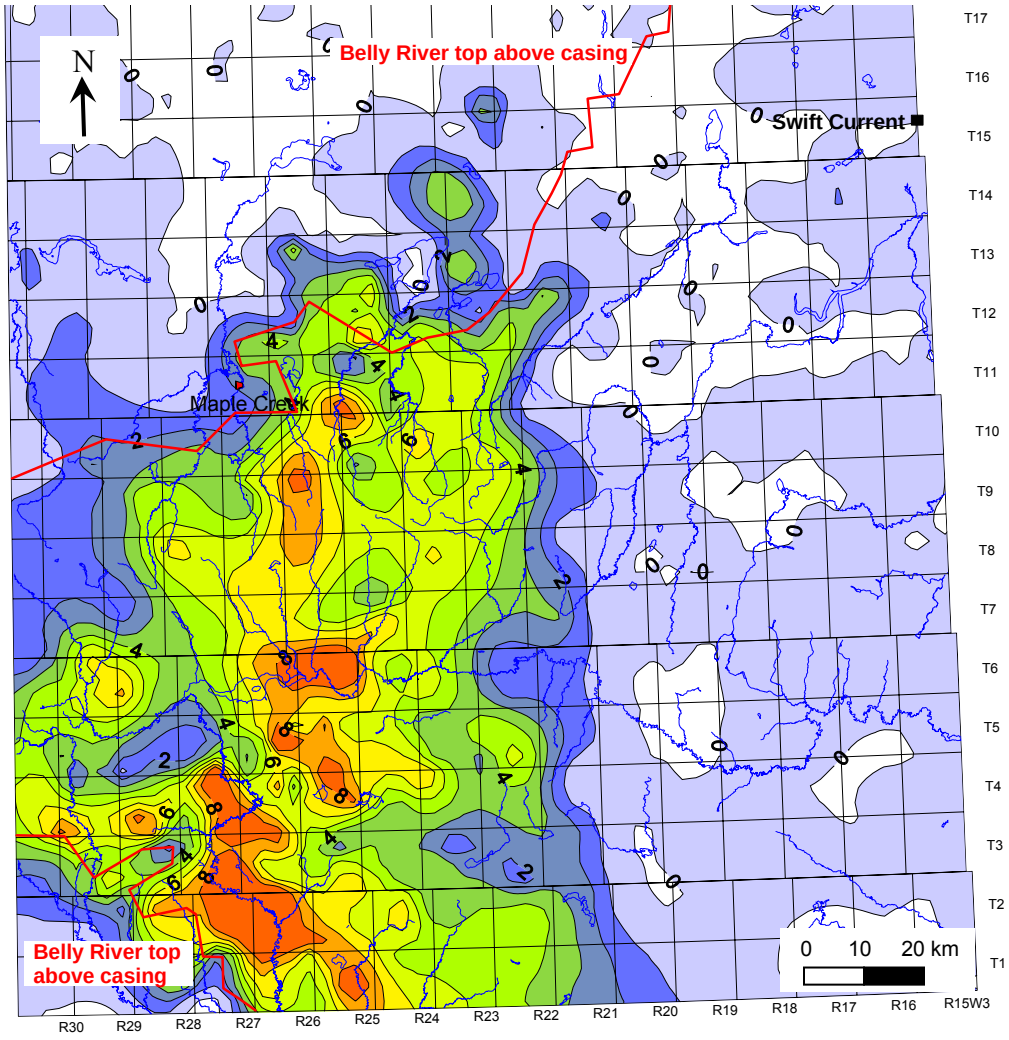

Figure 2.4: Total net coal thickness of Belly River coal seams; contour interval 1 m (after Frank, 2005).

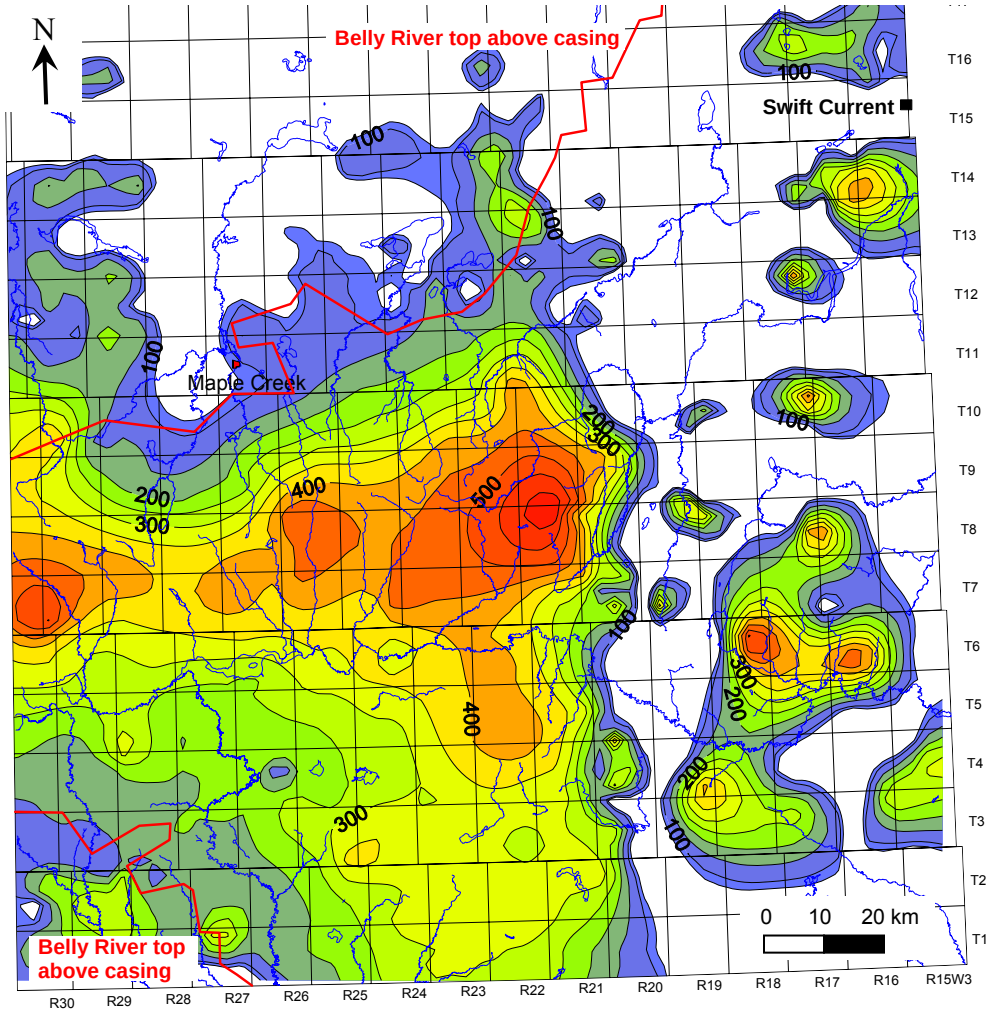

Figure 2.5: Thickness of overburden overlying the uppermost Belly River coal seam; contour interval 50 m (after Frank, 2005).

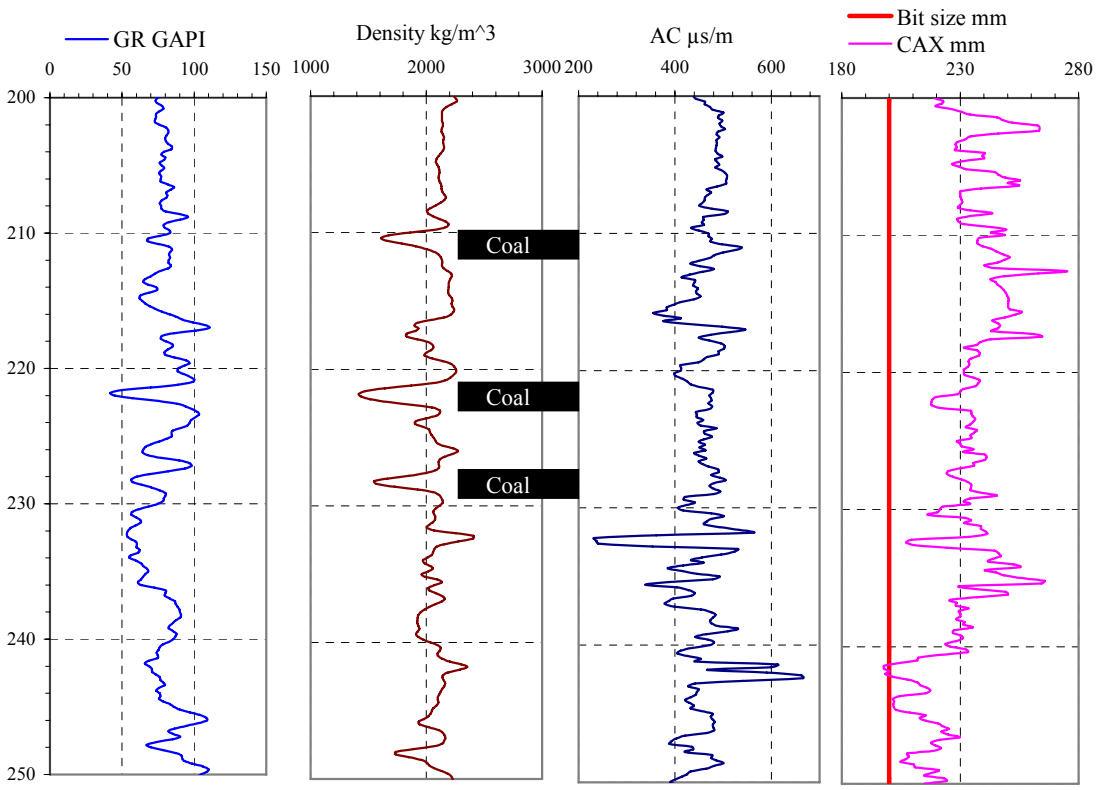

Figure 2.6: Gamma ray (GR), bulk density, compressive wave transit time (AC) and Caliper (CAX) logs for a Belly River section containing coal. well101/14-15-005-27W3-00.

2.2.3 Mannville Group Coals

The Mannville Group is divided into a lower sandstone-dominated formation (i.e., the Cantuar Formation) and an upper siltstone and shale-dominated formation (i.e., the Pense Formation). Depositional environments of Cantuar Formation rocks were mainly continental and coastal, whereas those of the Pense Formation strata were marginal marine (Christopher, 1984).

The coals of the Mannville Group in southwest Saskatchewan form seams of variable thickness and lateral extent that cover the west and northwest portion of the study area (Figure 1.1). Figure 2.7 shows a depth map for the top of the Mannville Group, generated using public-domain data retrieved using Energisite (Divestco, 2006) and Accumap (IHS Energy, 2006). The Mannville Group ranges in depth from slightly under

500 m at the northeast extremity of the study area, to nearly 1400 m in the south and southwest. The thickest coal seams, up to 5.5 m, have been identified within paleovalleys and embayments that occur along the margins of the Unity, Kindersley and Swift Current paleouplands (Bend and Frank, 2004).

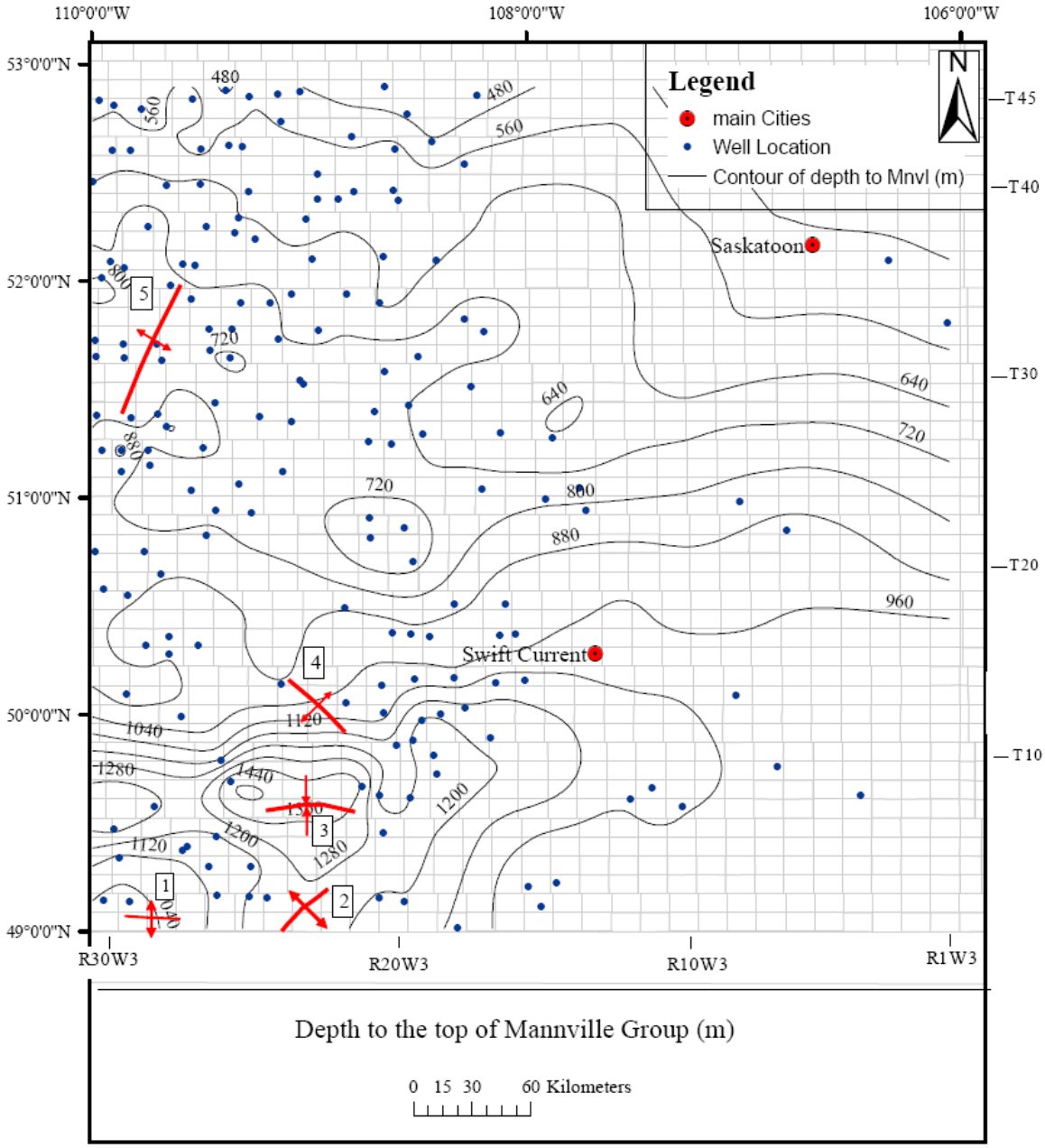

Figure 2.7: Depth (from ground surface) to the top of the Mannville Group. Basement tectonic features (after Christopher et al., 1971) are: (1) Battle Creek Anticline, (2) Val-Marie Arch, (3) Ponteix Syncline, (4) Swift Current Arch, and (5) Sweetgrass-North Battle Arch.

2.2.4 Viking Formation

The Viking Formation is characterized by mudstone, siltstone, silty sandstone, sandstone and conglomeritic elements in vertically-repeated, coarsening-upwards lithologic sequences (Christopher, 1971). Figure 2.8 shows a depth map for the top of the Viking Formation, generated using public-domain data retrieved using Energisite (Divestco, 2006) and Accumap (IHS Energy, 2006). Generally, the Viking Formation decreases in depth from south to north in the study area, from a maximum close to 1300 m to a minimum close to 400 m.

The Viking Formation does not contain coal deposits. However, because of its relevance to analyses discussed later in this thesis, a brief geological description of this formation is given here.

2.3 Effects of In-situ Stresses on Borehole Stability in Coal Beds

Borehole instability is primarily a function of how the rock surrounding a hole responds to the stress concentrations induced around it when it is drilled (Hawkes, 2003). If the well is drilled through a weak rock, these stress concentrations may lead to failure of the borehole. The basic factors affecting borehole instability include the magnitudes and directions of in-situ stresses, the mechanical properties of rocks, the characteristics of the drilling fluid and the influence of pore pressure and the radial flow of the fluid to or from the borehole (e.g., Gough and Bill, 1982; Fleming et al., 1990; Fjaer, 1992; Charlez, 1997; and Hawkes, 2003).

Field observations have shown borehole instability problems are still frequently encountered, even though techniques to manage the problems have been adopted. New challenges have also appeared as a result of the technology pushing towards deep, inclined and horizontal wells, often in weak rocks. Figure 2.9 shows the basic types of failure around a borehole. Compressive failure is caused by an insufficient mud weight in relation to the rock strength and stresses around the borehole; hole convergence is caused by flow of viscoplastic rocks which have yielded, and/or swelling of rocks with high reactive clay contents; while tensile failure is caused by an excessive mud weight compared with the smallest in-situ stress (Fjaer, el al., 1992).

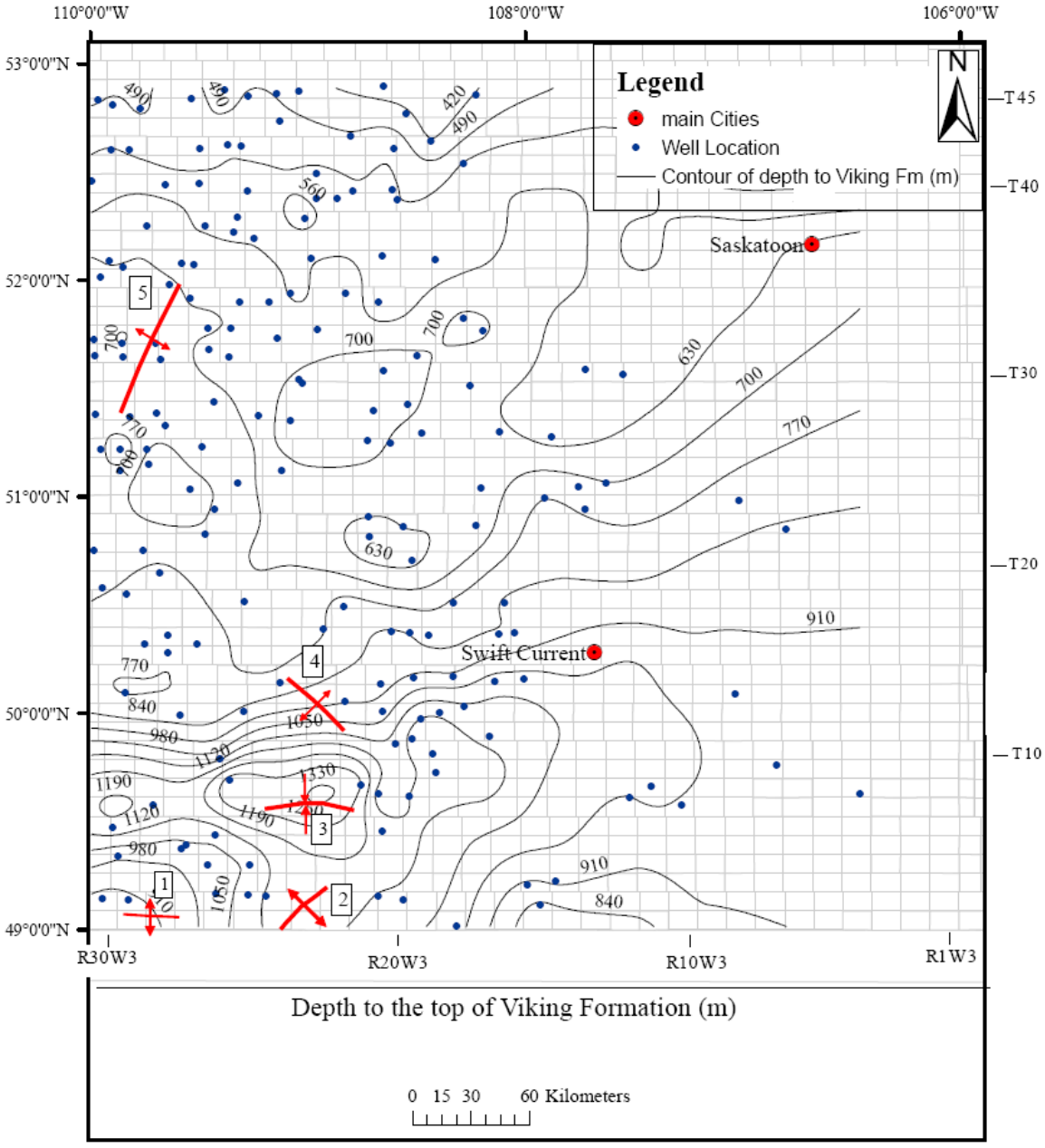

Figure 2.8: Depth (from ground surface) to the top of the Viking Formation. Basement tectonic features (after Christopher et al., 1971) are: (1) Battle Creek Anticline, (2) Val-Marie Arch, (3) Ponteix Syncline, (4) Swift Current Arch, and (5) Sweetgrass-North Battle Arch.

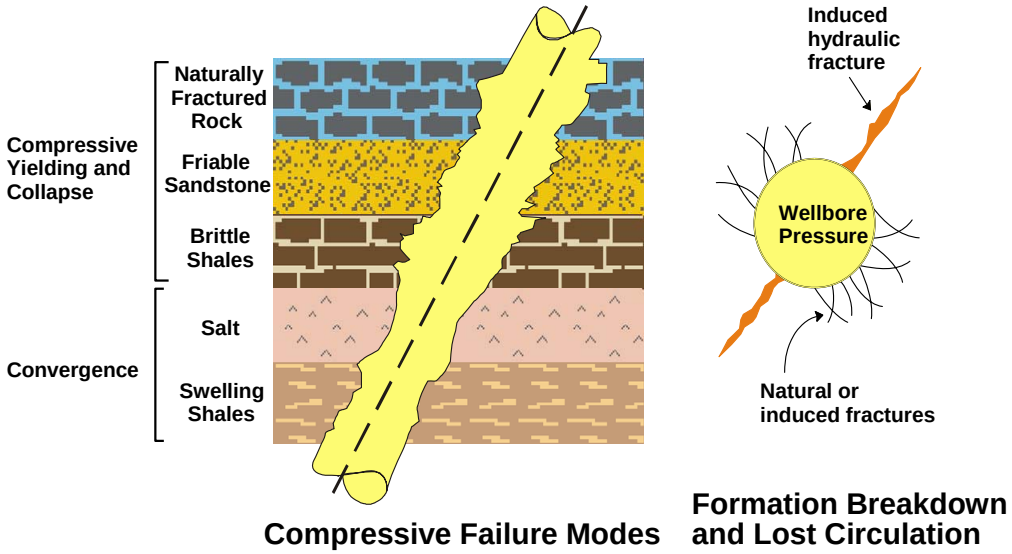

Figure 2.9: Stability problems during drilling (after Fjaer, et al., 1992).

Controlling borehole instabilities requires an understanding of the interaction between rock strength and in-situ stress. Because these cannot be altered or controlled, the only way to inhibit wellbore failure during drilling is to adjust engineering practices by choosing optimal trajectories and mud weights. Similarly, utilization of an appropriate trajectory can limit solids production by reducing the tendency for failure around a borehole (e.g., Fleming et al., 1990; Hawkes and McLellan, 1996; McLellan and Hawkes, 2001; Patrick, 2002; and Hawkes, 2007).

Many methods are available for modelling borehole stability, depending on the data availability and types of problems encountered during field development. Linear elastic models are popular because they are relatively easy to implement, require a modest number of input parameters, and are capable of assessing borehole instability risk for arbitrary well trajectories (McLellan and Hawkes, 1998). Linear elastic models are commonly used in conjunction with the assumption that instability and collapse occur when stresses exceed rock strength at any point on the borehole surface. This is generally a conservative assumption.

Solutions for the borehole problem based on Biot's poroelastic theory (i.e., poroelastic models) have shown that drilling through fluid-saturated formations gives rise to time-dependent stress and pore pressure fields in the vicinity of the borehole (McLellan and Hawkes, 1998). As a natural consequence, borehole stability in such

formations is of a time-dependent nature**.** Poroelasticity couples pore pressure changes near the borehole to the evolutions of effective stresses and strains.

Elastoplastic models are based on the premise that, when the stresses acting around a borehole exceed the strength of the surrounding rocks, a weak material such as coal will undergo plastic yielding. Elastoplastic models extend the stress stain analysis beyond the elastic limit. This model type predicts the stress concentration around a borehole wall more realistically than linear elastic models.

Hawkes (2003) described borehole instability models for coals to determine the minimum drilling mud weight required to prevent severe borehole collapse and to assess the risk of borehole collapse for a borehole pressure and well trajectory. In this study he used linear elastic, non-linear elastic and elastoplastic models, assuming isotropic continuum behaviour, in order to calculate the near-well stresses and to compare these stresses to a rock strength criterion to determine if shear yielding will occur. Also he employed a 2D finite element program to demonstrate stability modelling techniques for Ardley-Alberta coal in order to account for the possible effects of a pervasive plane of weakness that is oriented parallel to horizontal bedding planes.

2.4 Effects of In-situ Stress on Coal Permeability

Fluid flow in coalbeds occurs through the natural fractures, or cleats. Cleats are systematic, orthogonal fracture systems that commonly are perpendicular to bedding (Figure 2.10). They commonly form during coalification, and the face (dominant) cleat orientation reflects the far-field stress present during their formation (Ayers 2002). The face and butt cleat orientations are approximately parallel to the maximum and minimum horizontal stress axes, respectively (Moon and Roy 2004).

The permeability of a coal formation is one of the most important factors in CBM production. Several researchers (e.g., McKee et al., 1988; Seidles et al., 1992; Enever et al., 1994; Enever and McWatters, 1994; Sparks et al., 1995; and Bustin, 1997) have reported that coal permeability decreases with increasing effective stress; i.e. permeability is sensitive to changes in stress and pore pressure. McKee et al. (1988) developed a relationship for permeability, porosity and density as a function of effective stress. These relationships fit both laboratory and field data.

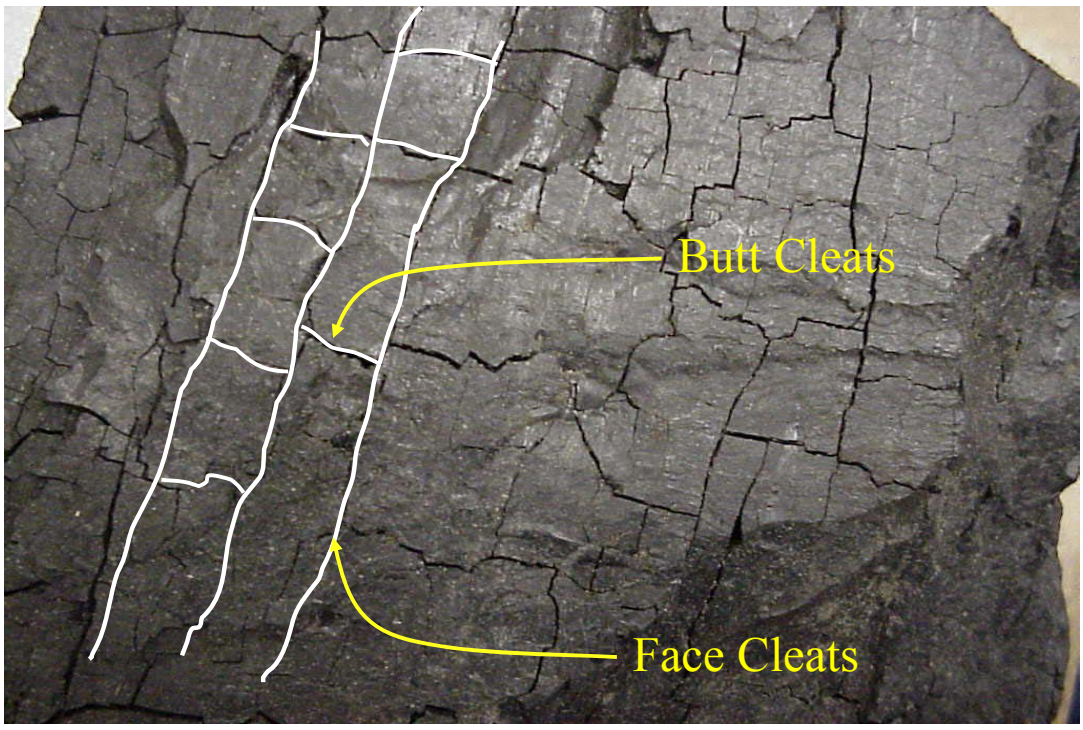

Figure 2.10: A photo of coal, showing face and butt cleats (after Ma, 2004).

Seidles et al. (1992) extended a "collection of matchsticks" model to stressed coals. They present equations for converting laboratory stress-permeability data to in-situ stress as a function of depth of burial in a basin. Sparks et al. (1995) and Enever et al. (1994) represent field-scale measurements of in-situ stress effects on the permeability of coal for both American and Australian coals (Figure 2.11). Sparks et al. (1995) show the relationship between minimum in-situ stress and CBM production (Figure 2.12). Of note in this latter example is the fact that, of all the stress regime parameters, it was the smallest in-situ stress component that was found to exert the strongest control on permeability (hence production). Presumably, the largest component of flow occurs in planes oriented normal to the smallest in-situ stress. This is especially true if cleats are oriented in this direction, as they often are (e.g., Campbell, 1979). This suggests that the smallest in-situ stress at a potential development site is the most important one to characterize with regards to permeability.

At this early stage of CBM development, very limited information about coal permeability in Saskatchewan is publicly available. Figure 2.13 shows a western Canadian coal permeability data, based largely on a compilation presented by Gentzis (2004). The lone data point for Saskatchewan was added to this plot during this project, based on a value reported to Saskatchewan Industry and Resources (SIR) for a well test run in a Belly River coal seam in Township 5, Range 25W3 in 2003.

Figure 2.13 suggests that there is an overall pattern of decreasing permeability with depth (hence stress). The considerable scatter observed in this figure is not surprising, given the varied coal types included in the compiled data.

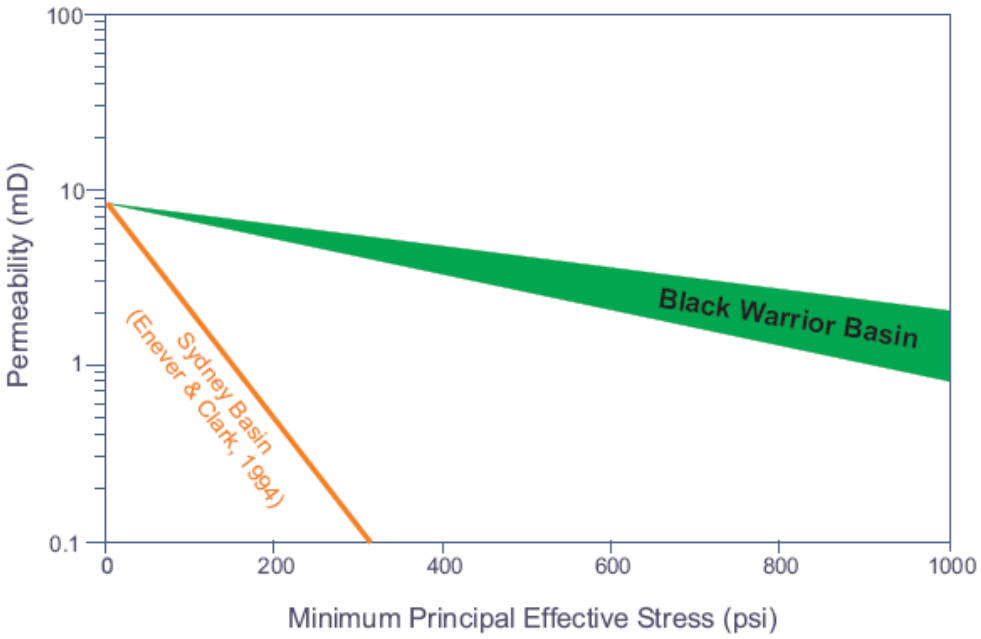

Figure 2.11: Comparison of permeability versus minimum effective stress in the Black Warrior Basin, U.S.A and the Sydney Basin, Australia (Sparks et al., 1995). [Note: A permeability of 1 millidarcy (mD) is equivalent to a hydraulic conductivity of 10^{-6}cm/s, when water is the pore fluid.]

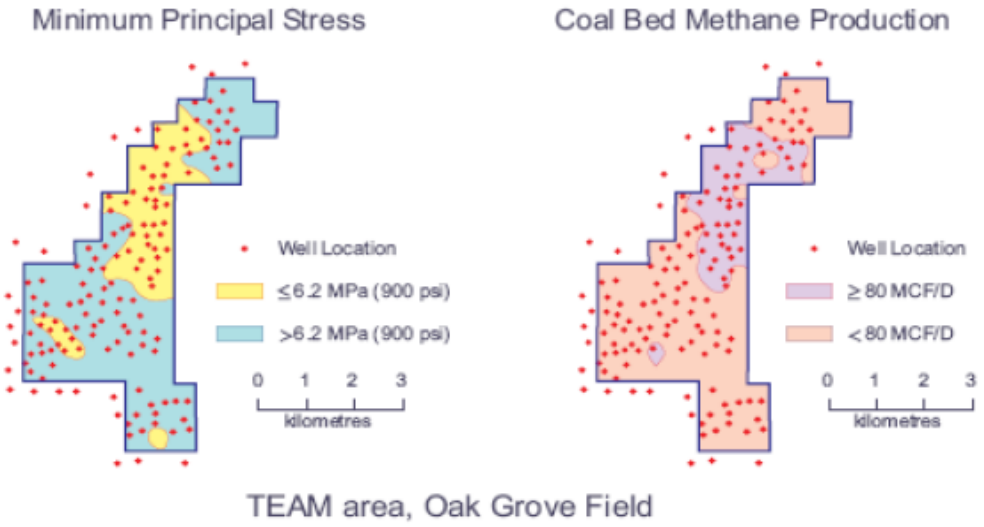

Figure 2.12: Relationship between in-situ stress and coalbed methane production (after Sparks et al., 1995).

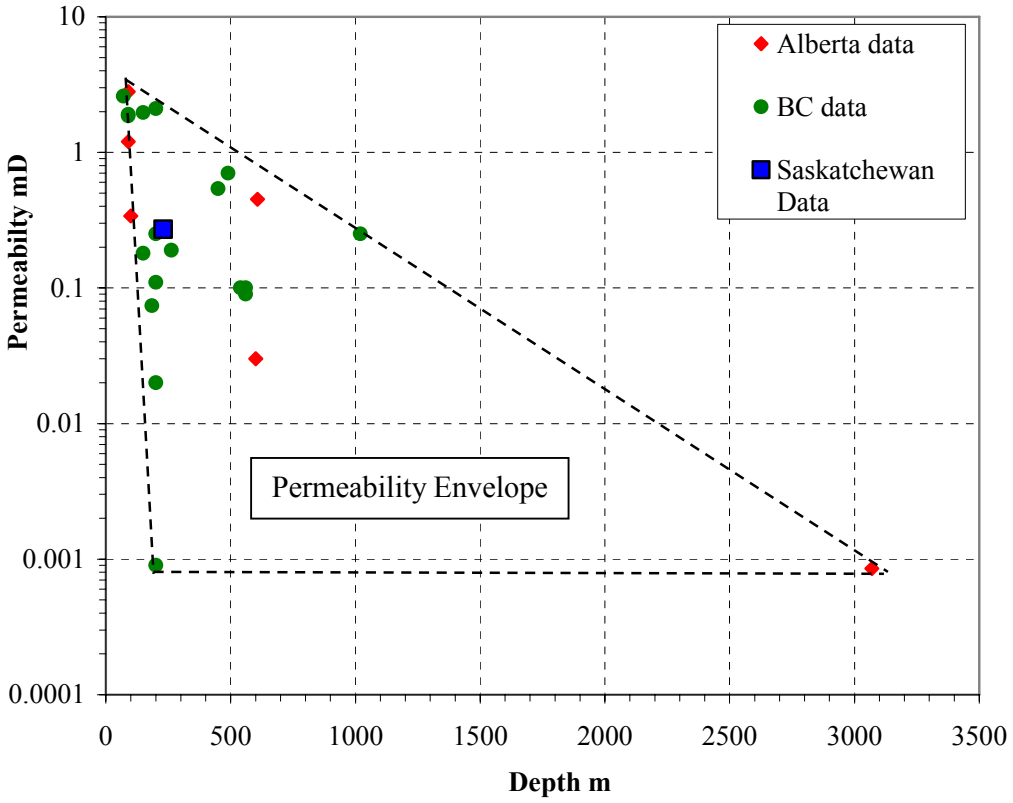

Figure 2.13: Permeabilities measured for coal seams in the Western Canada Sedimentary Basin plotted against depth. (Data compiled from Gentzis, 2004; Saskatchewan permeability data added from a public-domain well test report provided to the author by Saskatchewan Industry and Resources).

3. METHODOLOGY

3.1 Vertical Stress Magnitude

3.1.1 Introduction

Subsurface rock units carry the weight of the overlying rocks, sediments and pore fluids. The vertical stress at a given depth, z, results from this weight. The magnitude of this vertical (or "overburden") stress, σ_V, can be calculated by integrating bulk density measurements of the overburden as follows:

$$\sigma_V = 10^{-6} \times \int_0^z \rho_b g dz \qquad [3.1]$$

Where:

σ_V = vertical in-situ stress (MPa)

ρ_b = bulk density (kg/m^3)

z = depth from ground surface (m)

g = acceleration due to gravity (9.81 m/s^2)

In this thesis, as in most petroleum geomechanics studies, bulk density data were available from density logging tools. These tools measure densities at discrete intervals (often approximately 15 cm). As such, the following discrete form of equation 3.1 was used:

$$\sigma_V = \sum_{i=2}^{i=n} g \left(\frac{(\rho_b)_i + (\rho_b)_{i-1}}{2} \right) \Delta z_i \qquad [3.2]$$

Where i is an index increasing from 1 (at ground surface) to n (at the depth of interest).

3.1.2 Data Compilation and Quality Control

Vertical in-situ stress magnitudes were calculated in this project using bulk density data acquired from geophysical logs for 257 wells in the study area, using equation 3.2. Well locations were chosen to be as uniformly distributed as possible throughout the study area, penetrate to depths at least as great as the top of the Mannville Group, and with preference given to wells logged with relatively modern tools (e.g., post 1980s).

Although bulk density was the only data type used in the calculation of vertical stresses, several additional data types were also compiled in order to enable an assessment of bulk density log quality, and/or to provide context for the bulk density measurements. As such, the complete dataset typically compiled included the following:

- Bulk density,
- Bulk density correction,
- Caliper(s),
- Gamma-ray
- Sonic interval transit
- Well ID (UWI),
- Longitude and latitude
- Depths to geological formation tops, and
- Drill bit size(s).

These logs and well data are publicly available, and they were accessed using Energisite (Divestco, 2006) and Accumap (IHS Energy, 2006). The log data were obtained in digital format (Log ASCII Standard) and imported into Excel® for analysis. For vertical stress calculations, the vertical resolution of each bulk density dataset was down-sampled to 3 m. For each well, quality control was conducted by examining borehole enlargement (as parameterized by the ratio of caliper diameter to bit size), and by examining the magnitudes of bulk density corrections reported by the logging company (to compensate for the effects of borehole enlargement or excessive mudcake thickness). Tables 3.1 and 3.2 summarize the quality assessments made on the data that were ultimately retained for use in this project. A limited number of relatively low quality datasets were retained for use in areas where well coverage was sparse.

Table 3.1: Ratio of caliper diameter to bit size for wells used for vertical stress calculations.

Data Quality	*Range*	*Percentage of wells within this range*
Good	0.95-1.05	63
Fair	1.06-1.15	32
Poor	<0.95 or >1.15	5

Table 3.2: Average bulk density corrections for wells used for vertical stress calculations, expressed as a percentage of average bulk density.

Data Quality	*Range (%)*	*Percentage of wells within this range*
Good	1-3.5	60
Fair	3.6-5.5	35
Poor	5.5-6.8	5

3.1.3 Estimation of Near-Surface Bulk Densities

Two issues pertaining to near-surface bulk density data merit discussion:

- Bulk densities are not usually logged at shallow depths (e.g., above surface casing). As such, it was necessary to estimate bulk densities for unlogged intervals.
- Glacial deposits cover the bedrock throughout the study area. Given that these deposits have bulk densities markedly lower than most sedimentary rocks, it was necessary to estimate the thickness and bulk density of these deposits from a limited dataset.

For most wells analyzed, bulk densities for shallow deposits were addressed as follows. The average bulk density trend through the shallowest intervals logged was linearly extrapolated to the depth corresponding to the top of bedrock. In some cases, it was possible to reduce the size of the interval requiring extrapolation by splicing together bulk density datasets from neighbouring wells.

In order to address issue number two, 35 bulk density logs were found in the study area that were shallow enough to measure the thickness and bulk density of glacial deposits. Densities in these wells ranged from 1760 to 2095 kg/m^3. Thicknesses interpreted from this dataset, combined with a glacial deposit isopach map reported by Fenton et al. (1994), ranged from a few tens of metres to roughly 200 m. These data were used to estimate the thickness and bulk density of glacial deposits for each well included in the vertical stress investigation. Additional details on the densities of glacial deposits are included in Appendix A.

Figure 3.1 shows an example bulk density dataset, including the estimated near surface densities.

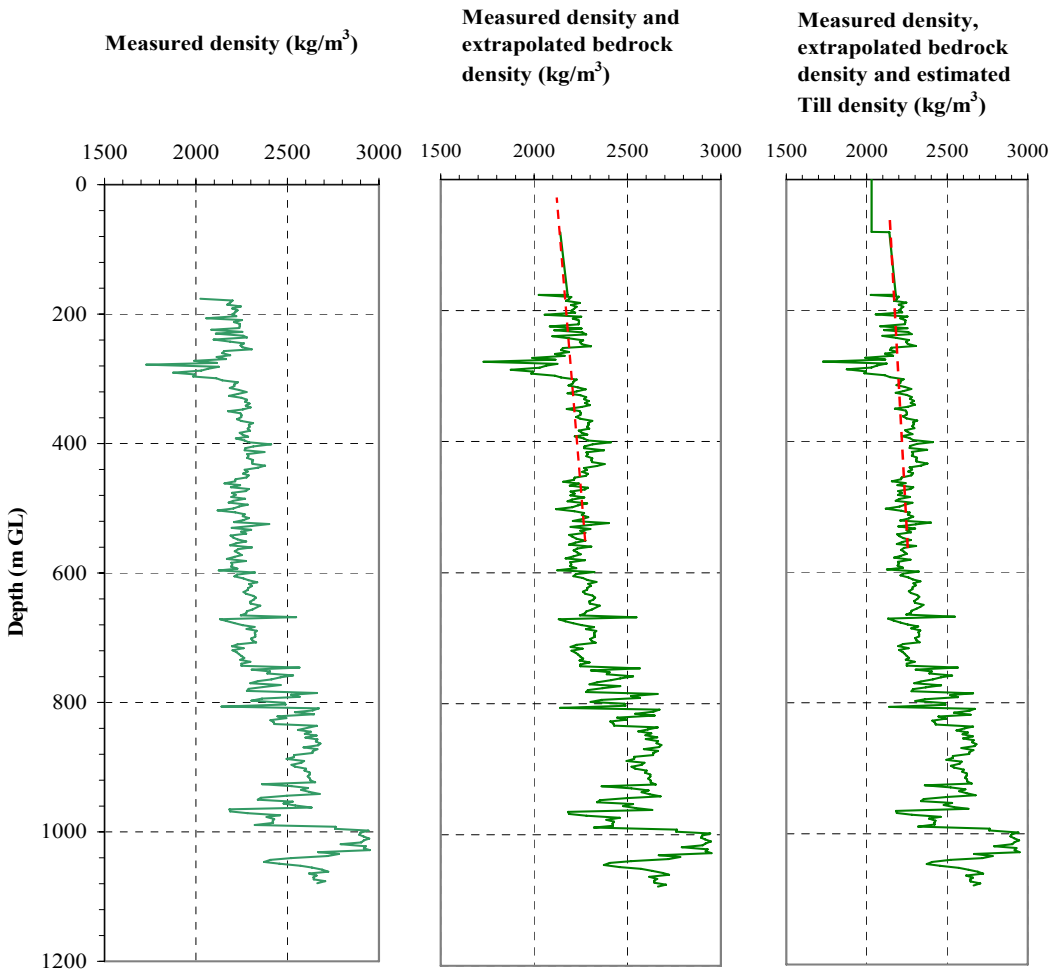

Figure 3.1: Sample bulk density dataset used for vertical stress calculation, including linear extrapolation of shallow bedrock densities, and estimated thickness and bulk density of glacial deposits. UWI 141/10-01-024-26W3-00.

3.2 Minimum Horizontal Stress Magnitude

3.2.1 Background

Warpinski (1989) introduced the following equation to calculate the magnitude of the minimum horizontal stress:

$$\sigma_{Hmin} = \frac{\upsilon_s}{1-\upsilon_s}\left(\sigma_V - \alpha P_{fm}\right) + \alpha P_{fm} + \sigma_{Tect} \qquad [3.3]$$

Where:

σ_{Hmin} = Minimum horizontal in-situ stress

σ_V = Vertical (overburden) in-situ Stress

P_{fm} = Formation pore pressure

α = Biot's coefficient = $1 - \frac{K_{bulk}}{K_{grain}} \approx 1$ for most soft rocks

K_{bulk} = Static bulk modulus of porous rock

K_{grain} = Static bulk modulus of constituent mineral grains

υ_s = Static Poisson's ratio

σ_{Tect} = Tectonic Stress

The tectonic stress is a function of rock stiffness (static Young's modulus) and the magnitude of lateral tectonic strains in the formation of interest. In passive basins, in which there has been no tectonic compression, this term is often neglected. In the Western Canada Sedimentary Basin, however, tectonic compression – resulting in the formation of the Rocky Mountains – has occurred in the relatively recent geological past. Therefore, it is inappropriate to neglect the tectonic stress term in equation 3.3. Unfortunately, there are insufficient data to predict tectonic stresses and strains in the study area with any measure of confidence, so calculation of minimum horizontal stress magnitudes using equation 3.3 was not pursued in this thesis.

3.2.2 Tests Used for Estimating Minimum Horizontal Stress:

In the petroleum industry, micro- and mini-frac tests are generally regarded as the best methods of estimating the minimum horizontal stress magnitude (σ_{Hmin}). Micro-frac tests involve initiating a hydraulic fracture within a short packed-off interval by slowly injecting a small volume (~1 m^3) of a low-viscosity fluid (e.g., water), and monitoring the pressure decline after injection ceases in order to identify the fracture closure pressure (*FCP*). Mini-frac tests are similar in nature, but involve larger volumes of injected fluid (which is often a water-based hydraulic fracturing fluid).

It is useful to define the commonly used concepts for a pressure time record for a hydraulic fracture as shown in Figure 3.2.

1. Fracture initiation pressure (p_i) is the pressure where the pressure-time curve first deviates from its initial, linear trend. It is believed that this is the pressure at which a (tensile) hydraulic fracture initiates.
2. Fracture breakdown pressure (p_b or *FBP*) is the maximum pressure during the test; it is the pressure at which the injected fluid flows into a hydraulic fracture at a significant rate. Fracture initiation pressure and fracture breakdown pressure may occur at the same point, depending on rock properties, fluid properties, and fluid injection rate.
3. Fracture propagation pressure (*FPP*) is the fluid pressure required to extend an existing hydraulic fracture.
4. Instantaneous shut-in pressure (*ISIP*): Is the fluid pressure in a hydraulic fracture immediately after pumping has stopped. *ISIP* is generally believed to be slightly larger than the minimum in-situ stress magnitude.
5. Fracture closure pressure (*FCP*) is the fluid pressure in a hydraulic fracture at the point where the fracture closes. This pressure is equal to the minimum in-situ stress.

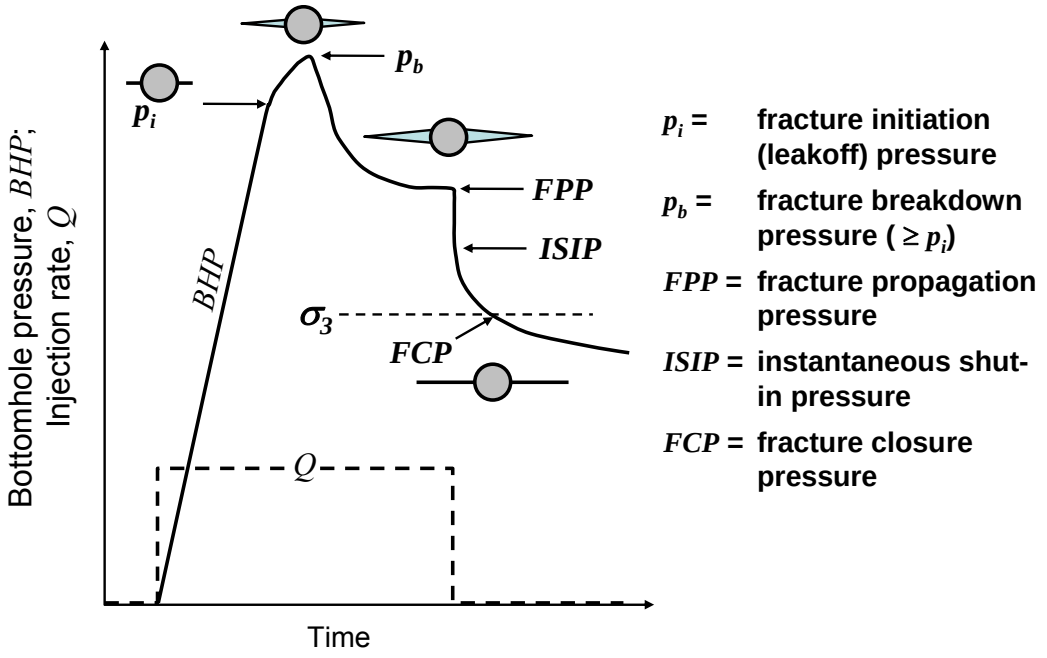

Figure 3.2: Typical pressure-time record for a micro- or mini-frac test. Fracture initiation pressure and fracture breakdown pressure may occur at the same point, especially in the case of a solids-free injection fluid.

As illustrated in Figure 3.2, *FCP* corresponds to the magnitude of the smallest principal stress (which is σ_{Hmin} in this case). The instantaneous shut-in pressure (*ISIP*), also shown in Figure 3.2, is typically slightly higher than the smallest principal stress. Mini-frac tests are similar to micro-frac tests, differing in that they typically involve a relatively high-rate injection of viscous fluids in volumes of 10 m^3 and more. Previous work in western Canada has shown that closure pressures from micro- and mini-frac tests are practically indistinguishable (Woodland and Bell, 1989).

A method for estimating minimum horizontal stress magnitudes using leak-off pressures (which are sometimes obtained during drilling operations, and are analogous in many ways to the fracture initiation pressure presented in Figure 3.2) was also considered for this project, following the procedures outlined in Hawkes et al. (2005). However, investigation of drilling data recorded in Saskatchewan Industry and Resources' well-file library indicated that too few leak-off tests have been run in the project area to support the use of this method.

3.2.3 Hydraulic Fracture Treatments for Well Stimulation

In principal, a hydraulic fracture stimulation treatment is similar in many ways to a mini-frac test. As in the case of the latter, fluid is injected into an isolated interval in order to create a hydraulic fracture. Key differences between the two, however, include the following:

- The volume and rate of fluid injection is much larger for a stimulation treatment.
- The fluid injected may be a two-phase (gas-liquid) mixture or even pure gas.
- Bottomhole pressures are typically not measured, hence they must be estimated based on pressures measured at the wellhead and knowledge of the properties of the fluid(s) in the well.
- Once a fracture has been initiated, a relatively coarse sand or some other type of proppant is added to the injection fluid with the intent of permanently placing these solids within the fracture.

The pressure record for a hydraulic fracture stimulation will usually look similar to the mini-frac dataset illustrated in Figure 3.2, but the duration of injection (hence fracture propagation) will be longer, and there may be no clearly defined fracture closure event.

3.2.4 Hydraulic Fracturing Data Compiled for the Project

Publicly accessible data compiled in the well-file library of the Saskatchewan Industry and Resources (SIR) were reviewed in search of micro- and mini-frac test data, with limited success. In light of this fact, it was decided that hydraulic fracture stimulation data should be used for interpreting minimum horizontal stress magnitude in the study area. While it is acknowledged that these data are less accurate than micro- and mini-frac tests, they have the advantage of being more readily available. As such, use of these data provided denser and more uniform data coverage throughout the study area.

Compilation of fracture stimulation data from SIR's well-file library was not feasible for this project. Fracture stimulation reports were often missing from the files entirely, and those that were present often included insufficient data for analysis. Although operating companies such as Husky Energy, Nexen Inc. and EnCana

Corporation generously offered to provide data for the project, it soon became apparent that data access through this route would also be unfeasible, partly because the operating companies do not keep a digital database of fracture stimulation records, but also because the data coverage available from a limited number of operating companies would be piece-meal in nature.

In light of these challenges, the University of Saskatchewan (U of S) entered into an agreement with BJ Services Canada (BJ) to access their database of fracture stimulation treatments in the study area. The agreement allowed U of S to use the data to interpret stress magnitudes, and to report these interpreted results on graphs and contour plots. The raw data itself, though, could not be presented in this thesis (with the exception of a limited number of samples for illustrative purposes) due to confidentiality issues.

There is one aspect of the BJ dataset with significant implications for this project. The geological formation possessing the most uniform data coverage throughout the study area is the Viking Formation.

Although the primary focus of this project was on the Belly River Formation and the Mannville Group, it was decided that it would be beneficial to pursue an analysis of minimum horizontal stress in the Viking Formation. Chapter 4 provides a discussion of findings relevant to the Belly River and Mannville that can be inferred from the Viking dataset. This discussion also reviews a limited amount of data from the Mannville Group and strata underlying the Belly River Formation.

BJ's database of Viking Formation treatment summaries was provided in an Excel® spreadsheet containing 2225 entries, dating from 1972 to 2005. The headings for each entry are listed in Table 3.3.

Rather than using the entire dataset for minimum horizontal stress interpretation, it was deemed necessary to extract the results that were most appropriate for this task. Most notably, given that bottomhole pressures were not measured during these treatments, calculated values for this parameter are more likely to be accurate for certain testing conditions (e.g., single-phase fluids; large cross-sectional flow areas). Other factors that guided the extraction of data for stress interpretations included: (a) the elimination of data redundancy (e.g., multiple tests in one well or neighbouring wells);

Table 3.3: Data fields in the database of Viking Formation fracture treatments.

Data Field	Comment / Description
UWI Display	Unique Well Identifier
Producing Formation	-
Well Type	Oil or gas
Job Type	Fluid type used, and a comment if gas was added or foam was used.
Date	-
Customer	-
Fluid Type	-
Configuration	Injection down casing, tubing, or both
Ave Rate (m3/min)	-
Top Perf (m)	Top depth of treatment zone
Casing (mm)	-
Tubing (mm)	-
Total Vol (m3)	-
Max Conc (kg/m3)	Maximum proppant concentration
Total Tonnes	Mass of proppant used
In Formation (Tonnes)	Mass of proppant placed in the formation
Sand Type(s)	Proppant type(s)
Sand-Off	Yes or no
Breakdown Press (MPa)	Measured at the wellhead
Ave Press (MPa)	Average wellhead pressure during injection
FG (kPa/m)	Instantaneous Shut-in Pressure, calculated at bottomhole conditions, and converted to gradient form by dividing by depth
Current Status	-

and (b) the need to obtain a dataset amenable to manual quality control measures (e.g., review of the complete treatment records and, if necessary, re-interpretation of the ISIP).

In the selection of treatment records to use for minimum horizontal stress analysis, preference was given to relatively recent data (BJ personnel indicated that algorithms for calculating bottomhole pressures have become more accurate in recent years). Treatments runs in wells with limited pressure depletion were preferred, as it is known that pressure depletion will reduce horizontal stresses to some extent (e.g., Addis, 1997). The database did not include reservoir pressures. As such, treatments run in reservoirs with limited production (as assessed using public-domain production data) were preferred. Where this could not be avoided, preference was given to oil reservoirs, in which pressures tend to deplete less than gas reservoirs. Wells that had sanded off (i.e., slurry injection terminated prematurely when the fracture stopped accepting proppant, resulting in a sudden pressure increase) were not used.

Compromises were made on some of the above-noted selection criteria, where necessary to obtain relatively uniform data coverage. Even so, it was not possible to find data for the entire study area presented in Figure 1.1. Consequently, the results of these minimum horizontal stress analyses presented in Chapter 4 will be mapped across a smaller area than the vertical stress results.

One hundred and six Viking Formation wells were ultimately selected for minimum horizontal stress analysis. Fifty-eight percent of these wells used were fractured after the year 2000.

3.2.5 Post-Fracture Shut-in Pressure Analysis

The end-result of the data compilation and filtering process described in the preceding section was a collection of instantaneous shut-in pressures (*ISIP*'s). However, as noted in section 3.2.1, fracture closure pressure (*FCP*) is generally regarded as the best estimate of minimum horizontal stress (σ_{Hmin}). Although it is not uncommon to use *ISIP* as an indicator of σ_{Hmin}, it represents an estimate that tends to be slightly high (e.g., De Bree and Walters, 1989). To quantitatively assess the relationship between *ISIP* and *FCP* in the Viking Formation dataset, post-fracture pressure shut-in data were analyzed in detail for a limited number of the wells in this dataset. This was accomplished using treatment data provided by BJ, which included measured wellhead pressures, calculated bottomhole pressures, and fluid (or slurry) injection rates recorded over the duration of each treatment.

Fracture closure pressure interpretation was conducted using the MinFrac computer program (Meyer and Associates, 2006). Several interpretation methods are available in this software, all of which tended to provide similar results for the data analyzed in this project. The common element to all of these methods is that they are based on analyses that identify different flow regimes that exist after shut-in, as fluid pressure declines from a magnitude that significantly exceeds the minimum in-situ stress. Most post-fracture interpretation methods are based on the four slow regimes identified in Figure 3.3. These flow regimes were identified and analyzed based on theoretical principles by Cinco and Samaniego (1981). The fracture linear flow regime is characterized by predominant flow along the length fracture. In the bi-linear flow regime,

linear flow along the fracture and linear flow from the fracture into the formation occur at roughly the same rate. Pressure decline during this regime is a linear function of $t^{1/4}$ (where t denotes time). In the formation linear flow regime, linear flow from the fracture into the formation is dominant. Pressure decline during this regime is a linear function of $t^{1/2}$. As pressure progressively dissipates during the preceding flow regimes, a point will be reached where the fluid pressure no longer exceeds the minimum in-situ stress, and the fracture will close. If the fracture closes "completely" (i.e., fracture permeability = formation permeability), a radial flow regime will develop. Pressure decline during this regime is a linear function of log(t). In reality, the final regime is often termed "pseudo-radial," as the fracture retains a higher permeability than the formation. It is important to note, however, that the fracture permeability after closure is significantly lower than it was in the preceding flow regimes, when it was being held open by high fluid pressures.

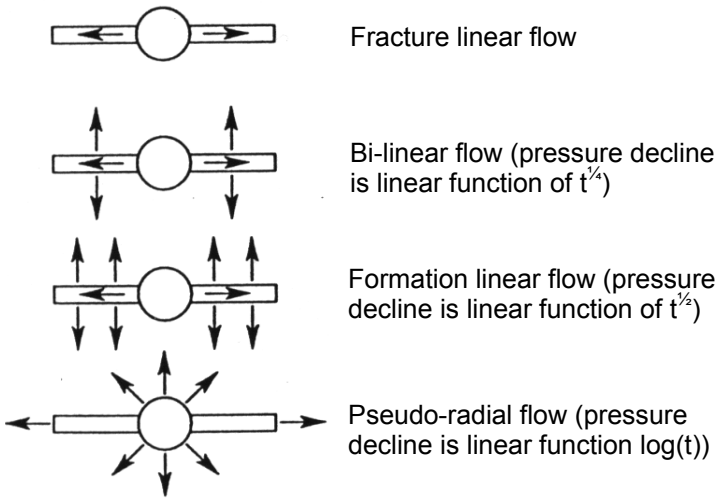

Figure 3.3: Schematic plot of mini-frac pressure decline data showing various flow regimes on log-log scale (after Hannan and Nzekwu, 1992).

As stated by Charlez (1997), the fracture linear and bi-linear flow regimes are usually very short-lived in high-permeability rocks. [Note: During this research, it was assumed that all of the fracture stimulation treatments were run in high-permeability rocks. This seems like a reasonable assumption; given that most formations of interest for conventional hydrocarbon production have permeabilities ranging from 10's to 100's of mD.] Consequently, the first major flow regime anticipated – after the rapid pressure drop to *ISIP* - is the formation linear regime. As demonstrated by several investigators (e.g., Nolte, 1989; Whitehead et al., 1989; Charlez, 1997), a plot of shut-in pressure against square root of time is an effective tool for interpreting fracture closure pressure. On such a graph, a linear trend in the early-time data is taken to indicate formation linear flow, and the first deviation from this trend indicates that fracture closure has occurred.

Figure 3.4 shows the shut-in data from one of the fracture stimulation treatments conducted in the Viking Formation. The bottomhole pressures shown on this graph were calculated by adding the wellhead pressures measured by BJ to the pressure associated with the fluid column in the wellbore. As reported by BJ, this treatment was run at a depth of 643.4 m, and the fluid density at shut-in was 1000 kg/m^3, yielding a wellhead-to-bottomhole pressure differential of 6.3 MPa.

As shown in Figure 3.4, injection stopped approximately 40.8 minutes after the treatment began. Pressure dropped rapidly after shut-in. The *ISIP* interpreted from this graph is 14.3 MPa.

Figure 3.5 shows the shut-in data for the same fracture stimulation treatment, plotted against the square root of time. Ignoring the extremely rapid pressure drop observed in the early time data, a linear trend is observed in the pressure decline range from approximately 14.2 to 13.9 MPa. The first deviation from this trend, at 13.9 MPa, is interpreted as the fracture closure pressure (*FCP*), hence the minimum in-situ stress magnitude.

Table 3.4 summarizes the *FCP*'s and *ISIP*'s interpreted from BJ's fracture stimulation treatment data for 12 wells in the study area for which fracture closure was interpreted to have occurred. On average, FCP is 0.90 times the *ISIP*, and the standard deviation of 0.03 is relatively small. [Note: This table includes data for two Mannville treatments– one of which was in coal – which were late additions to the project dataset.]

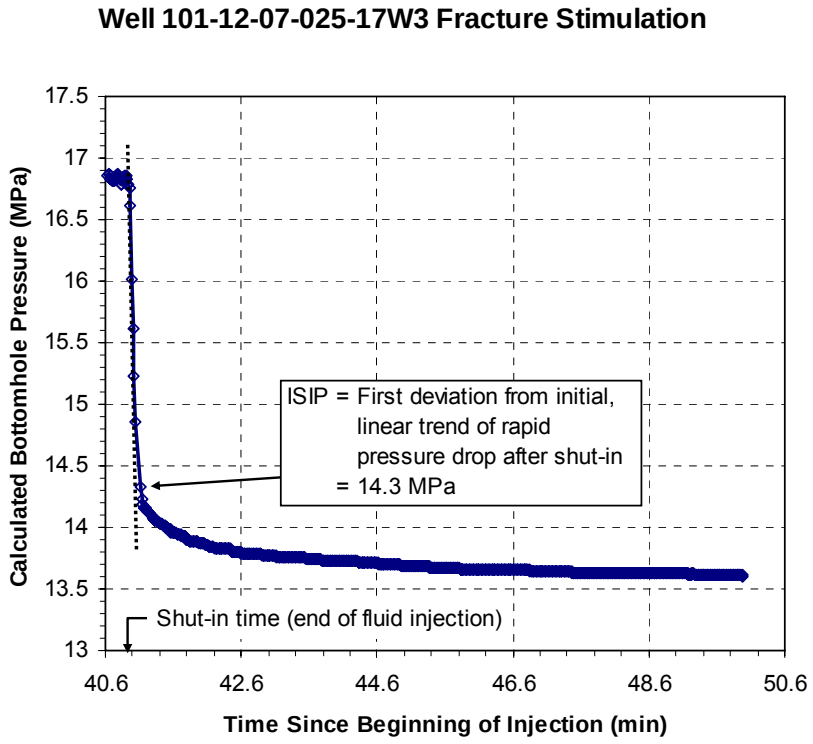

Figure 3.4: Post shut-in pressure decline data for a fracture stimulation treatment in the Viking Formation, well 12-07-025-17W3.

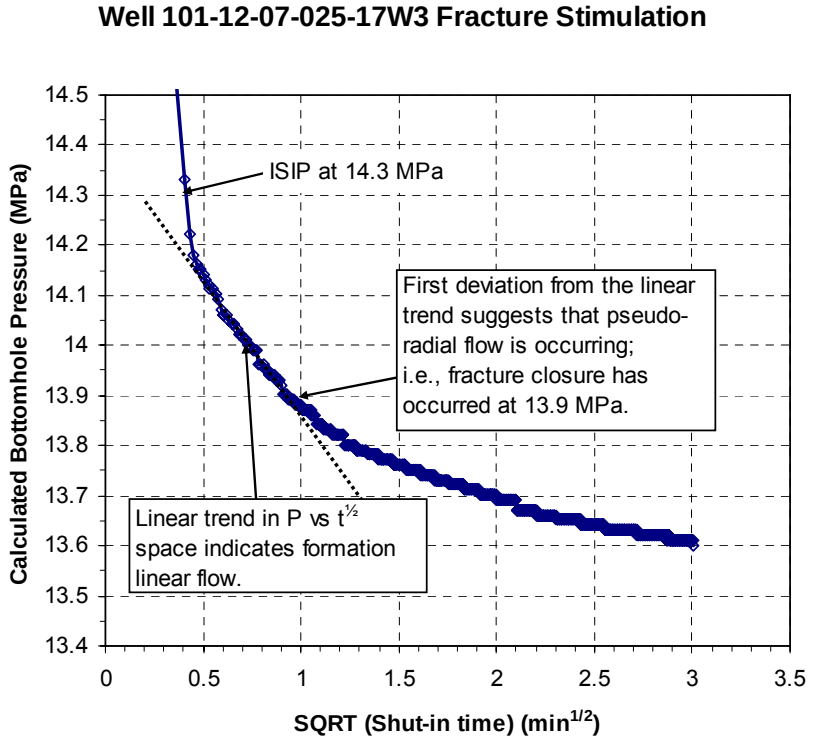

Figure 3.5: Shut-in pressure versus square root of time for a fracture stimulation treatment in the Viking Formation, well 12-07-025-17W3.

Table 3.4: Ratio of fracture close pressure (*FCP*) to instantaneous shut-in pressure (*ISIP*) interpreted from fracture stimulation data for ten Viking and two Mannville wells.

Unique Well Identifier	Top Perf (m)	σ_V (MPa)	ISIP (MPa)	FCP (MPa)	FCP/ISIP	Formation
131/08-34-042-23W3/0	541	11.67	11.88	10.54	0.89	Viking Fm
121/11-29-039-25W3/0	608.3	13.02	12.97	11.4	0.88	Viking Fm
100/14-25-032-24W3/0	847	17.96	13.5	12.17	0.9	Mnvl Coal
100/15-31-031-17W3/0	609	12.87	13.37	11.76	0.88	Viking Fm
131/06-14-029-17W3/0	694	14.82	15.31	14.02	0.92	Viking Fm
101/02-24-028-23W3/0	721	15.61	14.67	13.43	0.92	Viking Fm
141/10-02-028-17W3/0	724	15.59	14.31	12.47	0.87	Viking Fm
12-24-027-26W3/0	900	19.52	16.23	14.4	0.89	Mnvl Group
101/02-12-027-20W3/0	720	15.52	14.09	11.71	0.83	Viking Fm
131/10-06-026-17W3/0	672.5	14.49	13.1	11.66	0.89	Viking Fm
121/06-04-026-14W3/0	604	12.93	12.71	11.62	0.91	Viking Fm
101/12-07-025-17W3/0	643.4	13.8	14.3	13.9	0.97	Viking Fm
				Average:	0.9	
				Standard Deviation:	0.03	

There are two points worth noting about the results presented in Table 3.4. Firstly, they provide justification for a relatively simple means for estimating minimum in-situ stress magnitudes (i.e., multiplying *ISIP* by 0.90) in settings where fracture stimulation data are available, but mini-frac and micro-frac test data are not. Service companies tend to have "rule of thumb" *ISIP* multipliers that are similar to the 0.90 obtained in this work, but – to the author's knowledge - no public-domain documentation of such *ISIP* multipliers exists.

The second point of note pertains to well 101/12-07-025-17W3/0, for which the shut-in data were shown in Figure 3.4 and 3.5. The *FCP*/*ISIP* ratio of 0.97 interpreted for this well is anomalously large, compare to the other results presented in Table 3.4. In fact, the data for this well suggest that minimum horizontal stress magnitude (σ_{Hmin}) is roughly equal to the vertical stress magnitude (σ_V). For the other 11 wells analyzed, σ_{Hmin} was less than σ_V.

3.3 Maximum Horizontal Stress Magnitude

There is no direct measurement technique for measuring the maximum horizontal stress magnitude (σ_{Hmax}). Possibly the best available method for estimating the magnitude

of σ_{Hmax} is to back-calculate its value from a micro- or mini-frac test that was run in an uncased borehole in competent rock. If a bottomhole measurement of fracture breakdown pressure is available for such a test, as well as the σ_{Hmin} magnitude interpreted from either ISIP or FCP, σ_{Hmax} can be calculated using linear elastic analysis of borehole stresses (i.e., Kirsch's equations), as described below.

Assuming that pore pressure in the rock surrounding a borehole remains constant as pressure changes occur within the borehole (i.e., the so-called "non-penetrating" fluid case), the effective tangential stress (σ_θ') around the circumference of the borehole is given by:

$$\sigma_\theta' = \sigma_{H\max} + \sigma_{H\min} - 2(\sigma_{H\max} - \sigma_{H\min})\cos(2\theta) - P_w - P_0 \qquad [3.4]$$

Where:

P_w = well pressure (i.e., fluid pressure within the borehole)

P_o = pore pressure

θ = angular position of the point of interest on the borehole wall, wrt σ_{Hmax}

Tensile failure is most likely to occur where the effective tangential stress reaches a minimum. According to equation 3.4, this occurs at $\theta = 0°$, in which case σ_θ' is given by:

$$\sigma_\theta' = 3\sigma_{H\min} - \sigma_{H\max} - P_w - P_0 \qquad [3.5]$$

The condition for tensile failure (i.e., hydraulic fracturing) to occur is:

$$\sigma_\theta' = T_0 \qquad [3.6]$$

Where:

T_0 = tensile strength of the rock

The well pressure at which tensile fracture initiation occurs (which is commonly regarded as the "fracture breakdown" pressure) is denoted P_b. As such, the relationship between effective tangential stress, tensile strength and well pressure at the point of fracture breakdown is:

$$\sigma_\theta' = T_0 = 3\sigma_{H\min} - \sigma_{H\max} - P_b - P_0 \qquad [3.7]$$

Re-arranging equation 3.7, it is possible to solve for the magnitude of the maximum horizontal stress as follow:

$$\sigma_{H\max} = 3\sigma_{H\min} - P_b + T_0 - P_0 \qquad [3.8]$$

The magnitude of the maximum horizontal stress can be calculated in cases were all of the parameters on the right hand side of equation 3.8 are known.

3.4 Horizontal Stress Orientations

A commonly used method for estimating stress orientations is the analysis of borehole breakouts (e.g., Plumb and Hickman, 1985; Bell, 2003; Zoback et al., 2003). These breakouts are intervals in a well where caving has occurred on opposite sides of a borehole, so that it is laterally elongated, and are indicative of anisotropic compression around the borehole (i.e., $\sigma_{Hmin} \neq \sigma_{Hmax}$). In near-vertical wells (i.e., within 5° of vertical) through transversely isotropic rocks, breakout caving elongates the wellbore parallel to σ_{Hmin} (Figure 3.6). Breakouts are best displayed on borehole imaging logs, but logging tools possessing oriented calipers (e.g., dipmeter logs) are also suitable for documenting breakouts. As such, vertical wells in the study area possessing image logs and dipmeter logs were sought for analysis in this project.

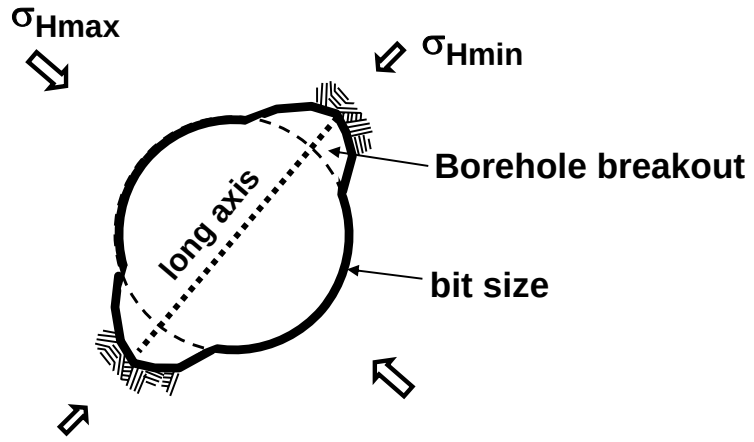

Figure 3.6: Orientation of a borehole breakout in a vertical well indicates the direction of the minimum horizontal stress.

4. RESULTS AND DISCUSSION

4.1 Vertical Stress Magnitude

4.1.1 Selection of Geological Reference Surfaces

The form of the raw output generated in this work was a continuous depth profile of vertical stress for each well analyzed. It is more convenient to present this information in the form of contour maps, which illustrate the regional variations in stress magnitude as calculated for geological surfaces of interest. The surfaces selected for this project, and justification for each, are as follows (listed from youngest to oldest):

- Top of Lea Park Formation: Although coals of the Belly River Formation were one of the primary features of interest in this project, the top of this formation has not been determined throughout the entire study area (e.g., in areas where the formation top lies above surface casing depths). The Lea Park Formation immediately underlies the Belly River Formation, and its top depth is well established throughout the study area.
- Top of Viking Formation: Although this formation was not of interest with respect to coal seams, vertical stresses were mapped at its top to allow comparison to the minimum horizontal stresses interpreted for this formation using fracture stimulation data.
- Top of Mannville Group: The top of this coal-bearing group is well established throughout the study area.

Vertical stresses calculated for these three reference surfaces are presented in tabular form in Appendix A.

4.1.2 Vertical Stress – Top of Lea Park Formation

One hundred and ninety-nine wells were used in the calculation of vertical stress (σ_V) magnitudes at the top of Lea Park formation. A contour map of σ_V magnitude is shown in Figure 4.1. The map shows a north and northeastward decrease in vertical stress from approximately 14 MPa to 2 MPa. This trend is generally consistent with decreasing burial depth (see Figure 4.2). There are three notable low stress areas, all of which are related to basement structural features. The first area, at the southwest corner of the study area, shows low stress values due to relatively shallow depths overlying the Battle Creek anticline. The second area, around 49º 20' N and 108º W, shows low stresses overlying the Val Marie arch. The third area shows low stresses overlying the Sweetgrass - North Battleford arch (around 52º N, near the Alberta-Saskatchewan border). The depth of sediments (hence vertical stress magnitude) increases around 49º 30' N and 107º 45' W, due to the presence of the Ponteix syncline.

Figure 4.3 shows a contour map of vertical stress gradient at the top of the Lea Park Formation. Throughout this thesis, stress and pressure gradients are calculated as secant gradients. For example, the vertical stress gradients mapped in Figure 4.3 were calculated as follows:

$$\sigma_V grad = \frac{\sigma_V}{vertical\ depth} \qquad [4.1]$$

The map shows a northeastward decrease in stress gradient, from approximately 22 kPa/m to 18.4 kPa/m. This largely reflects the fact that, at shallower depths in the north-northeastern part of the study area, a larger proportion of the overburden consists of glacial deposits rather than rock. It should be noted that, in these areas, it was common for 50% or more of the overburden density to be estimated, given the lack of density data at these relatively shallow depths. However, generously allowing for 10% uncertainty in the overburden densities, the vertical stress gradients in the north-northeast part of the study area are notably lower than the gradients in the south-southwest.

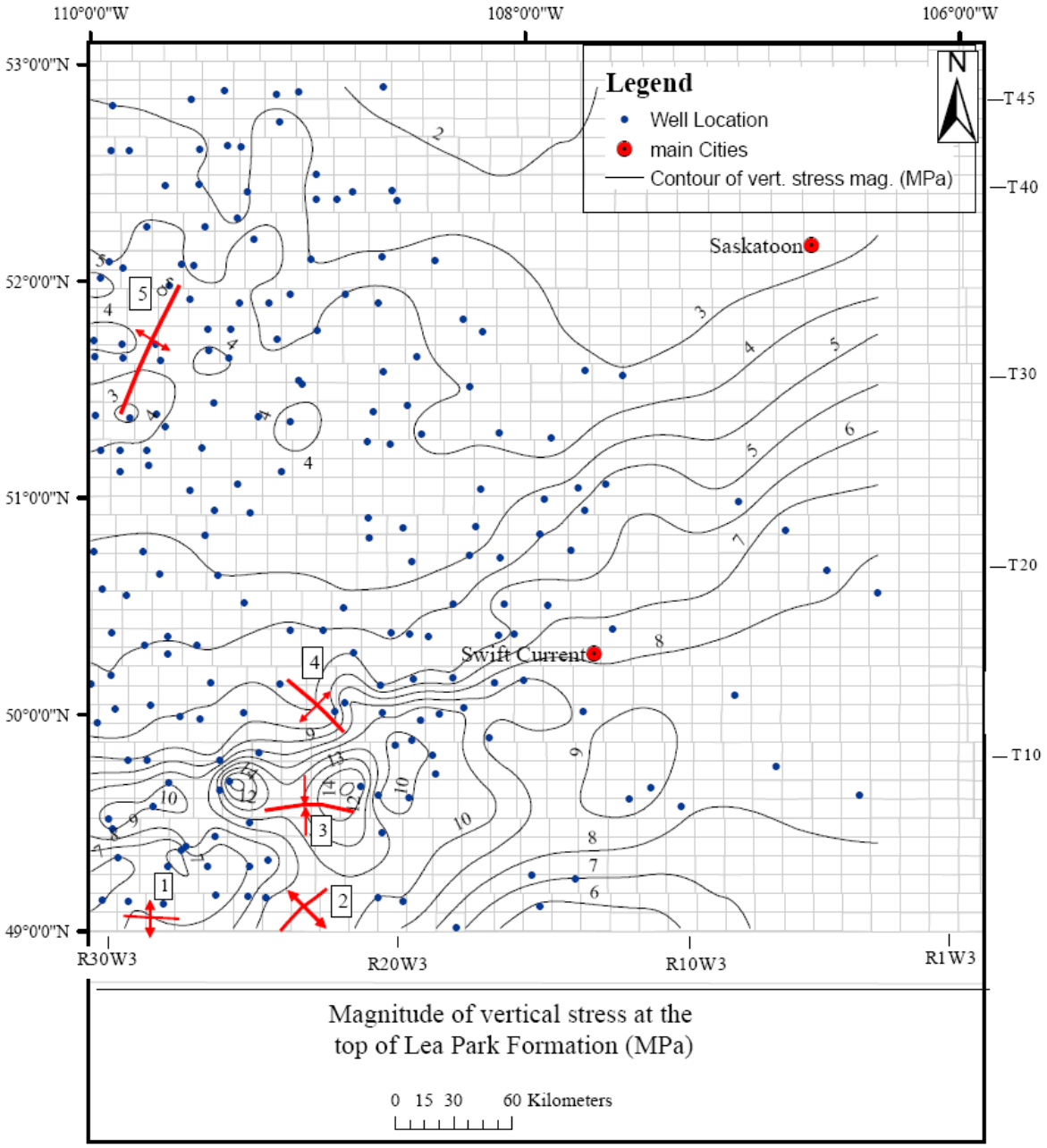

Figure 4.1: Vertical stress magnitude at the top of the Lea Park Formation in southwest Saskatchewan. Basement tectonic features (after Christopher et al., 1971) are: (1) Battle Creek Anticline, (2) Val-Marie Arch, (3) Ponteix Syncline, (4) Swift Current Arch, and (5) Sweetgrass-North Battle Arch.

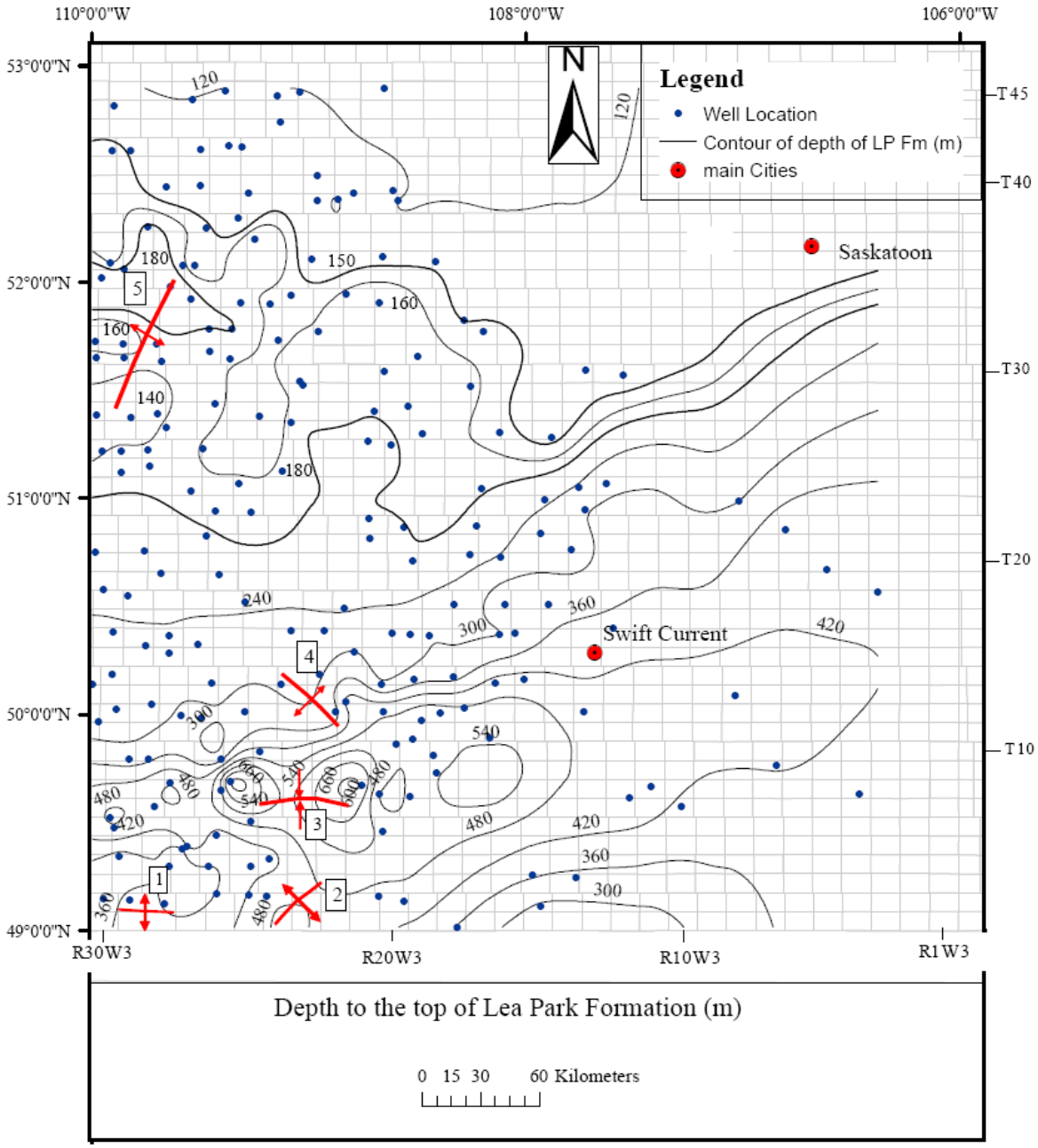

Figure 4.2: Depth (from ground surface) to the top of the Lea Park Formation. Basement tectonic features (after Christopher et al., 1971) are: (1) Battle Creek Anticline, (2) Val-Marie Arch, (3) Ponteix Syncline, (4) Swift Current Arch, and (5) Sweetgrass-North Battle Arch.

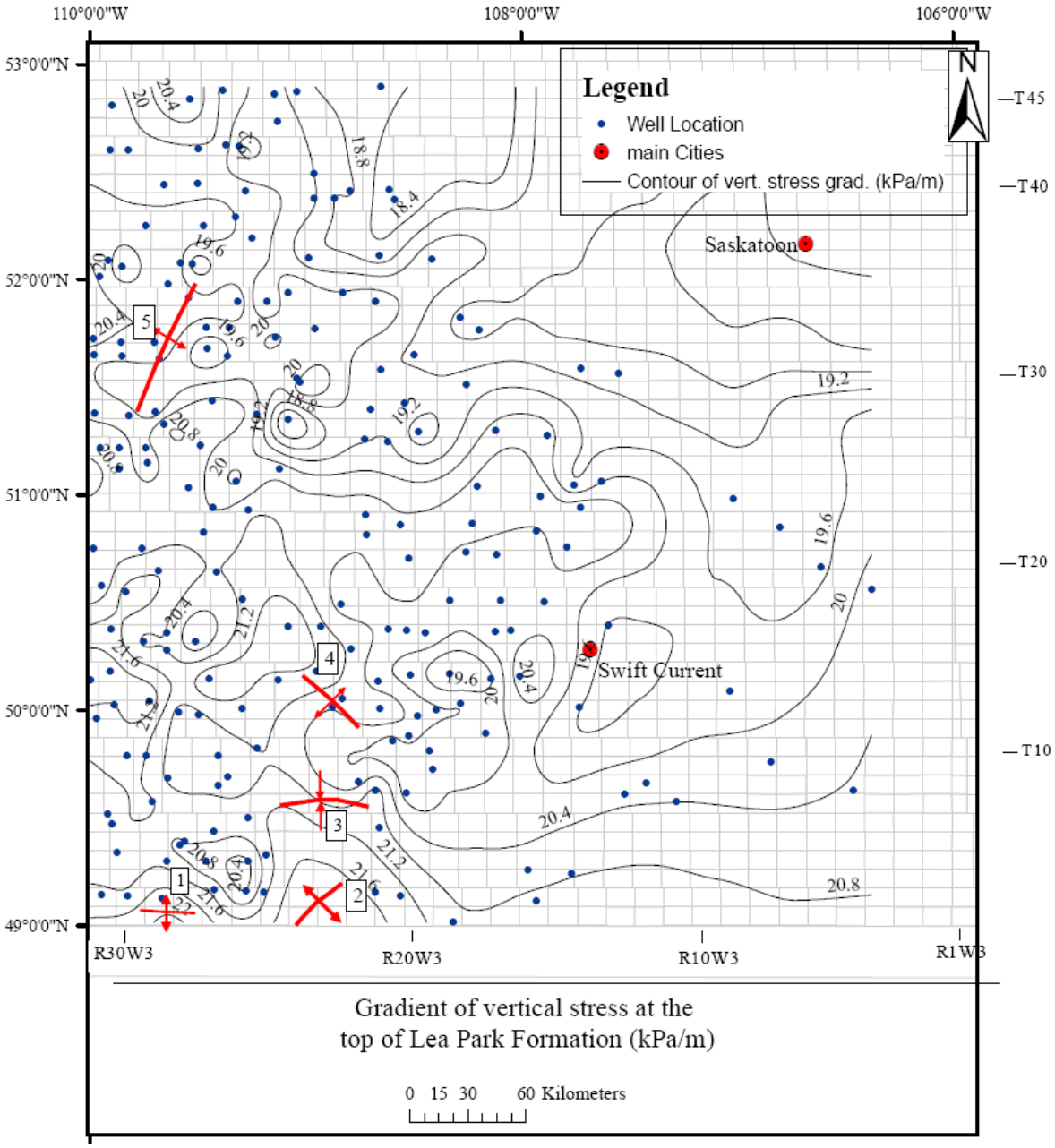

Figure 4.3: Vertical stress gradient at the top of the Lea Park Formation in southwest Saskatchewan. Basement tectonic features (after Christopher et al., 1971) are: (1) Battle Creek Anticline, (2) Val-Marie Arch, (3) Ponteix Syncline, (4) Swift Current Arch, and (5) Sweetgrass-North Battle Arch.

4.1.3 Vertical Stress – Top of Viking Formation

One hundred and seventy-nine wells were used for vertical stress calculations at the top of the Viking Formation. Figure 4.4 shows a contour map of vertical stress magnitude. The map shows that vertical stresses are highest - around 27 MPa - at the southwest extremity of the study area, and lowest – under 10 MPa – at the northeast extremity. This general trend is consistent with burial depth (see Figure 2.8). Similar to the Lea Park Formation, three areas of relatively low stress are visible, overlying: (1) the Battle Creek anticline; (2) the Val Marie arch; and (3) the Sweetgrass - north Battleford arch.

Figure 4.5 is a contour map showing the vertical stress gradient at the top of the Viking Formation. There is a slight decrease is vertical stress gradient – from roughly 22.2 kPa/m to 20.2 kPa/m - from west to east across the map area, indicating that overburden density decreases slightly from west to east across the study area. This is consistent with the trend observed in the Alberta Basin by Bachu and Michael (2002). The only noteworthy anomaly is an area of relatively low gradients (as low as 20 kPa/m) that corresponds roughly with the location of the Swift Current arch (southwest of the city of Swift Current).

4.1.4 Vertical Stress – Top of Mannville Group

One hundred and seventy-five wells were used for vertical stress calculations at the top of the Mannville Group. Figure 4.6 shows a contour map of vertical stress magnitude. The map shows that the vertical stress magnitude decreases from south-southwest to north-northeast, from roughly 31 MPa to under 9 MPa. This general trend is consistent with burial depth (see Figure 2.7), and is very similar to the contour map for the Viking Formation – although the effects of basement features seem slightly less pronounced.

Figure 4.7 is a contour map showing the vertical stress gradient at the top of the Mannville Group. The fact that gradient maps of this type tend to over-emphasize subtle features is especially evident for this dataset. Overall, the trend is very similar to that observed for the Viking Formation. There is a slight decrease is vertical stress gradient –

from roughly 22.6 kPa/m to 20.2 kPa/m - from west to east across the map area, and area of slightly lower gradients near the Swift Current arch.

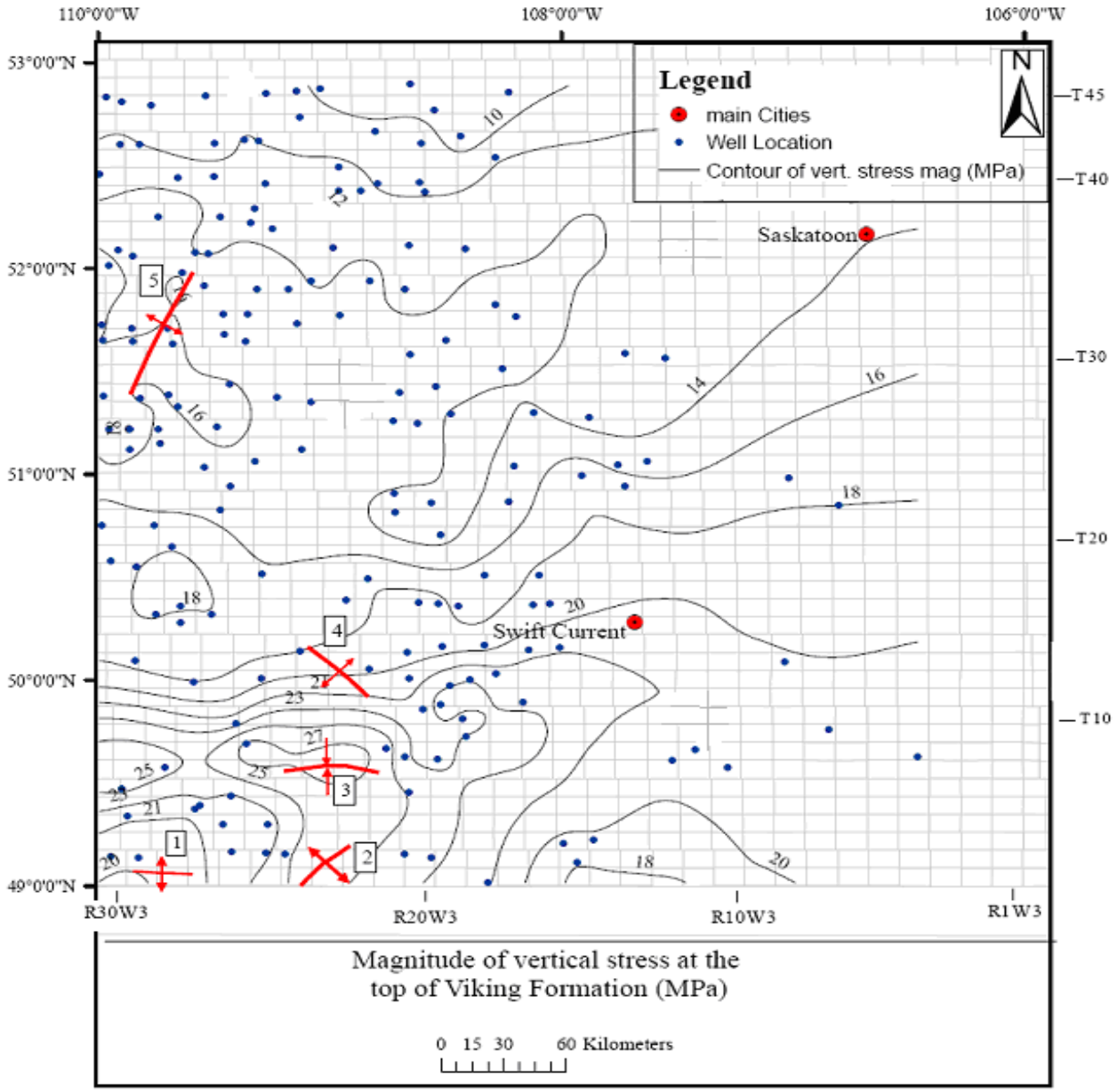

Figure 4.4: Vertical stress magnitude at the top of the Viking Formation in southwest Saskatchewan. Basement tectonic features (after Christopher et al., 1971) are: (1) Battle Creek Anticline, (2) Val-Marie Arch, (3) Ponteix Syncline, (4) Swift Current Arch, and (5) Sweetgrass-North Battle Arch.

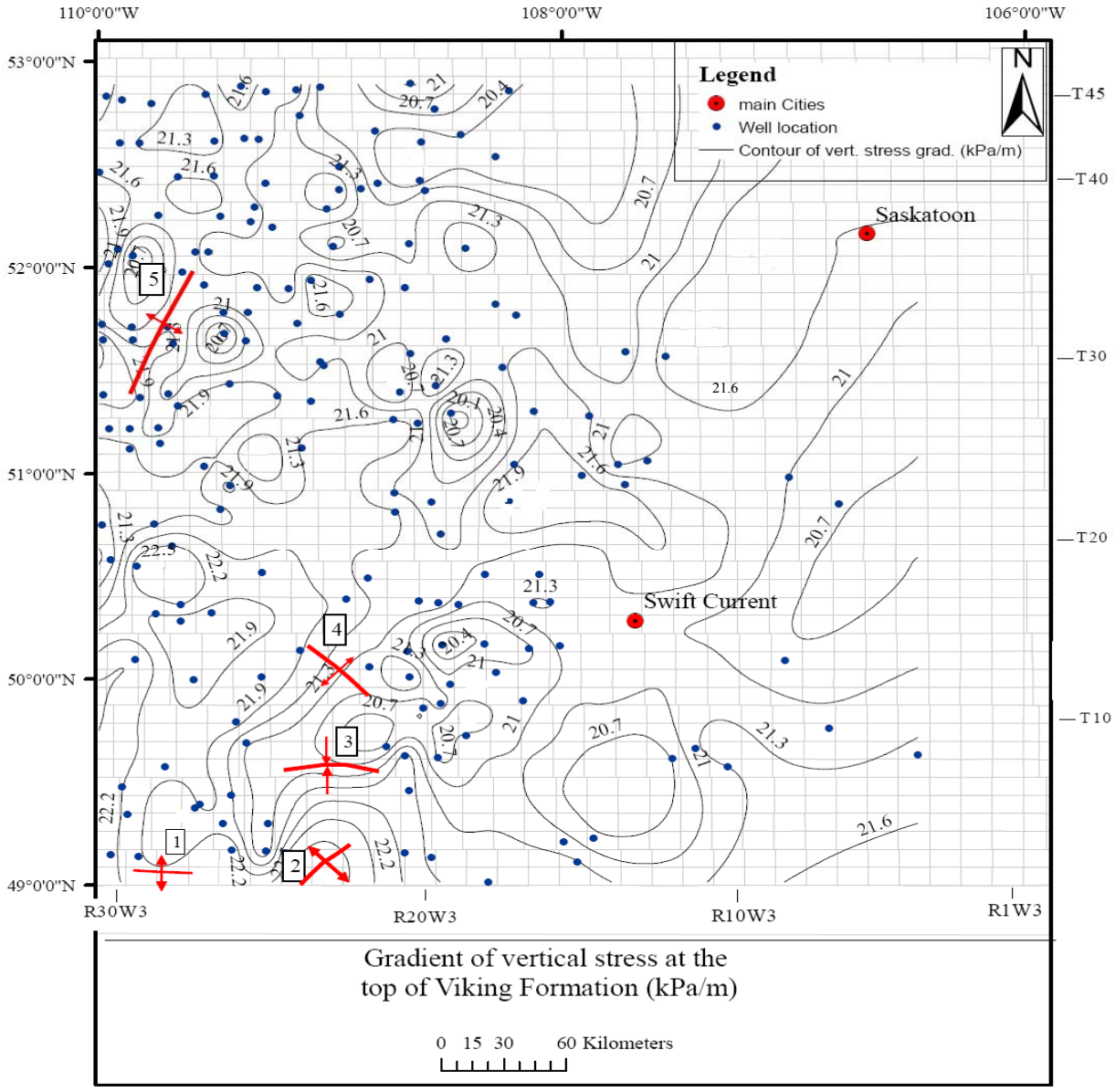

Figure 4.5: Vertical stress gradient at the top of the Viking Formation in southwest Saskatchewan. Basement tectonic features (after Christopher et al., 1971) are: (1) Battle Creek Anticline, (2) Val-Marie Arch, (3) Ponteix Syncline, (4) Swift Current Arch, and (5) Sweetgrass-North Battle Arch.

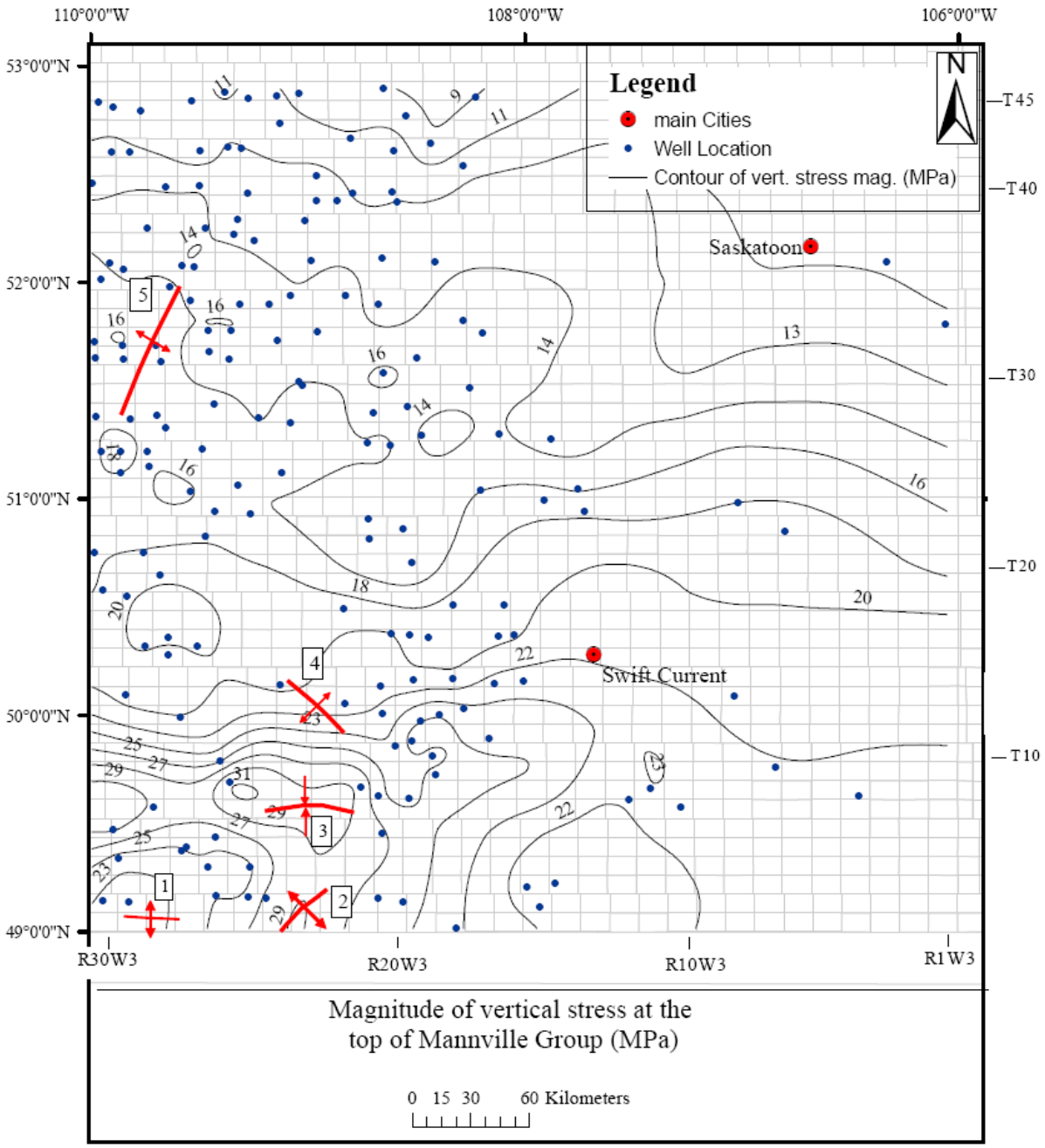

Figure 4.6: Vertical stress magnitude at the top of the Mannville Group. Basement tectonic features (after Christopher et al., 1971) are: (1) Battle Creek Anticline, (2) Val-Marie Arch, (3) Ponteix Syncline, (4) Swift Current Arch, and (5) Sweetgrass-North Battle Arch.

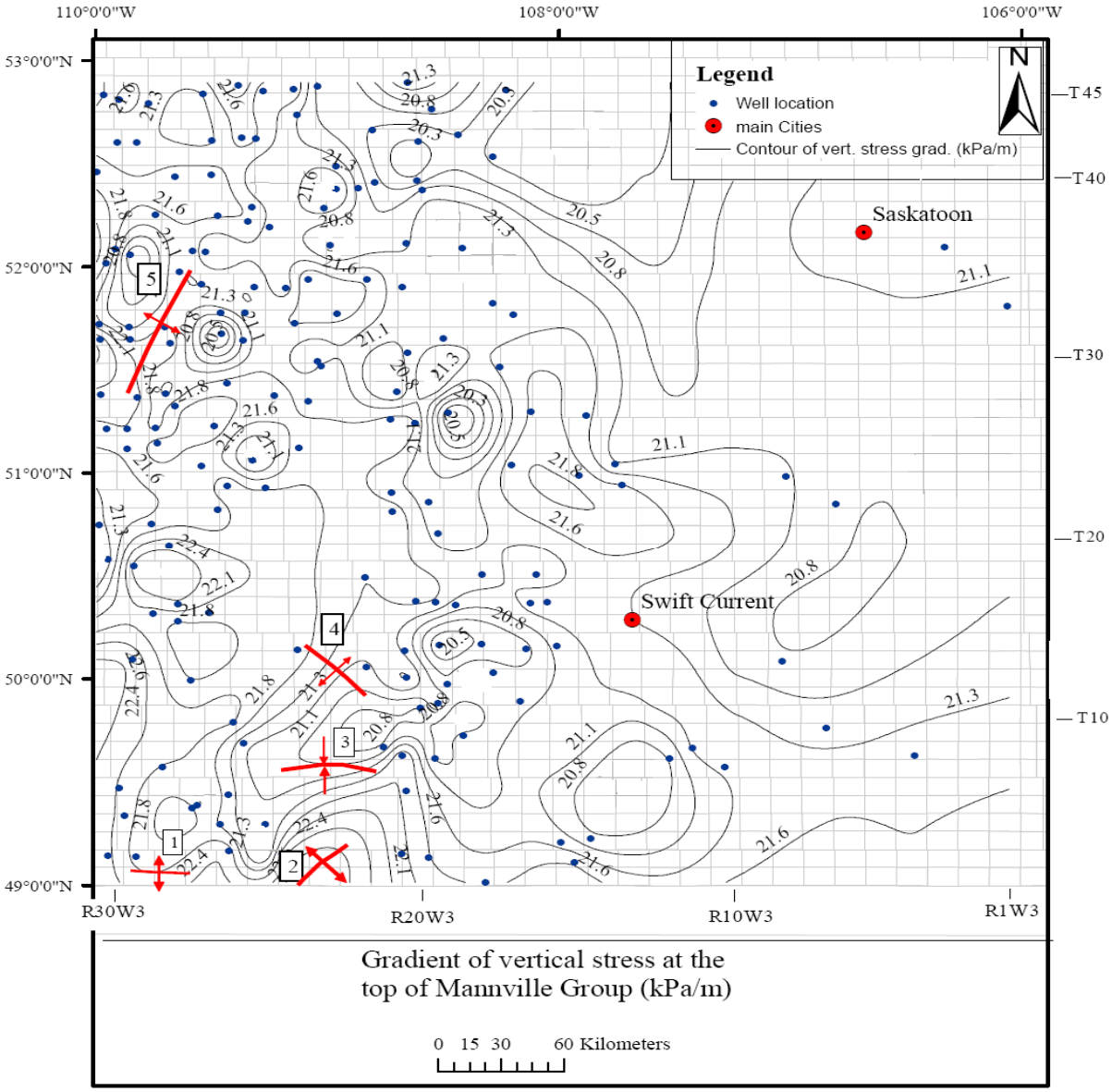

Figure 4.7: Vertical stress gradient at the top of the Mannville Group. Basement tectonic features (after Christopher et al., 1971) are: (1) Battle Creek Anticline, (2) Val-Marie Arch, (3) Ponteix Syncline, (4) Swift Current Arch, and (5) Sweetgrass-North Battle Arch.

4.2 Minimum Horizontal Stress Magnitude

4.2.1 Minimum Horizontal Stress – Top of Viking Formation

A contour map of minimum horizontal stress magnitudes interpreted from fracture stimulation data in the Viking Formation is shown in Figure 4.8. The data used to generate this map are presented in tabular form in Appendix B. The map shows a general trend of decreasing stress from south-southwest to north-northeast, from approximately 18 MPa to 8 MPa. This general trend is consistent with burial depth (see Figure 2.8) and vertical stress (see Figure 4.4). Compared to the vertical stress magnitudes, the correlation between minor anomalies and basement structural features appears to be weaker. The region of relatively high horizontal stress (centered around 49° 20' N, 108° 30' W) roughly corresponds to the Ponteix syncline. There is a weak pattern of relatively low stress near the Saskatchewan-Alberta border, at 52° 25' N, which roughly coincides with the Sweetgrass - north Battleford arch.

It is significant to note that the minimum horizontal stress magnitudes are less than the vertical stress magnitudes throughout the entire map, which is consistent with the expectation that σ_{Hmin} is the least principal stress in the study area (see section 2.1).

Figure 4.9 is a contour map of the minimum horizontal stress gradient, calculated in the same fashion as the vertical stress gradient (see section 4.1.2), in the Viking Formation (at the top of the perforated zone). Gradients are mostly in the 18 to 20 kPa/m range in the northern half of the study area. The limited data available south of township 24 suggest that gradients are slightly lower (17 to 18 kPa/m) in the central part of the map area, and lower still (14 to 17 kPa/m) in the southern part. In interpreting these data, it is important to bear in mind the discrepancy in data density across the map area. More specifically, only 14 data points were obtained south of township 24.

It is believed that shales and shaley rocks tend to have higher horizontal stresses than sandstones (e.g., Warpinski et al., 1989). This is generally attributed to the higher Poisson's ratios of many types of shale, relative to sandstones. Equation 3.3 demonstrates that, all else being equal, higher values of Poisson's ratio lead to higher horizontal stress magnitudes. As noted by Christopher et al., 1971), there is a facies change in the Viking Formation from southwest to northeast, from a relatively thick succession of

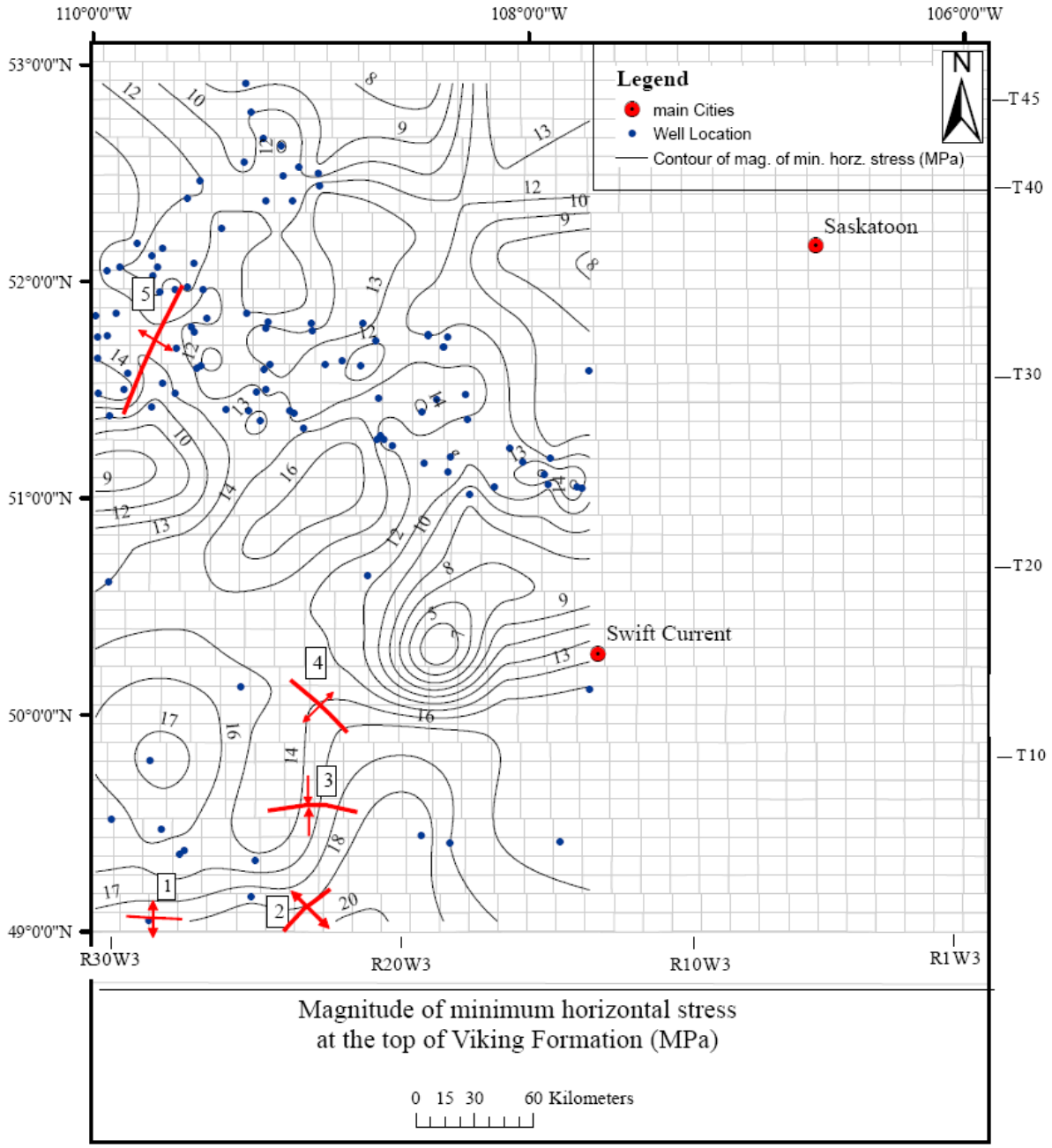

Figure 4.8: Minimum horizontal stress magnitude in the Viking Formation, southwest Saskatchewan. Basement tectonic features (after Christopher et al., 1971) are: (1) Battle Creek Anticline, (2) Val-Marie Arch, (3) Ponteix Syncline, (4) Swift Current Arch, and (5) Sweetgrass-North Battle Arch.

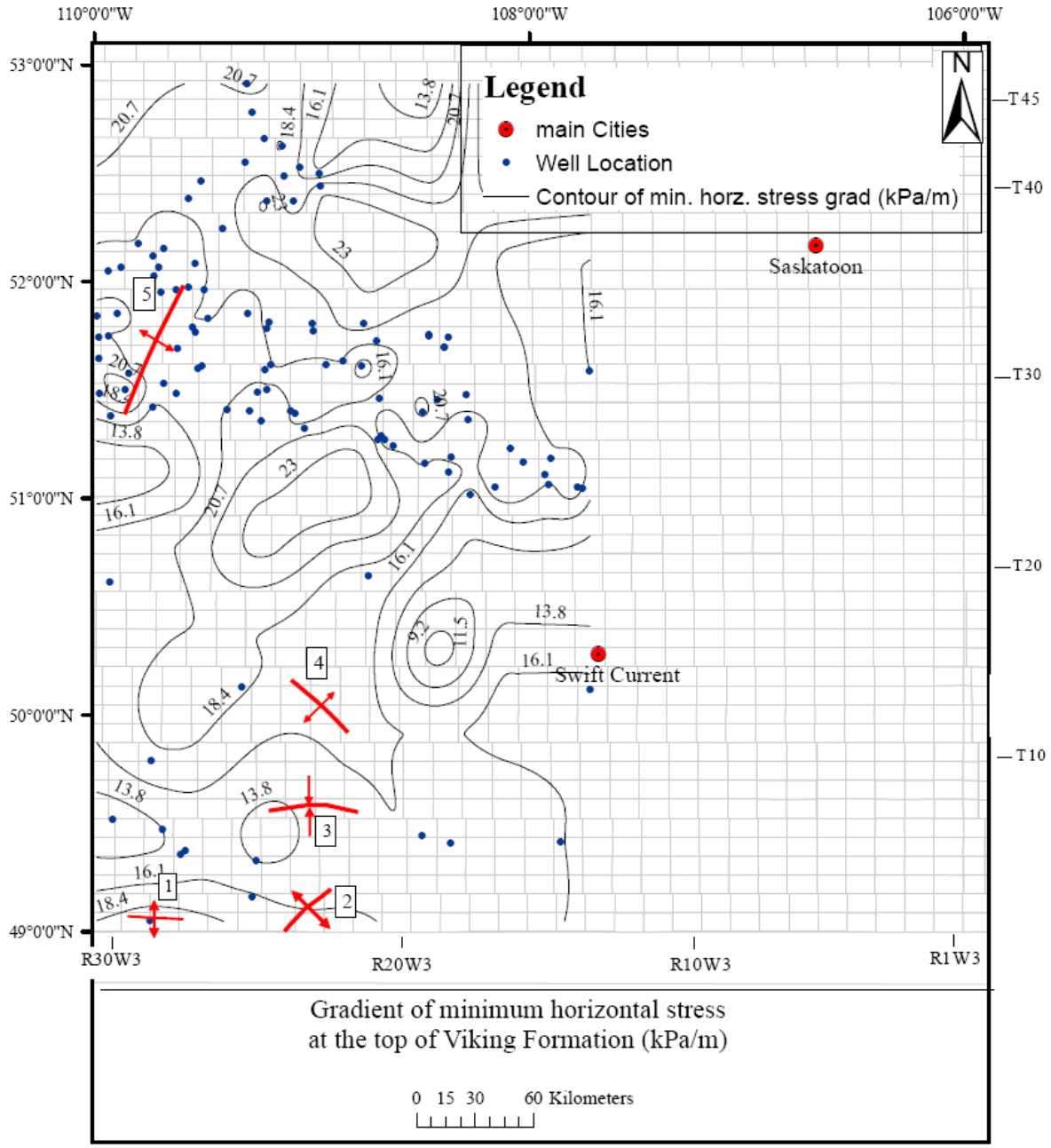

Figure 4.9: Minimum horizontal stress gradient in the Viking Formation, southwest Saskatchewan. Basement tectonic features (after Christopher et al., 1971) are: (1) Battle Creek Anticline, (2) Val-Marie Arch, (3) Ponteix Syncline, (4) Swift Current Arch, and (5) Sweetgrass-North Battle Arch.

predominantly sandy strata to a much thinner Viking sequence containing siltstone and mudstone elements. This lithology change might account, in part, for the relatively high stress gradients observed in the north-northwest part of the map area. More investigation of: (1) minimum horizontal stresses in the southern half of the map area; and (2) lithologies and rock mechanical properties throughout the map area (e.g., using mechanical properties measured on cores and calculated from full-wave sonic logs) would be required to assess this effect with greater confidence.

4.2.2 Minimum Horizontal Stress – Top of Mannville Group

Data were obtained for only 15 Mannville Group fracture stimulation treatments in the study area. In order to obtain more minimum horizontal stress estimates, this limited dataset was supplemented using stresses interpreted for the Viking Formation. This was accomplished using a simple gradient model, shown graphically in Figure 4.10, and implemented algebraically as follows:

$$\sigma_{H\min} = \left(\sigma_{H\min}\right)_{ref} + \left(\sigma_{H\min}\ grad\right)_{ref} \times \left\lfloor TVD - TVD_{ref} \right\rfloor / 1000 \qquad [4.2]$$

Where:

σ_{Hmin} = magnitude of minimum horizontal stress at the depth of interest (MPa)

$(\sigma_{Hmin})_{ref}$ = magnitude of minimum horizontal stress at a reference depth (MPa)

$(\sigma_{Hmin}\ grad)_{ref}$ = gradient of σ_{Hmin} at a reference depth (kPa/m)

TVD= vertical depth of point of interest (m)

TVD_{ref} = vertical depth of reference point (m)

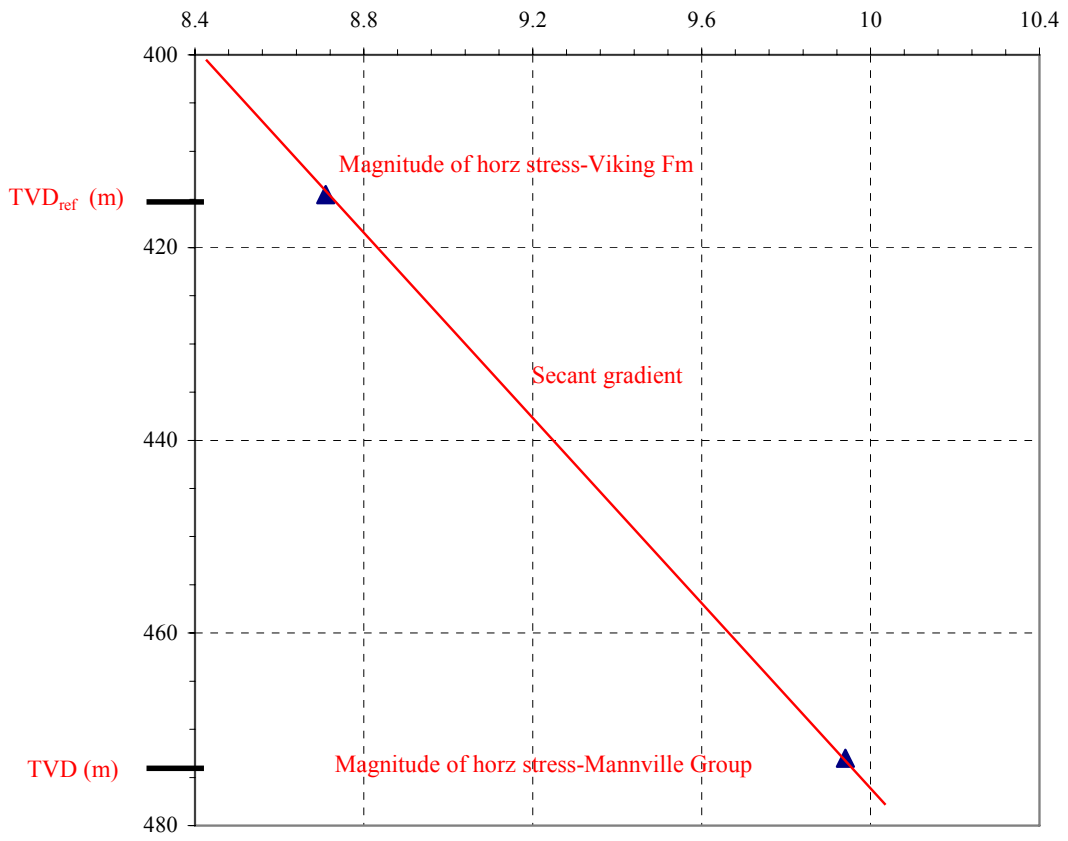

Figure 4.10: Graphical representation of the simple gradient model that was used to estimate the minimum horizontal stress magnitude at the top of the Mannville Group in the study area, using magnitudes interpreted for the Viking Formation.

The Viking Formation data points were used as the reference data in equation 4.2, in order to calculate σ_{Hmin} magnitudes at the top of the Mannville Group. [Note: This essentially amounts to linearly extrapolating σ_{Hmin} interepreted in the Viking upwards to the top of the Mannville, assuming that σ_{Hmin} is zero at ground surface.] Given that the Viking Formation and Mannville Group lie close together in the stratigraphic column (i.e., they are only separated by the Joli Fou shale - see Figure 2.3) and they are of the same general lithology (i.e., predominantly sandstone, throughout much of the study area), it seems reasonable to expect that this linear extrapolation method should provide results that are reasonably representative for the Mannville Group. Further investigation of fracture stimulation data in the Mannville would be required to confirm this, as well as more detailed analysis of the lithologies and mechanical properties of the Mannville and Viking strata – and their effects on horizontal stresses.

The resultant contour map of minimum horizontal stress magnitude is shown in Figure 4.11. The map shows a general trend of decreasing stress from south-southwest to north-northeast, from approximately 20 MPa to 10 MPa. This general trend is consistent with burial depth (see Figure 2.7) and vertical stress (see Figure 4.6).

Figure 4.12 shows the gradient of minimum horizontal stress at the top of Mannville Group. The gradient varies from 14 kPa/m to 22 kPa/m, which is less than vertical stress gradient at the top of this group. The figure also shows two anomalies areas where the minimum horizontal stress gradient is less than 17 kPa/m

4.2.3 Minimum Horizontal Stress – Belly River Formation

No fracture stimulation data were obtained for the Belly River Formation, or the underlying Lea Park Formation (which is predominantly a non-reservoir quality shale). Given that the Belly River Formation is stratigraphically separated from the Viking Formation by several shale formations of the Colorado Group, as well as the Milk River and Lea Park Formations (see Figure 2.3), it is more difficult to argue that a representative value can be obtained by linear extrapolation of the Viking dataset.

Table 4.1 lists the two results interpreted from fracture stimulation data - and one mini-frac test result provided by Husky Energy - which were close to the depth of the Belly River Formation. These data, which yielded somewhat high minimum horizontal stress gradients of 18.9, 20.0 and 22.5 kPa/m, were obtained in the Milk River Formation in the southwestern part of the study area. The fact that the latter formation is more shaley in character than the Belly River may account, in part, for these relatively high values (which are similar to vertical stress gradients interpreted at the top of the Lea Park Formation). However, lithology effects aside, it has been noted elsewhere in the Western Canada Sedimentary Basin that minimum horizontal stresses become larger than vertical stress magnitude at depths less than a few hundred metres (Woodland and Bell, 1989; Bell et al., 1994). This is likely a result of elevated horizontal stresses that existed in these rocks as a result of significantly elevated overburden loads experienced in the past (e.g., before removal of younger rock strata by erosion, and during periods of glaciation), which have not yet dissipated. Based on this limited amount of information on minimum horizontal stress magnitudes, as well as the vertical stress data presented in section 4.1.2,

it is suggested that σ_{Hmin} may be close to or greater than σ_V in parts of the study area – particularly where Belly River depths become least (i.e., in the north and northeast).

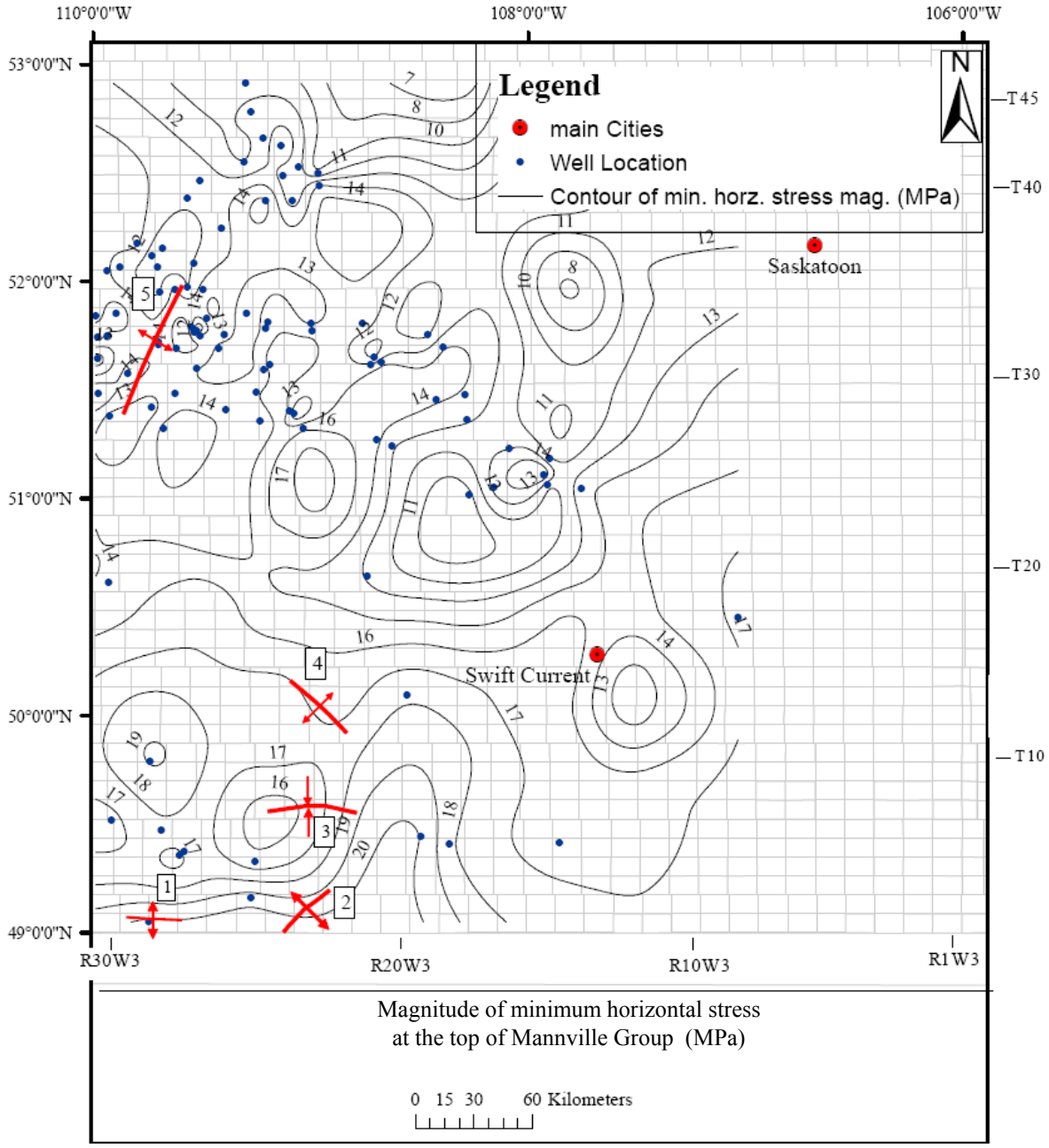

Figure 4.11: Minimum horizontal stress magnitude at the top of the Mannville Group, southwest Saskatchewan. Basement tectonic features (after Christopher et al., 1971) are: (1) Battle Creek Anticline, (2) Val-Marie Arch, (3) Ponteix Syncline, (4) Swift Current Arch, and (5) Sweetgrass-North Battle Arch.

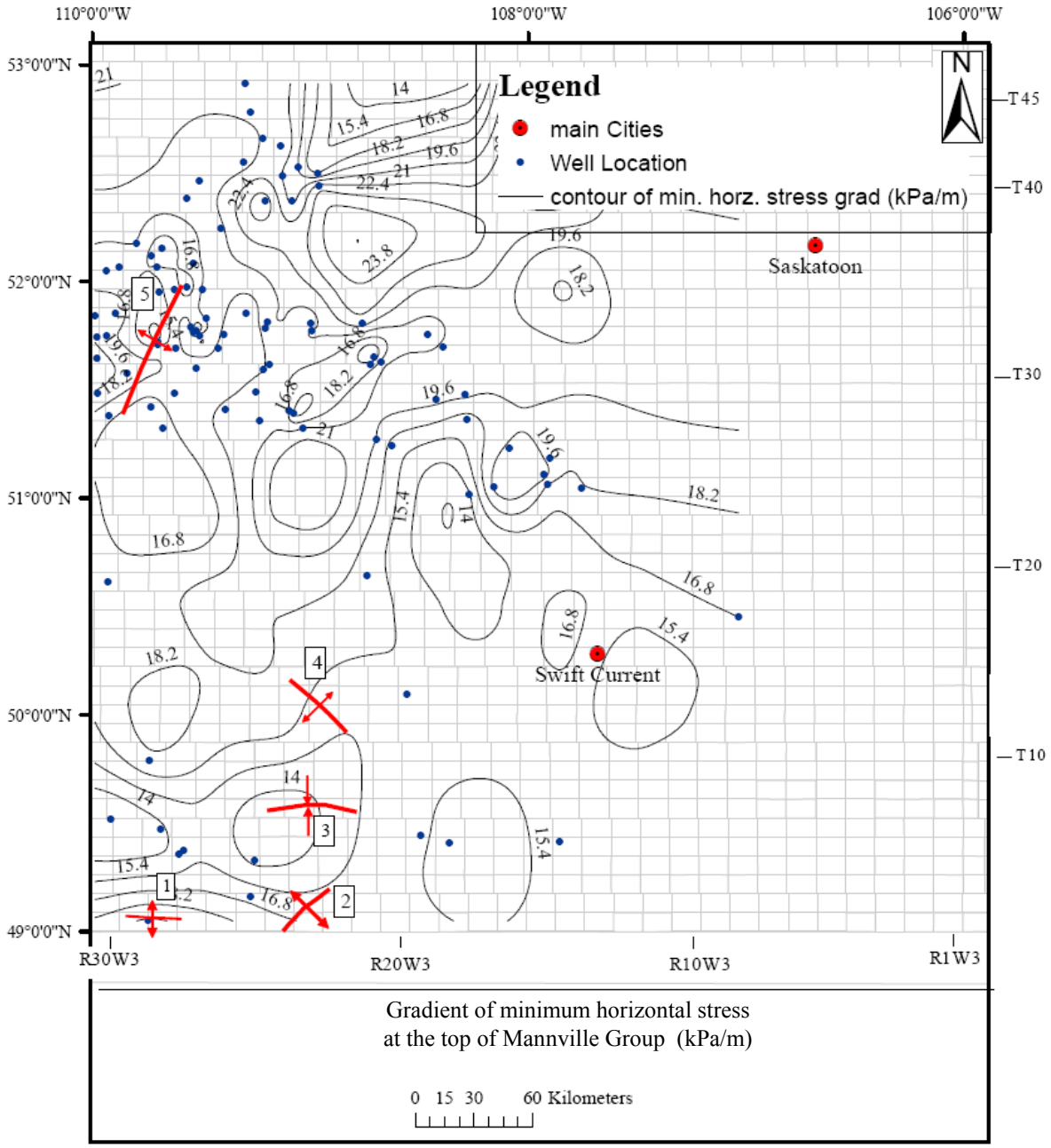

Figure 4.12: Minimum horizontal stress gradient in the top of Mannville Group, southwest Saskatchewan. Basement tectonic features (after Christopher et al., 1971) are: (1) Battle Creek Anticline, (2) Val-Marie Arch, (3) Ponteix Syncline, (4) Swift Current Arch, and (5) Sweetgrass-North Battle Arch.

Table 4.1: Minimum horizontal stresses interpreted from fracture stimulation treatments and a mini-frac test in the Milk River Formation.

UWI	Top of Treatment Zone (m)	σ_v Magnitude (MPa)	σ_v Gradient (kPa/m)	σ_{Hmin} Magnitude (MPa)	Source	σ_{Hmin} Gradient (kPa/m)
06-32-002-28W3	497	11	22.13	9.41	0.9 ×ISIP	18.93
08-04-006-19W3	750	15.3	20.40	16.9	0.9 ×ISIP	22.53
16-30-022-17W3	330	6.97	21.12	6.75	Mini-Frac	20.45

4.2.4 Pore Pressure Effects

The minimum horizontal stress results obtained in this project very clearly identify the influence of burial depth on stress magnitudes, and suggest a secondary influence of lithology. It is also known that pore pressures affect horizontal stresses. As such, an extensive compilation of pore pressures interpreted from drill-stem tests in the Mannville Group (Christopher, 2003) was used to assess the relationship between pore pressures and horizontal stresses in the study area.

Figure 4.13 is a contour map of pore pressure at the top of the Mannville Group, converted from the data of Christopher (2003), who presented these data in the form of potentiometric surface elevations. There is a general trend of pore pressure decrease from about 12 MPa in the southwest to about 3 MPa in north-northeast. This general trend is consistent with burial depth (see Figure 2.7). Figure 4.14 shows the pore pressure gradient (i.e., pore pressure divided by vertical depth) at the top of Mannville Group. Compared to a normal hydrostatic gradient (typically 10 to 11 kPa/m), the northern and south-eastern parts of the study area show gradients that are slightly below normal (i.e., 6 to 9 kPa/m). These sub-normal gradients are consistent with Christopher's (2003) interpretation that hydraulic communication between the Mannville Group and underlying Mississippian and Devonian strata occurs in parts of the study area through faults and fracture zones. Two areas of relatively normal pressure gradients are present in the study area. One is located in the southwest corner of the study area, and the other is centered roughly 100 km northeast of Swift Current.

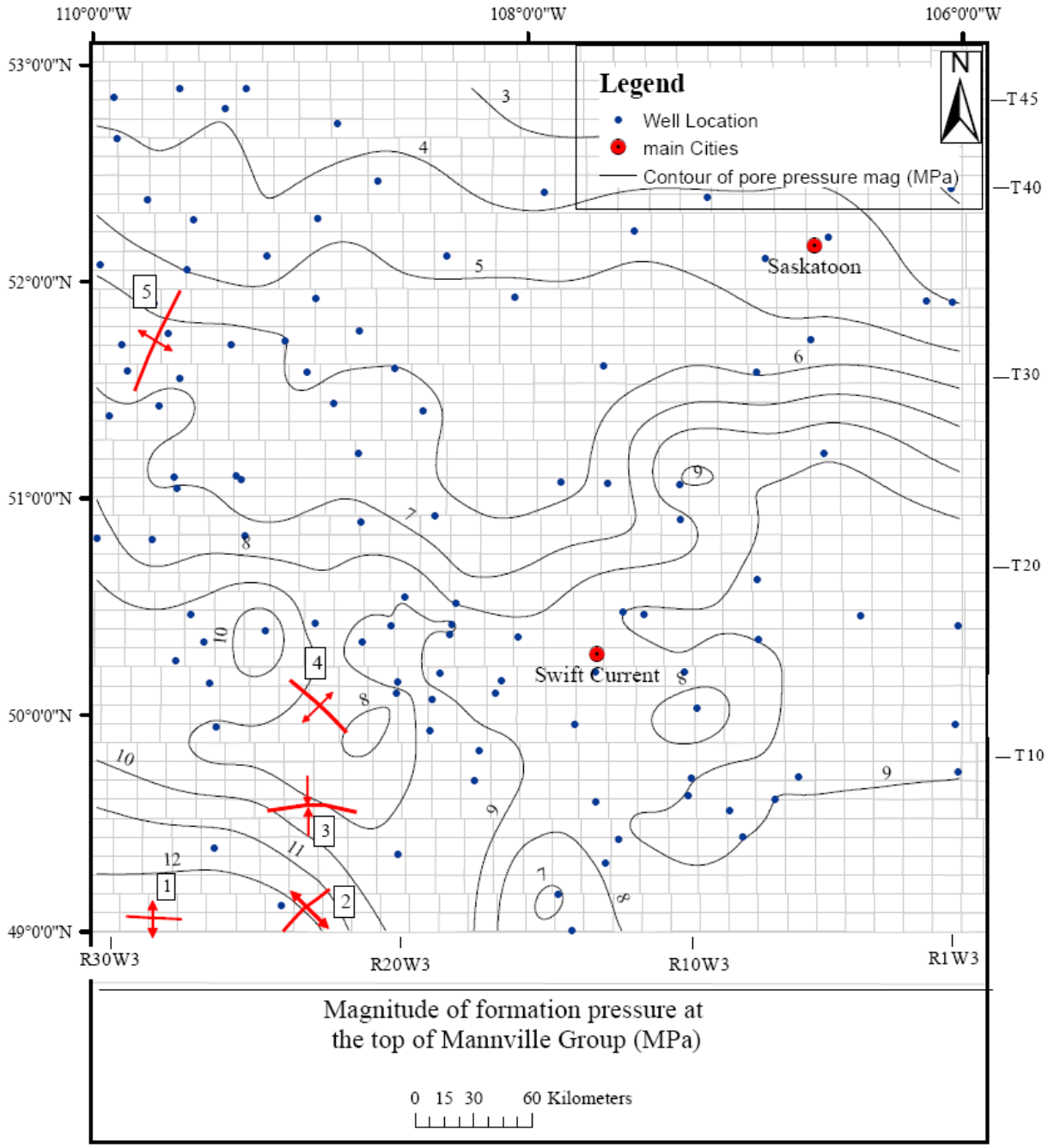

Figure 4.13: Pore pressure at the top of the Mannville Group in southwest Saskatchewan (converted from potentiometric surface data presented by Christopher, 2003). Basement tectonic features (after Christopher et al., 1971) are: (1) Battle Creek Anticline, (2) Val-Marie Arch, (3) Ponteix Syncline, (4) Swift Current Arch, and (5) Sweetgrass-North Battle Arch.

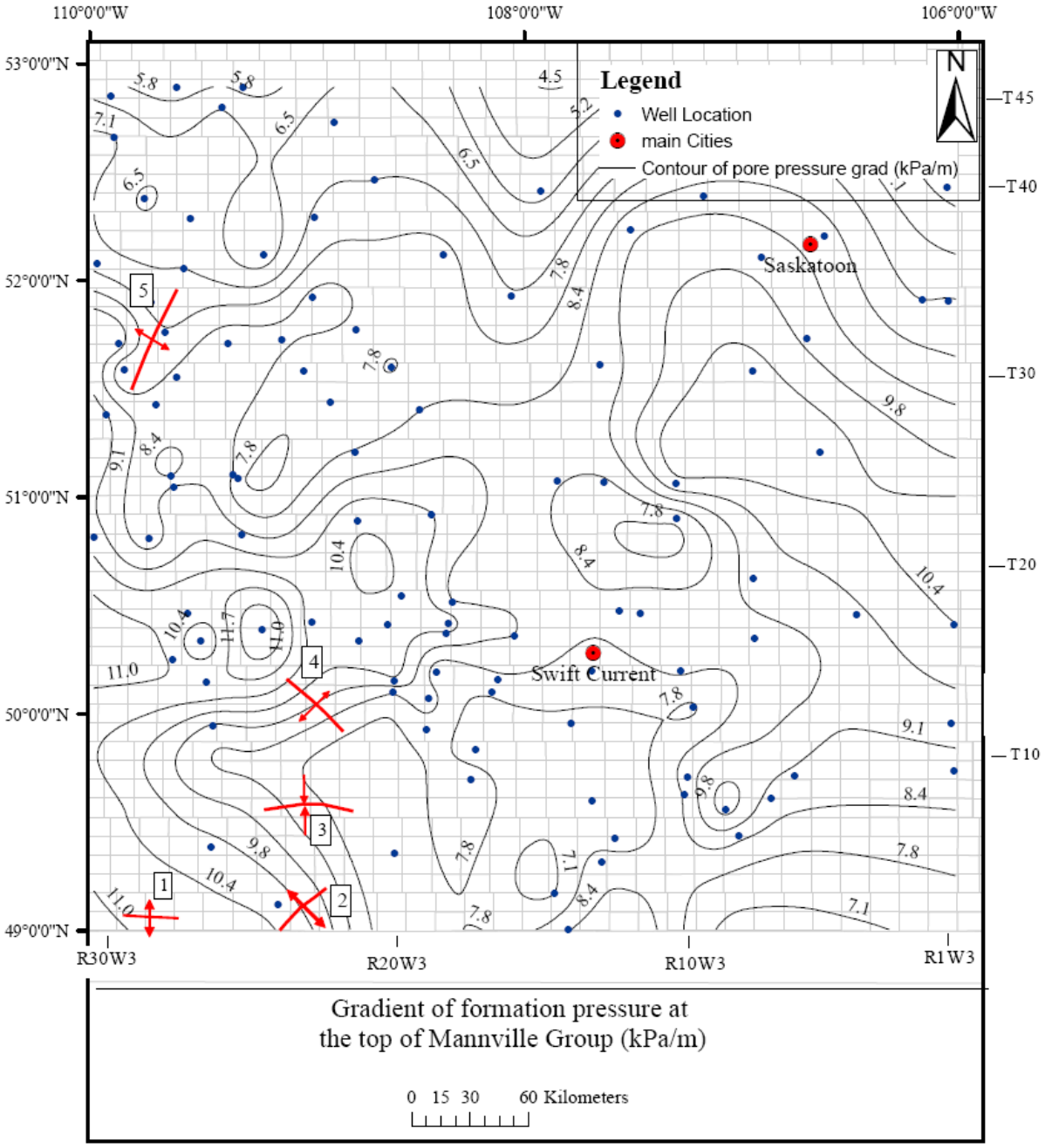

Figure 4.14: Pore pressure gradient at the top of the Mannville Group in southwest Saskatchewan (converted from potentiometric surface data presented by Christopher, 2003). Basement tectonic features (after Christopher et al., 1971) are: (1) Battle Creek Anticline, (2) Val-Marie Arch, (3) Ponteix Syncline, (4) Swift Current Arch, and (5) Sweetgrass-North Battle Arch.

Figure 4.15 shows a plot of Mannville Group pore pressures and minimum horizontal stress magnitudes against depth. Also shown on the plot, to provide a basis for comparison, are vertical stress magnitudes and gradient reference lines of 10, 13, 18 and 23 kPa/m. This plot suggests that, at depths greater than 1000 m, relatively low pore pressures correspond to relatively low horizontal stresses. This relationship (low pressure – low horizontal stress) is expected theoretically and has been observed in other sedimentary basins (e.g., Addis, 1997).

4.2.5 Measurement in Coal

Another point of interest illustrated in Figure 4.15 is the relatively high minimum horizontal stress magnitude interpreted for the only fracture stimulation treatment that was run in a coal seam. In fact, the minimum horizontal stress magnitude is nearly as high as the vertical stress magnitude in this case. Without additional data for coals, it is not possible to assess if this data point is representative or anomalous. As noted in section 4.2.1, shales and shaley rocks generally have higher horizontal stresses that sandstones. More explicitly, theoretical expressions for horizontal stresses indicate that rocks with higher values of Poisson's ratio will have higher horizontal stresses (e.g., Warpinski et al., 1989; also see equation 3.3). Shales generally have relatively high Poisson's ratios compared to sandstones, hence the elevated stresses observed in the former. Given that coals also tend to have relatively high Poisson's ratios, it seems reasonable to expect that they will often have horizontal stresses higher than a sandstone would under similar conditions. This provides some support to the suggestion that the lone coal measurement analyzed in this project might be representative. However, additional stress measurements in coals in the study area will be required to confirm this, as well as an investigation of coal mechanical properties, such as Poisson's ratio.

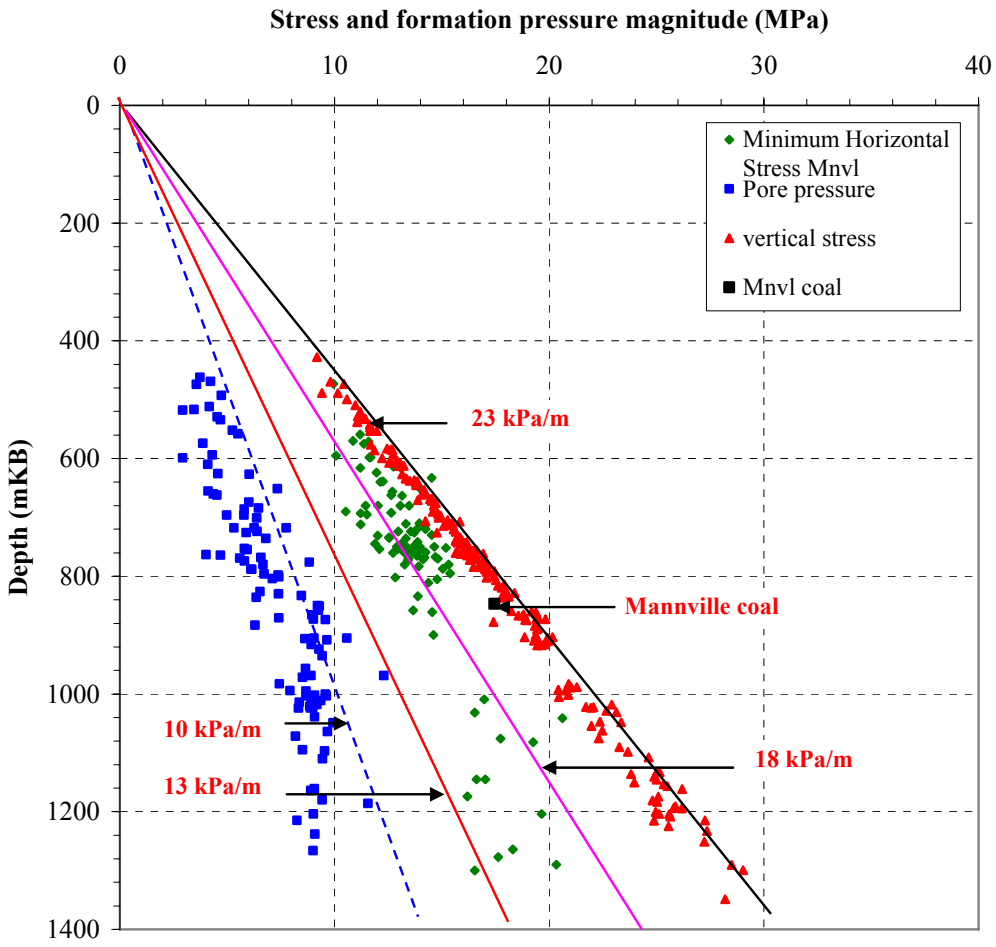

Figure 4.15: Relationship between pore pressure, minimum horizontal stress and vertical stress in the Mannville Group, southwest Saskatchewan.

4.3 Maximum Horizontal Stress Magnitude

No suitable data for estimating the value of the maximum horizontal stress (σ_{Hmax}) were found within the study area. The only remotely relevant σ_{Hmax} value reported in the literature (Bell et al., 1994) was interpreted from two micro-frac tests conducted in the Deadwood Formation at depths of 2168 m and 2213 m in Regina (well 3-8-17-9W2). For these two tests, σ_{Hmax} values were, on average, 1.33 times larger than σ_{Hmin} and virtually equal to (i.e., 0.99 times) σ_V. These data are consistent with the stress regime map presented in Figure 2.2. Given that the study area is slightly closer to the Rocky

Mountains than the Regina test well, it is suggested that a rough estimate for σ_{Hmax} is in the range of 1.3 to 1.4 times σ_{Hmin}, which should generally yield a number equal to or slightly greater than the vertical stress magnitude.

It is unclear how the results obtained in this research relate to stress regime information interpreted by Gendzwill and Stauffer (2006). Based on seismic data obtained in the vicinity of the potash mine near Colonsay, Saskatchewan (which is east of the study area), they reported numerous normal faults at shallow depths (< 400 m) which they attribute to Tertiary through Quaternary extensional tectonics. Their results suggest a normal fault stress regime; i.e., a vertical stress magnitude that is greater than the maximum horizontal stress.

4.4 Horizontal Stress Orientations

Six measurements of horizontal stress orientation in the study area were previously reported by Bell et al. (1994). During this project, seven additional measurements were interpreted from Formation MicroImager (FMI) logs retrieved from the well-file library of Saskatchewan Industry and Resources in Regina. Two additional stress orientations interpreted by Husky Energy were also provided to the investigator. EnCana Corporation provided access to a number of their FMI logs from the study area, but no borehole breakouts were found in these logs.

All thirteen horizontal stress orientations are listed in Table 4.2. Figure 4.16 shows well locations that have data that were used for interpretation horizontal stress orientation. Figure 4.17 shows a roseplot for the seven wells analyzed during this project. These data have an average minimum horizontal stress orientation of 140º, with a circular standard deviation of 13º. Figure 4.18 shows a roseplot for all thirteen wells available in the study area. This composite dataset has an average minimum horizontal stress orientation of 137º, with a circular standard deviation of 12º.

Figure 4.19 shows the horizontal stress orientations on a map of southwest Saskatchewan. The general trend of σ_{Hmin} in the study area is northwest-southeast, which (as expected) is parallel to the trend of the Rocky Mountains. There is a notable counter-clockwise inflection in this trend on the vicinity of the Swift Current arch. It is also notable that three of the new data points are rotated 20° to 30° counter-clockwise from

Table 4.2: Orientation of horizontal stresses in southwest Saskatchewan.

UWI	Longitude	Latitude	σ_{Hmin} azimuth	σ_{Hmax} azimuth	Source
06-28-04-27W3	49.326	-109.582	100.1	10.1	Bell 1994
11-05-05-27W3	49.359	-109.605	127.4	37.4	Bell 1994
16-07-09-18W3	49.726	-108.422	142.5	52.5	Bell 1994
06-01-021-19W3	50.815	-108.706	124	34	Husky Energy
16-30-022-17W3	50.869	-108.228	170	80	Husky Energy
10-28-28-24W3	51.426°	-109.316	142	52	FMI log
09-06-35-26W3	51.979	-109.695	150.5	60.5	Bell 1994
02-16-36-28W3	52.088	-109.939	143.7	53.7	FMI log
11-36-38-27W3	52.314	-109.731	136.8	46.8	Bell 1994
12-05-39-26W3	52.328	-109.718	136.8	46.8	Bell 1994
09-29-42-25W3	52.648	-109.556	117.7	27.7	FMI log
06-07-43-24W3	52.668	-109.476	162.9	72.9	FMI log
21-10-52-23W3	53.471	-109.305	120.7	30.7	FMI log

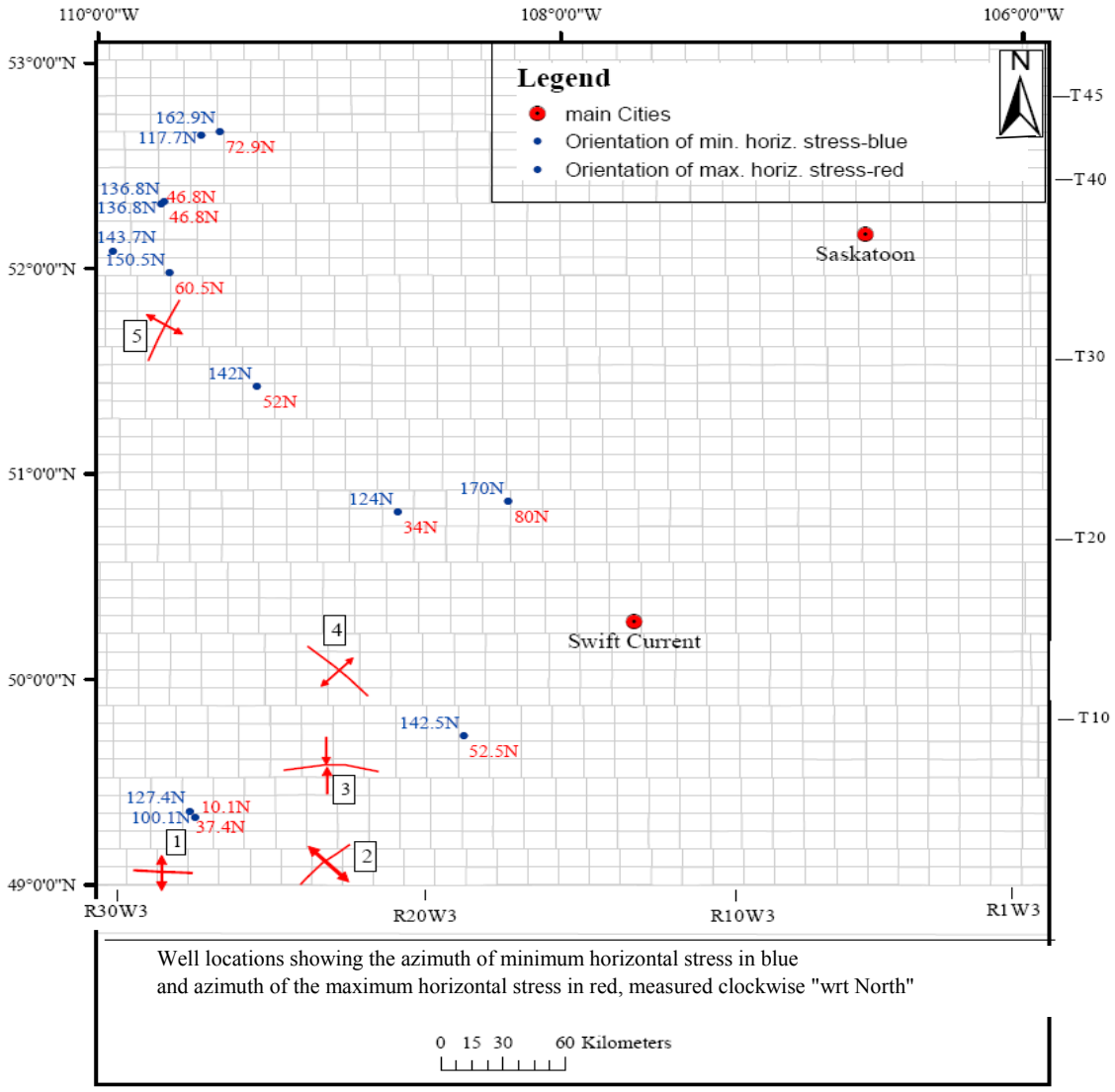

Figure 4.16: Well locations having data that were used for interpretation of horizontal stress orientations. Basement tectonic features (after Christopher et al., 1971) are: (1) Battle Creek Anticline, (2) Val-Marie Arch, (3) Ponteix Syncline, (4) Swift Current Arch, and (5) Sweetgrass-North Battle Arch.

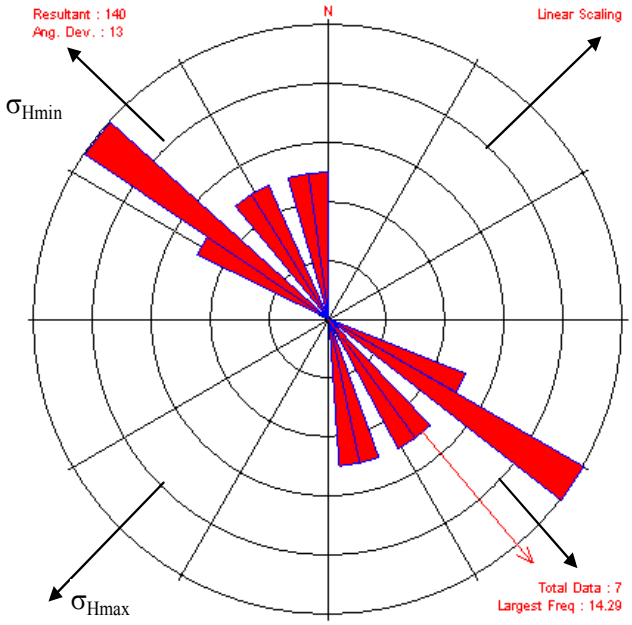

Figure 4.17: Roseplot of borehole breakout data for the seven wells analyzed in this project.

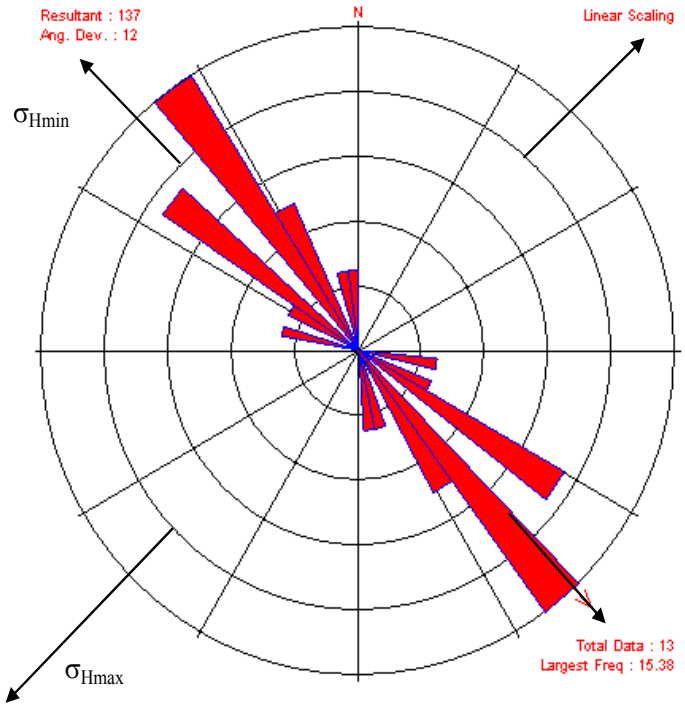

Figure 4.18: Roseplot of borehole breakout data from all wells in the study area, including six wells reported by Bell et al. (1994).

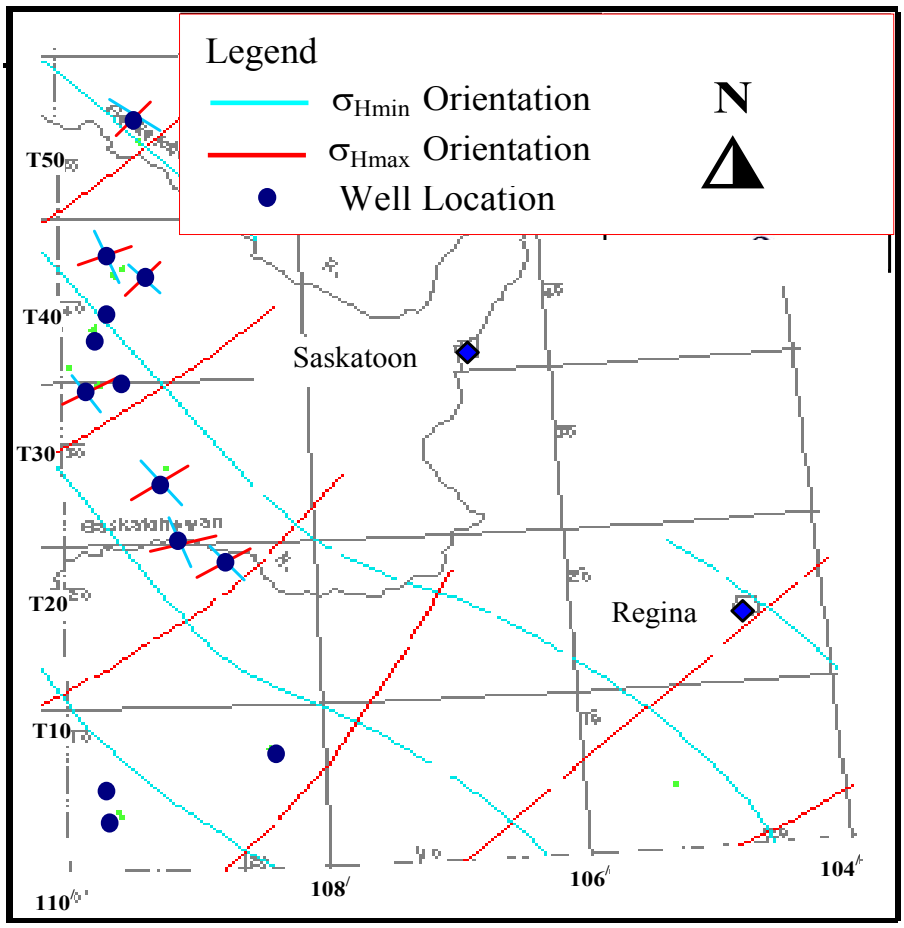

Figure 4.19: Horizontal stress trajectories in southwest Saskatchewan determined from borehole breakouts. The blue lines represent the orientation of the minimum horizontal stress. Continuous trajectory lines were taken from Bell et al. (1994). Short trajectory lines show local orientations interpreted in this project.

the regional trend interpreted from Bell et al.'s (1994) data, and one of the new data points is rotated by roughly 50°. The latter anomalous data point is considered dubious, but the repeatability of the former minor anomalies suggests that they could be real.

Another method used to constrain the orientation of horizontal stresses is the analysis of natural fractures. Stauffer and Gendzwill (1987) studied fracture systems in late Cretaceous to late Pleistocene strata in Saskatchewan (Figure 4.20). They found a consistent pattern of orthogonal fractures trending northeast-southwest and northwest-southeast. They attributed the origin of the fractures to uplift and tectonically derived stresses. This trend is in general agreement with the horizontal stress orientations interpreted in the Western Canadian Sedimentary Basin.

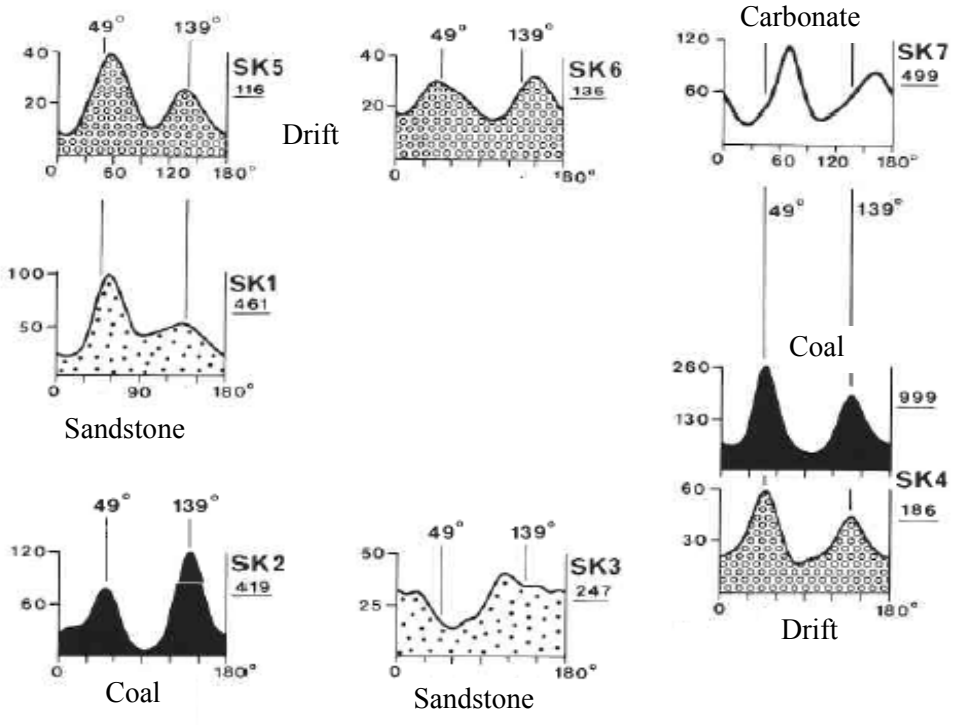

Figure 4.20: Frequency distribution diagrams of natural fracture strike directions in late Cretaceous to late Pleistocene strata in Saskatchewan (after Stauffer and Gendzwill, 1987)

5 PRACTICAL IMPLICATIONS OF STRESS REGIME ON COALBED METHANE DEVELOPMENT

5.1 Coal Permeability

In-situ stress has been shown to be related to coal bed permeability in several basins in Australia and in North America. Measurements of in-situ stress, pore pressure and permeability have been made in coal seams in numerous wells in the north and south Bowen basins, and the Sydney Basin and in the Glouscester basin in Australia. Figure 5.1 shows a compilation of effective stress and permeability measurements made in coal seams in four basins in Australia (Enever et al., 1998).

In this study the magnitudes of minimum horizontal stresses at the top of Mannville Group were converted to effective stresses by subtracting relevant pore pressure, using the following relationship:

$$\sigma_{H\min}' = \sigma_{H\min} - P_o \qquad [5.1]$$

Where:

σ_{Hmin}' = effective minimum horizontal stress

σ_{Hmin} = minimum in-situ stress

P_o = pore pressure

Figure 5.2 shows a depth profile of effective minimum horizontal stress magnitudes at the top of Mannville Group of southwest Saskatchewan. These data points generally fall between gradient lines of 6 and 14 kPa/m, a gradient line close to 10 kPa/m representing average conditions.

Figure 5.3 shows a modified version of the western Canadian coal permeability data presented in Figure 2.12. In the latter figure, coal permeabilities were plotted against depth, rather than minimum effective in-situ stress. For use in this project, the depth axis was converted to effective stress by multiplying depth by an average effective stress

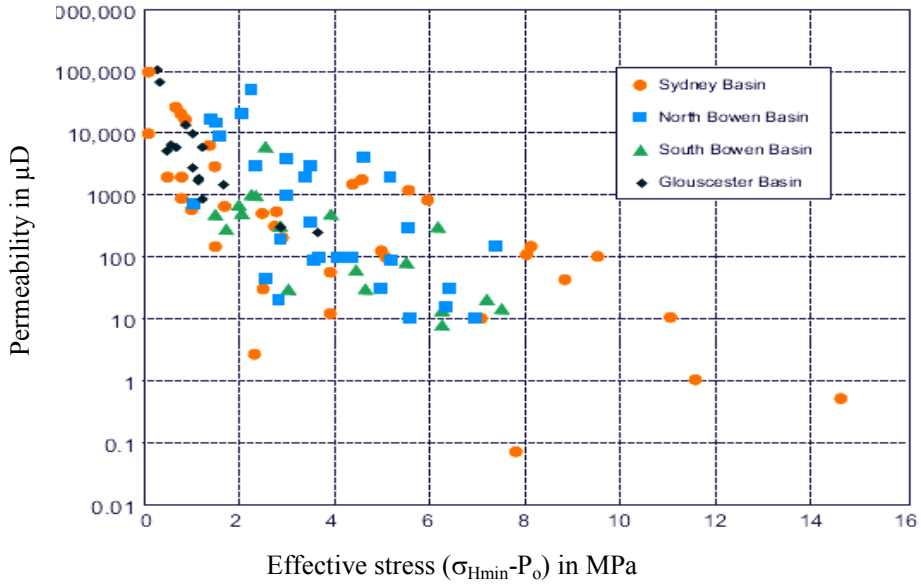

Figure 5.1: Combined effective stress and permeability measurements made in coal seams in four basins in Australia (from Enever et al., 1998).

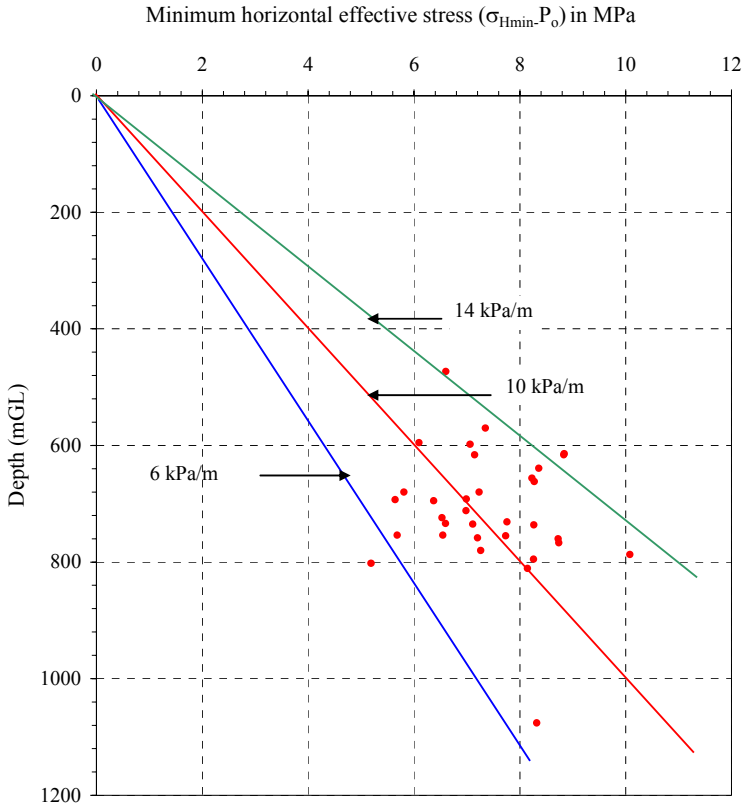

Figure 5.2: Value of the effective minimum horizontal stress (σ_{Hmin}-P_o) at the top of Mannville Group of southwest Saskatchewan plotted against depth.

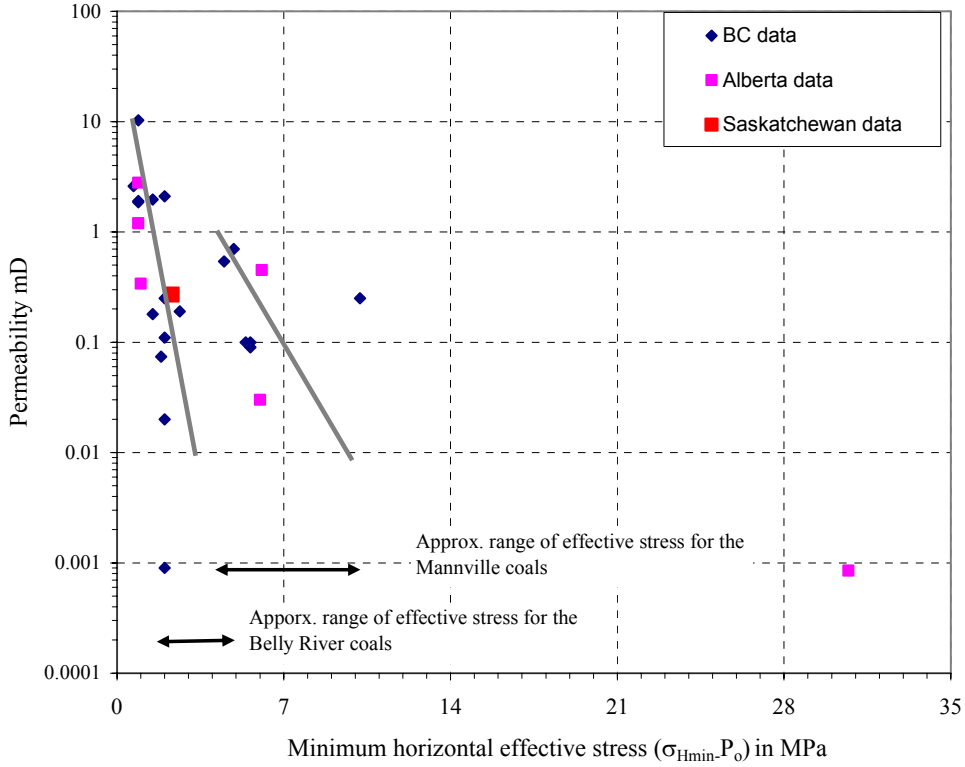

Figure 5.3: Permeability measurements made in coal seams in BC, Alberta and Saskatchewan, plotted against estimated effective horizontal stress (BC and Alberta data from Gentzis, 2004; Saskatchewan data obtained from SIR).

gradient of 10 kPa/m, based on the assumption that the conditions interpreted above for Mannville coals are reasonably representative of conditions for the other coals included in Figure 5.3.

Although there is considerable scatter in the Canadian data shown in Figure 5.3, the plot does suggest the expected general trend of decreasing permeability with increasing effective stress. Based on the stress and pore pressure data presented in this thesis, it is anticipated that minimum effective stresses in the Belly River coals will typically be a few MPa, and in the 5 to 10 MPa range for the Mannville coals. A very rough estimate of permeabilities based on the data in Figure 5.3 suggests that permeabilities could be in the 0.01 to 10 millidarcy range for the former, and 0.01 to 1 millidarcy range for the latter. Clearly, more well testing and core testing of

permeabilities in Saskatchewan's Belly River and Mannville coals is needed in order to establish both absolute values of permeability, as well as the stress-dependence of permeability.

The face cleats of coal are commonly oriented parallel to σ_{Hmax} (Campell, 1979, Bell and Bachu, 2003,). Given the horizontal stress orientations presented in this thesis, it seems reasonable to expect that the orientation of face cleats in the study area can be inferred from Figure 4.19. From this figure, it seems reasonable to expect that coal permeabilities in the study area will be greatest in a roughly southwest-northeast direction. This is partially consistent with results presented by Stauffer and Gendzwill (1987), who interpreted a northwest-southeast orientation (striking 139° clockwise from north) for a prominent fracture set in coals in southern Saskatchewan. However, Stauffer and Gendzwill (1987) also interpreted a second, more prominent fracture set in these coals that was oriented northeast-southwest (striking 49° clockwise from north) (Figure 4.20). As such, it is possible that coal permeabilities are actually greatest in the northwest-southeast direction. In spite of these contradictory results, it seems reasonable to expect that coal permeabilities should be lowest in the north-south or east-west directions.

5.2 Hydraulic Fracturing

There is a high probability that hydraulic fracture stimulation will be required to achieve economic production rates in the Belly River and Mannville coals. The minimum horizontal stress magnitudes presented in this thesis can be used to estimate the bottomhole pressure that will have to be exceeded in order to create and propagate hydraulic fractures in these coals. In cases where minimum horizontal stresses were not interpreted (e.g., for the Belly River Formation throughout the entire study area; for the Mannville Group group outside of the area that was successfully mapped), the vertical stress magnitude may be used as an upper bound estimate of σ_{Hmin}. In fact, given the inferred possibility that σ_{Hmin} magnitudes in the coals will be higher than the values interpreted for sandstones in this project (see section 4.2.5), it may be appropriate to design fracture treatments on the assumption that the σ_V magnitude is representative of the smallest principal stress. From an operational perspective, this should ensure that

fracture stimulation jobs are designed with adequate pumping capacity to create hydraulic fractures. However, it is currently unclear what the orientation of these fractures may be. Hydraulic fractures induced in coals where σ_{Hmin} is the minimum in-situ stress will be oriented vertically, and propagate in the direction of the maximum horizontal stress (as shown in Figure 4.19). Hydraulic fractures induced in coals where σ_V is the minimum in-situ stress will be oriented horizontally.

5.3 Borehole Stability

5.3.1 Modelling Approach

Borehole stability modelling was conducted using Phase2 (Rocscience, 2006), a software application which uses the finite element method to predict induced stresses and rock yielding around underground openings (e.g., tunnels and boreholes) in elastic-brittle-plastic materials. A schematic representation of the type of output generated using such a model is shown in Figure 5.4. For a given bottomhole pressure (i.e., mud density), such a model predicts the cross-sectional area of rock that will yield (i.e., become damaged and weakened). This yielded zone area is commonly normalized by dividing by the cross-sectional area of the drill bit. This parameter, named normalized yielded zone area (NYZA), is explicitly defined in Figure 5.4.

The analyses conducted in this project must be considered as preliminary estimates of borehole stability. Although key parameters such as in-situ stresses and pore pressures have been interpreted and/or compiled with reasonable confidence in this project, there are – to the author's knowledge - no public-domain mechanical properties available for Mannville or Belly River coals in the Western Canada Sedimentary Basin. In order to provide some basis for estimating rock mechanical properties, a literature review was conducted. The results are reported in Appendix C. More specific comments on rock mechanical properties actually used for this project are given in the following section.

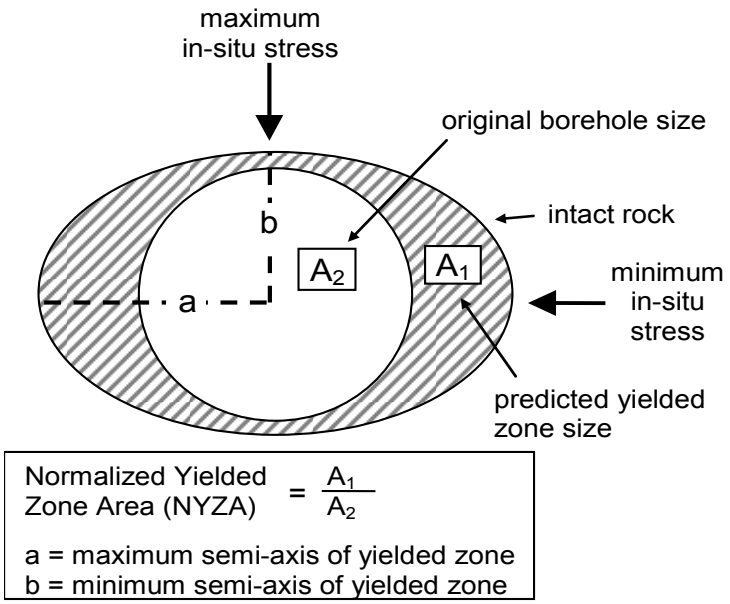

Figure 5.4 Cross-sectional view of a yielded borehole (McLellan and Hawkes, 2001).

5.3.2 Mannville Coals

Some of the Mannville coal seams are several metres thick and, as a consequence, they may be developed using horizontal wells. This development strategy has proven effective for Mannville coals in the Alberta Basin. The main objective of the borehole stability analyses conducted in this project was to investigate the minimum borehole pressure (i.e., drilling fluid density) required to prevent severe borehole collapse while drilling horizontal wells in Mannville coals. It is especially crucial to answer this question for horizontal wells in weak rocks such as coals, in which instability problems may easily become unmanageable if bottomhole pressures are too low.

Representative rock mechanical properties were obtained by back-analyzing borehole enlargement in Mannville coals, as measured by caliper logs in well 3-14-28-27W3 (which are shown in Figure 5.5). Conditions at this well were considered to be representative for much of the deeper Mannville coal deposits that are likely to be developed in the study area, for which borehole instability risks are greatest. Rock mechanical properties were adjusted until model-predicted yielded zone size matched the enlarged hole size measured with calipers. The values for these properties were

constrained using mechanical properties compiled for various coals from various countries, including Canada (see Appendix C; and Hawkes, 2003). As such, the values obtained from back-analysis are realistic. However, it is of utmost importance to measure these mechanical properties on core samples, and conducting refined borehole stability analyses, before making final mud density selections for horizontal wells in Mannville coals.

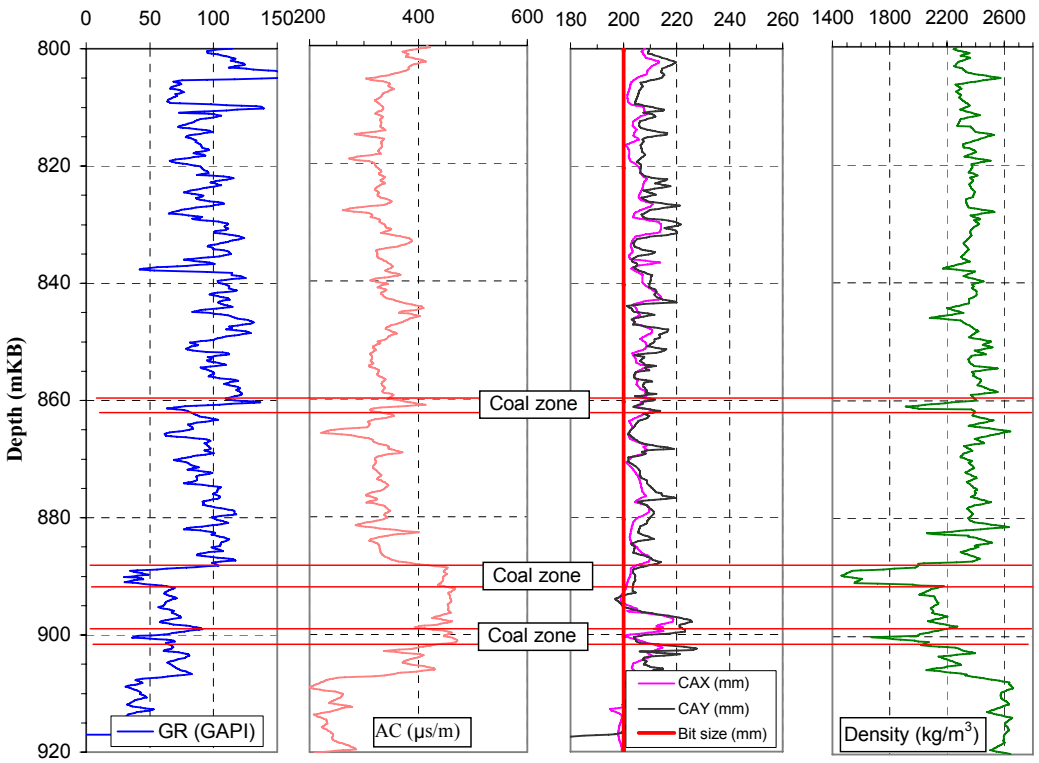

Figure 5.5: Gamma ray, sonic transit time, dual-arm caliper (CAX, CAY), and density log reading through Mannville coal and adjacent strata for FCE MARENGO S A3-14-28-27.

The input parameters used are summarized in Table 5.1. A horizontal well trajectory parallel to the minimum horizontal stress was selected as the base case for analysis. As discussed in section 5.2, this orientation is likely to provide the best production rates (because permeability should be greatest in a plane normal to such a borehole, especially if cleats are present), and it represents a conservative case in terms of stability (i.e., the maximum extent of rock yielding should occur for horizontal wells drilled in this orientation). The extent of borehole yielding predicted for the base case is shown in Figure 5.6.

Table 5.1: Input parameters for borehole stability modelling- Mannville coal.

Parameter	Value
Depth	900 m
Vertical stress gradient	21.5 kPa/m
Maximum horizontal stress gradient	23.8 kPa/m
Minimum horizontal stress gradient	18.2 kPa/m
Minimum horizontal stress orientation	330º
Horizontal well azimuth	330º
Formation pressure gradient	9.4 kPa/m
Drilling mud density	1000 kg/m^3
Mud pressure leakoff into formation	None
Rock Mechanical properties:	
Unconfined compressive strength	10.8 MPa
m_{peak}	4
s_{peak}	1
Young's modulus	1.7 GPa
Poisson's ratio	0.35
$m_{residual}$	1
$s_{residual}$	0.5

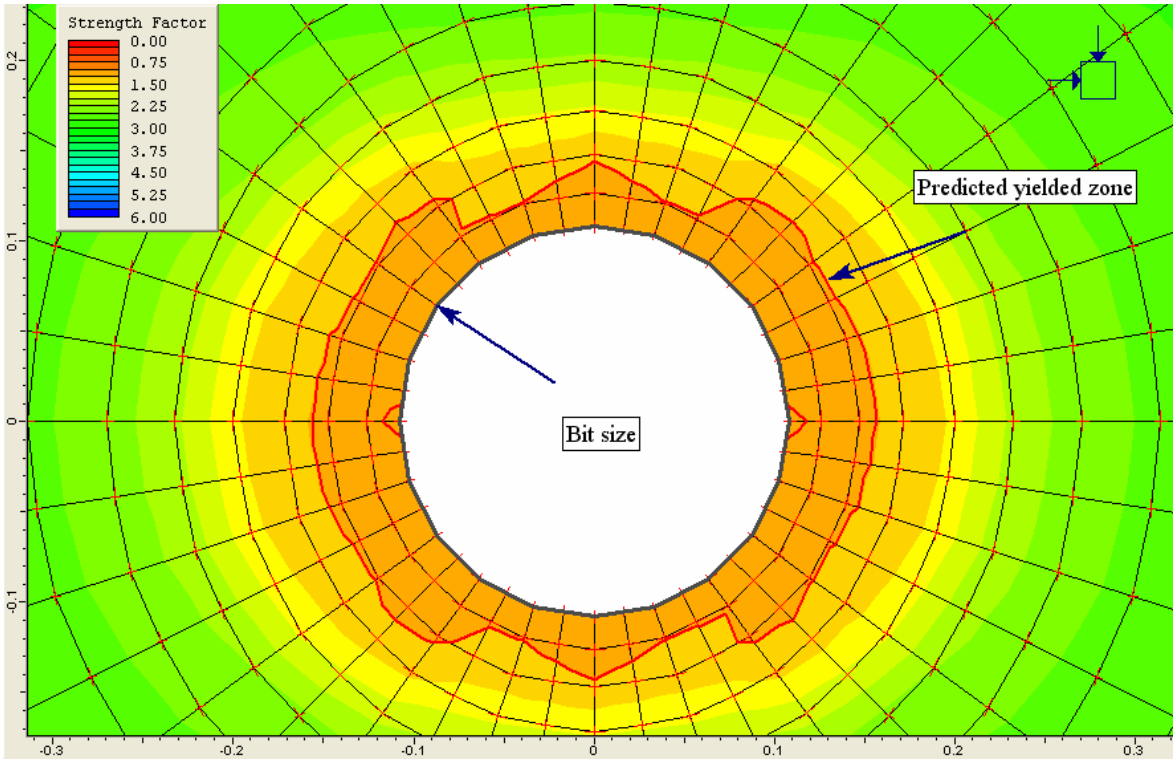

Figure 5.6: Cross-sectional view of rock yielding around a horizontal well for base-case conditions in the Mannville coal, predicted using Phase2. The contours show strength factor, which is the ratio of shear strength to applied shear stress.

Given the uncertainty in rock mechanical properties, a sensitivity analysis was run using unconfined compressive strengths 10% greater than and less than the base case value. The results, shown in Figure 5.7, indicate that NYZA values are less than 0.7 for all cases considered, even for unweighted mud systems (~1000 kg/m^3). Similarly, to confirm that the base case well trajectory is actually the most conservative case (i.e., the most yielding occurs), a sensitivity analysis to trajectory was run. The results, shown in Figure 5.8, confirm expectations.

As a rough guideline, NYZA values greater than 1 are often regarded as indicators of unacceptable borehole instability (e.g., McLellan and Hawkes, 2001). Given that the NYZA's predicted in this study were all less than 1, this suggests that horizontal drilling of the Mannville coals should be feasible. In fact, the results suggest the possibility that underbalanced drilling might even be feasible. However, this possibility was not explored. Analyses of underbalanced should only be considered once better values have been obtained for rock mechanical properties. Similarly, borehole stability analyses for

well completions design should only be conducted after new data are available. Conservatively, until further analyses have proven otherwise, it should be assumed that slotted liners or screens would be required to prevent catastrophic hole collapse in horizontal wells in Saskatchewan's Mannville coals during production. Based on public data from the Corbett Field in Alberta, most horizontal wells in Mannville coals have been completed with slotted liners, although a few have been completed barefoot (i.e., linerless) – suggesting that this cheaper completion method merits some consideration in Saskatchewan.

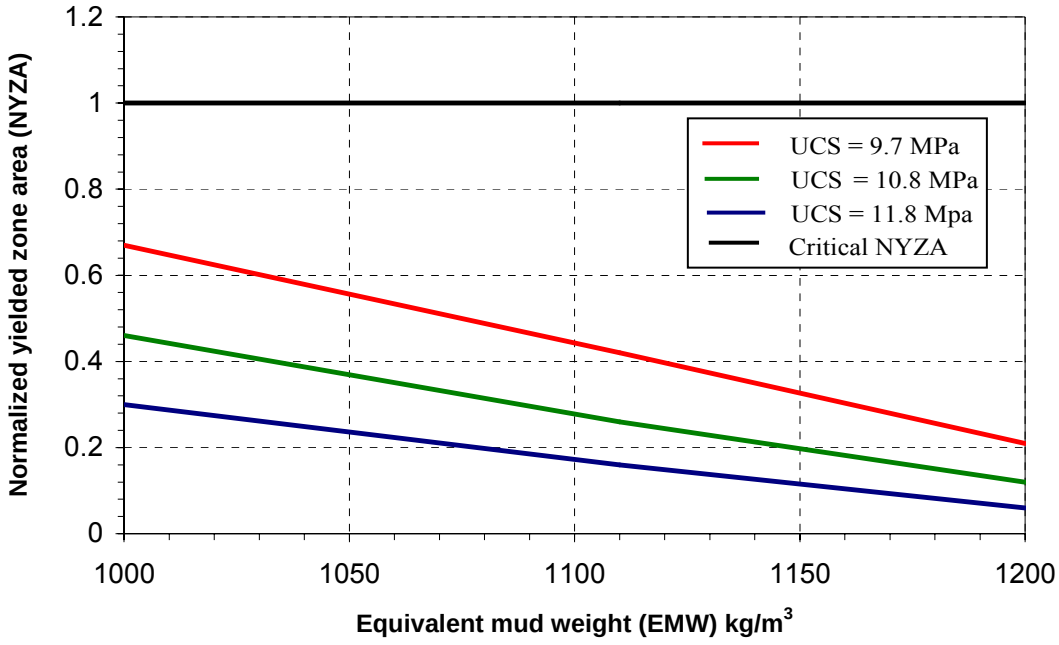

Figure 5.7: Sensitivity of borehole yielding to unconfined compressive strength (UCS) for a horizontal well in the Mannville coal at 900 m depth. UCS for the base case is 10.8 MPa.

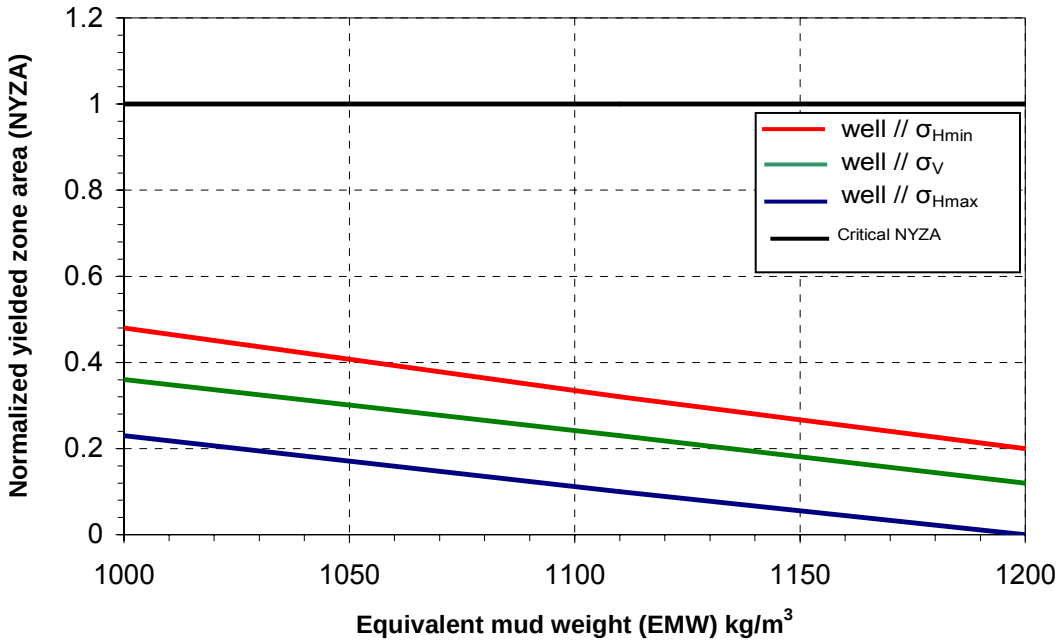

Figure 5.8: Sensitivity of borehole yielding to well trajectory for a horizontal well in the Mannville coal at 900 m depth. The base case trajectory is parallel to σ_{Hmin}.

5.3.3 Belly River Coals

Given that the Belly River coals exist as numerous thin seams, these coals will likely be developed using vertical wells, with hydraulic fracturing used to stimulate production in most of the seams. The drilling risks for vertical wells passing through thin, weak zones occurring at shallow depths are often manageable. Appendix D gives a description of preliminary borehole stability analyses conducted for the Belly River coals, following the procedures described above for Mannville coals. The results reported in Appendix D seem to support the belief that borehole instability risks are low for the Belly River coals.

6. CONCLUSIONS AND RECOMMENDATIONS

6.1 Conclusions

- The main objective of this research was to map in-situ stress magnitudes and orientations across southwest Saskatchewan, and assess which areas might be most prospective for coalbed methane production on the basis of the in-situ stress regime. The guiding principle was the concept, proven elsewhere, that coal permeability, fracturing pressures, induced fracture orientations, and borehole stability are all very sensitive to in-situ stresses.
- Previous work has shown that the Belly River Formation and Mannville Group contain coal seams with potential for coalbed methane production in southwest Saskatchewan.
- Work conducted for this thesis has shown that vertical stress magnitudes in the coal-bearing strata of southwest Saskatchewan are dominantly controlled by present-day burial depth, although decreasing overburden densities from west-southwest to east-northeast have a secondary effect.
- Vertical stresses at the top of the Lea Park Formation (i.e., base of the Belly River Formation), in the region of greatest interest for Belly River coal development (i.e., south of T15, west of R20W3), are in the 6 to 12 MPa range.
- Vertical stresses at the top of the Mannville Group in the region of greatest interest for coal development (i.e., west-central and northwest parts of the study area) are in the 12 to 18 MPa range.
- Work conducted for this thesis has shown that minimum horizontal stresses can be estimated in the study area by multiplying the instantaneous shut-in pressure measured during a hydraulic fracture stimulation by a factor of 0.90.
- Data for interpreting minimum horizontal stresses in southwest Saskatchewan are limited, compared to vertical stresses. Available data suggest that depth is a

dominant controlling factor, but that pore pressures (sub-normal pressures cause lower stresses) and lithology also have notable effects (shaley rocks, and perhaps coals, have higher stresses).

- Insufficient data were obtained for estimating minimum horizontal stresses in the Belly River Formation. The limited available data, along with stress interpretations published for the Alberta Basin, suggest that minimum horizontal stress magnitudes may be close to the vertical stress magnitudes. In the north-northeastern part of the study area, where the Belly River Formation occurs at relatively shallow depths (e.g., 100 to 200 m), it is even possible that minimum horizontal stresses are greater than vertical stresses.
- Hydraulic fractures induced in Belly River coals where σ_{Hmin} is the minimum in-situ stress will be oriented vertically, and propagate in the direction of the maximum horizontal stress azimuth. Based on a previously published dataset, which has been supplemented during this project, this azimuth generally trends southwest-northeast in the study area, with a counterclockwise deflection over the Swift Current arch. Hydraulic fractures induced in coals where σ_V is the minimum in-situ stress will be oriented horizontally.
- Minimum horizontal stresses at the top of the Mannville Group in the region of greatest interest for coal development (i.e., the northwest part of the study area) are estimated to be in the 10 to 14 MPa range.
- No data for maximum horizontal stress magnitude interpretation were available for the study area. Based on a limited amount of previously published data, a rough guideline for estimating this stress component is to multiply the minimum horizontal stress by a factor in the 1.3 to 1.4 range, which should typically yield a value slightly greater than the vertical stress magnitude.
- The stress regime in the study area is complex, and not yet fully understood. Notably, the interpretation of normal faults in Tertiary and Quaternary strata reported previously in the earth science literature has not been reconciled with the results obtained in this research.

- Published coal permeability data compiled during this project suggest that permeabilities may vary over two or three order of magnitude for the stress ranges anticipated in the Belly River and Mannville coals in southwest Saskatchewan.
- First-order analyses of borehole stability, conducted during this project using estimated rock mechanical properties, suggest that it may be feasible to drill horizontal wells in Mannville coal seams without the need for weighted mud systems.

6.2 Recommendations

- More stress tests should be run in the Belly River and Mannville coals, in order to provide a more complete and accurate picture of minimum horizontal stresses in these strata. Ideally, micro- or mini-frac tests would be used for this purpose and tests within and above the coal seams would be conducted to measure the effects of lithology on horizontal stress.
- Results of these stress tests should be used to predict fracture stimulation behaviour; notably, fracturing pressures, fracture orientation (e.g., vertical vs. horizontal), and fracture containment behaviour (for vertical fractures).
- Coal cores should be obtained and used for laboratory tests to determine coal permeability as a function of stress, and coal mechanical properties.
- These revised coal properties and stress data should be used for more comprehensive modelling of borehole instability risks during drilling and completion operations. These analyses would enable predictions of the feasibility of underbalanced drilling, and linerless openhole completions for horizontal wells in the Mannville Group.
- The stress maps generated in this project should be "stitched" together with similar maps previously published for the Alberta Basin, in order to provide one continuous dataset across southwest Saskatchewan and southeast Alberta.
- Fracture stimulation data for a larger number of Cretaceous-age strata should be compiled and analyzed for minimum horizontal stress magnitudes.

- Lithological attributes and mechanical properties of these Cretaceous-age reservoirs should be compiled (ideally based on core observations and measurements, but realistically estimated from geophysical logs).
- The above-noted dataset should be interpreted to provide a more complete picture of minimum horizontal stress variations – both areally and with depth in southwest Saskatchewan.

7. REFERENCES

Addis, M.A. 1997, 'The stress-depletion response of reservoirs,' SPE Paper 38720, in *Proceedings of the SPE Annual Technical Conference and Exhibit*, San Antonio, USA, pp. 55-65.

Ayers, W., 2002, Coalbed gas systems, resources, and production and a review of contrasting cases from the San Juan and Powder River basins: AAPG Bulletin, **86**, pp. 1853-1890.

Bachu, S. and Michael, K. 2002, *Hydrogeology and Stress Regime of the Upper Cretaceous-Tertiary Coal-bearing Strata in Alberta*, EUB/AGS Earth Sciences Report 2002-04, Alberta Geological Survey, Edmonton, Canada, 81 p.

Bell, J.S. 2003, 'Practical methods for estimating in situ stresses for borehole stability applications in sedimentary basins,' *Journal of Petroleum Science and Engineering*, vol. 38, pp. 111-119.

Bell, J.S. and Bachu, S. 2003, 'In situ stress magnitude and orientation estimates for Cretaceous coal-bearing strata beneath the plains area of central and southern Alberta,' *Bulletin of Canadian Petroleum Geology*; March 2003; v. 51; no. 1; pp. 1-28.

Bell, J.S., Price, P.R. and McLellan, P.J. 1994, 'In-situ stress in the Western Canada Sedimentary Basin,' in *Geological Atlas of the Western Canada Sedimentary Basin*, comp. G.D. Mossop and I. Shetsen, Canadian Society of Petroleum Geologists and Alberta Research Council, Calgary, Canada, pp. 439–446.

Bend, S.L. and Frank, M.C. 2004, 'CO_2 sequestration and coalbed-methane potential of lower Mannville group (lower Cretaceous) coals, southern Saskatchewan - Preliminary investigations,' in *Summary of Investigations 2004*, vol. 1, Misc. Rep. 2004-4.1, Saskatchewan Industry and Resources Geo-Publications, Regina, Canada.

BJ Services Company Canada Ltd. and Rakhit Petroleum consulting Ltd. 2006, Joint venture, "Multi-client study stress analysis - central Alberta,"

Bustin, R.M. 1997, 'Importance of fabric and composition on the stress sensitivity of permeability in some coals, northern Sydney basin, Australia: Relevance to coalbed methane exploitation,' American association of petroleum geologists bulletin, v. 81, no. 11, p. 1894-1908.

Campbell, J.D. 1979, 'Major cleat trends in Alberta plains coal,' *CIM Bulletin*, vol. 72, pp. 69-75.

Charlez, Ph. A. 1997, 'Rock mechanics, Petroleum applications,' Vol.2, Paris editions: Technip.

Christopher, J.E. 2003, *Jura-Cretaceous Success Formation and Lower Cretaceous Mannville Group of Saskatchewan*, Report 223, Saskatchewan Industry and Resources Geo-Publications, Regina, Canada.

Christopher, J.E. 1984, '*The Lower Cretaceous Mannville Group, northern Williston Basin region*,' Canada; *in* Stott, D.F. and Glass, D.J. (eds.), The Mesozoic of Middle North America, Can. Soc. Petrol. Geol., Mem. 9, p109-126.

Christopher, J.E., Kent, D.M. and Simpson, F. 1971, *Hydrocarbon Potential of Saskatchewan*, Saskatchewan Energy and Mines, Report 157, Saskatchewan Industry and Resources Geo-Publications, Regina, Canada.

Cinco, H. and Samaniego, F. 1981, 'Transient Pressure Analysis for Fractured Wells,' *Journal of Petroleum Technology*, vol. 33, no. 9, pp. 1749-1766.

Collin, P. M. (2002). Geomechanics and Wellbore stability design of an offshore horizontal well, North Sea, SPE/PS-CIM/CHOA, presented at SPE international thermal operations and heavy oil symposium and international horizontal well technology conference, Calgary, AB, Canada.

de Bree, P. and Walters, J.V. 1989,. 'Micro/minifrac test procedures and interpretation for in situ stress determination,' *International Journal of Rock Mechanics and Mining Science & Geomechanics Abstracts*, vol. 26, pp. 515–521.

Divestco Inc. 2006, *EnerGISite Well Log Data*, Digital library of geophysical logs and DTS reports, accessed at www.energisite.com.

Enever, J.R., Pattison, C.I., McWatters, R.J. and Clark, I.H. 1994, 'The relationship between in-situ stress and reservoir permeability as a component in developing an exploration strategy for coalbed methane in Australia,' SPE 28048, in *Proceedings of the SPE/ISRM Rock Mechanics in Petroleum Engineering conference*, Delft, the Nethrelands.

Fenton, M.M., Schreiner, B.T., Nielsen, E. & Pawlowicz, J.G. 1994, 'Quaternary geology of the western plains,' Chapter 26 in *The Geological Atlas of the Western Canada Sedimentary Basin*, ed. G. Mossop & I. Shetsen, Canadian Society of Petroleum Geologists, Calgary, Alberta & Alberta Research Council, Edmonton, Canada.

Ferdous, H., Bergman, K., and Qing, H. 2006, 'Viking lowstand deposits in west central Saskatchewan: Depositional model for the reservoir units in Dodsland-Hoosier area, Saskatchewan, Canada,' *CSPG/CSEG/CWLS Convention*, Calgary, Canada.

Fjaer, E., Holt, R.M., Horsrud, P., Raaen, A.M. and Risnes, R. 1992, 'Petroleum related rock mechanics, developments in Petroleum science,' 33, Elsevier, New York.

Fleming, N.H., Ronaldi, R., Bruce, S., and Haryanto, J. 1990, 'The application of mechanical borehole stability theory to development well planning,' IADC/SPE 19943, presented at the 1990 IADC/SPE conference, held in Huston, Texas, U.S.A. February 27-March 2, 1990.

Foroughi, M.H., Shariar, K., and V S Vutukuri, V.S.1999, 'Modification of Some Failure Criteria for Rock and Coal' paper ID 9901025, presented at the Tenth Australian Tunnelling Conference

Frank, M.C. 2005, Coal distribution in the upper Cretaceous Belly River group of southwest Saskatchewan. Open File 2005-3, Saskatchewan Industry and Resources, Regina, Canada.

Gentzis, T. 2004, 'Economic CBM in the foothills: The puzzle,' presentation at the *CSUG Conference*, Calgary, Canada.

Gendzwill, D. and Stauffer, M. 2006, 'Shallow faults, Upper Cretaceous clinoforms, and the Colonsay Collapse, Saskatchewan,' Canadian Journal of Earth Science v. 43, pp. 1859-1875.

Gough, D.I. and Bell, J.S. 1982, 'Stress orientations from borehole wall fractures with examples from Colorado, east Texas and northern Canada,' Canadian Journal of Earth Sciences, v. 19, no. 7, pp. 1358-1370.

Gulrajani, S. N., and Nolte, K.G., 2000, 'Fracture evaluation using pressure diagnostics, chapter 9 of reservoir stimulation,' 3rd edition, edited by Economides, M.J., and Nolte, K.G.

Hawkes, C.D. October 21, 2003, 'Assessing the mechanical stability of horizontal borehole in coal seams. Workshop on rock mechanics and ground control in the soft rock and coal industries,' held with conjunction with the 16th mine operator's conference, Saskatoon, Saskatchewan, Canada.

Hawkes, C.D. September 30, 2004, 'Estimation of minimum in-situ stress magnitudes in the Edmonton region' final report submitted to Alberta Geological Survey.

Hawkes, C.D. 2007, 'Assessing the mechanical stability of horizontal boreholes in coal,' *Canadian Geotechnical Journal*,' v. 44, n. 7, pp. 797-813.

Hawkes, C.D., and McLellan P.J. June 19-21, 1996, 'Modelling of yielded zone enlargement around a wellbore,' Proceeding of the 2nd North American rock mechanics symposium, Montreal, Quebec, Balkema.

Hawkes, C.D., Bachu, S., Haug, K. and Thompson, A.W. 2005, 'Analysis of in-situ stress Regime in the Alberta Basin, Canada, for performance assessment of CO_2 geological sequestration sites,' in *Proceedings of the Fourth DOE/NETL Annual Conference on Carbon Capture and Sequestration*, Alexandria, Virginia, USA, 22 p.

Hubbert, M.K. and Willis, D.G. 1957, 'Mechanics of hydraulic fracturing,' *Transaction of the American Institute of Mining, Metallurgical, and Petroleum Engineers*, v. 210, pp. 153-166.

IHS Energy. 2006, *Accumap User's Guide*, IHS Energy, Calgary, Canada.

Jones, A.H., Bell, G.J., and Schraufnagel, R.A. 1988, 'A revive of the physical and mechanical properties of coal with implications for coal-bed methane well completion and production,' Gas Research Institute report (Contract number 5081-214-0577, 5081-214-1084, 5081-214-1460).

Kaiser, P.K., Mackay, C., and Morgenstern, N.R. 1982, 'Performance of a shaft in a weak rock (Bearpaw shale)', ISRM symposium, Aachen, 1982.05, 26-28.

Kwon, O., Kronenberg, A.K., Gangi, A.F., Johnson, B., and Herbert, B.E. 2004, 'Permeability of illite-bearing shale: Anisotropy and effects of clay content and loading,' Journal of geophysical research, vol. 109, B10205, doi:10.1029/2004JB003052.

Leckie, D.A. and Smith, D.G. 1993, 'Regional setting, evolution, and depositional cycles of the Western Canada Foreland Basin. In: Foreland Basins and Fold Belts,'

Macqueen, R.W. and Leckie, D.A. (eds.). *AAPG Memoir 55*, pp. 9-46.

Ma, T. 2004. "An introduction to coalbed methane", special session 31: Back to basic series, presented at the Canadian International Petroleum Conference, Calgary, Alberta, Canada, June 8-10, 2004.

McLennan, J.D., Hasegawa, H.S., Roegiers, J-C. and Jessop, A.M. 1986. 'Hydraulic fracturing experiment at the University of Regina Campus', Canadian Geotechnical Journal, v. 23, p. 548-555.

McLellan, P.J., Lawrence, K., and Cormier K. 1992. 'A multiple-zone acid stimulation treatment of a horizontal well, Midale, Saskatchewen', Journal of Canadian Petroleum Technology, v. 31, no. 4, p. 71-82.

Mclellan, P.J. and Hawkes, C.D. 1998, 'Application of probabilistic techniques for assessing sand production and borehole stability risks,' paper SPE 47334, presented at SPE/ISRM Eurock '98, Trondheim, Norway, July 8-10,1998.

McLellan, P.J. and Hawkes, C.D. 2001, 'Borehole stability analysis for underbalanced drilling,' *Canadian Journal of Petroleum Technology*, vol. 40, no. 5, pp. 31-38.

McKee, C.R., Bumb, A.C. and Koenig, F. 1988, 'Stress-dependent permeability and porosity of coal and other geologic formations, SPE 12858, SPE Formation Evaluation, vol. 3, no. 1, pp. 81-91.

Meyer and Associates. 2006, *Meyer Fracturing Simulators*, 4th edition, Meyer and Associates, Inc., Natrona Heights, PA, USA.

Moon, V. and Roy, T. 2004, '*Geological controls on rock mass classification of coal from Huntly East Mine, New Zealand'* Engineering Geology **,**Volume 75, Issue 2, pp 201-213

National Energy Board of Canada. 2003, *Canada's Energy Future: Scenarios for Supply and Demand to 2025*, www.neb-one.gc.ca/energy/supplydemand/2003/index_e.htm.

Nolte, K.G. 1979, 'Determination of fracture parameters from fracturing pressure decline,' SPE 8341, presented at the 54th annual fall technical conference and exhibition of SPE/AIME, held in Las Vegas, Nevada, U.S.A. September 23rd -26 1979.

Nolte, K.G. 1988, 'Prenciples for fracture design based on pressure analysis,' SPE 10911, presented at the 1982 SPE Cotton Valley Symposium held in Tyler TX May 20.

Palmer Ian and Mansoori John 1996, 'How permeability depends on stress and pore pressure in coalbeds: A new model,' SPE 36737, presented at the 1996 Annual Technical conference and exhibition held in Denver.

Plumb, R.A. and Hickman, S.H. 1985, 'Stress-induced borehole elongation: A comparison between the four-arm dipmeter and the borehole televiewer in the Auburn geothermal well,' *Journal of Geophysical Research*, vol. 90, no. B7, pp. 5513-5521.

Porter, J.W., Price, R.A. and McCrossan, R.G. 1982, 'The Western Canada Sedimentary basin' *Phil. Trans. R. Soc. Lond.* A 305, pp 169-192.

Saskatchewan Geological Survey. 2003, *Geology, and Mineral and Petroleum Resources of Saskatchewan*, Misc. Report 2003-7, Saskatchewan Industry and Resources Geo-Publications, Regina, Canada, 173 p.

Seidle J.P., Jeansonne M.W., and Erickson D.J. 1992, 'Application of Matchstick geometry to stress dependent permeability in coals,' SPE 24361, presented at the 1992 Rocky Mountain region meeting held in Casper, Wyoming, May 18- 21 , 1992.

Sparks, D.P., McLendon, T.H., Saulsberry, J.L. and Lambert, S.W. 1995, 'The effects of stress on coalbed reservoir performance, Black Warrior Basin, U.S.A.,' SPE Paper 30743, in *Proceedings of the Society of Petroleum Engineers Annual Technical Conference and Exhibition*, Dallas, USA, pp. 339-351.

Stauffer, M.R. and Gendzwill, D.J. 1987, 'Fractures in the northern plains, stream patterns, and mid-continent stress,' Canadian Journal of Earth Science 24, 1086-1097.

Warpinski, N.R. 1989, 'Elastic and viscoelastic calculations of stresses in sedimentary basins,' *SPE Formation Evaluation*, vol. 4, no. 4, pp. 522-530.

Whitehead, W.S., Gatens, J.M. and Holditch, S. A. 1989, 'Determination of in-situ stress profiles through hydraulic fracturing measurements in two distinct geologic areas,' *International Journal of Rock Mechanics & Mining Sciences*, vol. 26, pp. 637-645.

Woodland, D. C., and Bell, J. S. 1989, 'In situ stress magnitudes from mini-frac records in Western Canada,' *Journal of Canadian Petroleum Technology*, vol. 28, no. 5, p. 22-31.

Zipf, Jr. and R.,K., 2006, 'Numerical modelling procedures for practical coal mine design,' Proceedings of the 41st U.S. Rock Mechanics Symposium, Golden, Colorado, June 17-21, 2006. Alexandria, VA: American Rock Mechanics Association, NIOSHTIC-2 No. 20030405

Zoback, M.D., Barton, C.A., Brudy, M., Castillo, D.A., Finkbeiner, T., Grollimund, B.R., Moos, D.B., Ward, C.D. and Wiprut, D.J. 2003, 'Determination of stress orientation and magnitude in deep wells,' *International Journal of Rock Mechanics & Mining Sciences*, vol. 40, pp. 1049-1076.

APPENDIX A: VERTICAL STRESS DATA

Figure A.1 shows glacial till thickness, and Figure A.2 shows estimated density of glacial till in the study area, measured in uncased boreholes. The criterion for choosing till thickness and density values was based on a sudden increase in density with depth. The thicknesses interpreted in this manner were cross-referenced with an isopach map of glacial till published by Fenton et al. (1994). Table A-1 shows depth to the glacial till and their densities estimated from bulk density logs. Table A.2 lists the vertical stresses calculated for the Lea Park Formation, Viking Formation and the Mannville Group. Table A.3 lists the data quality indicators for these calculated vertical stresses.

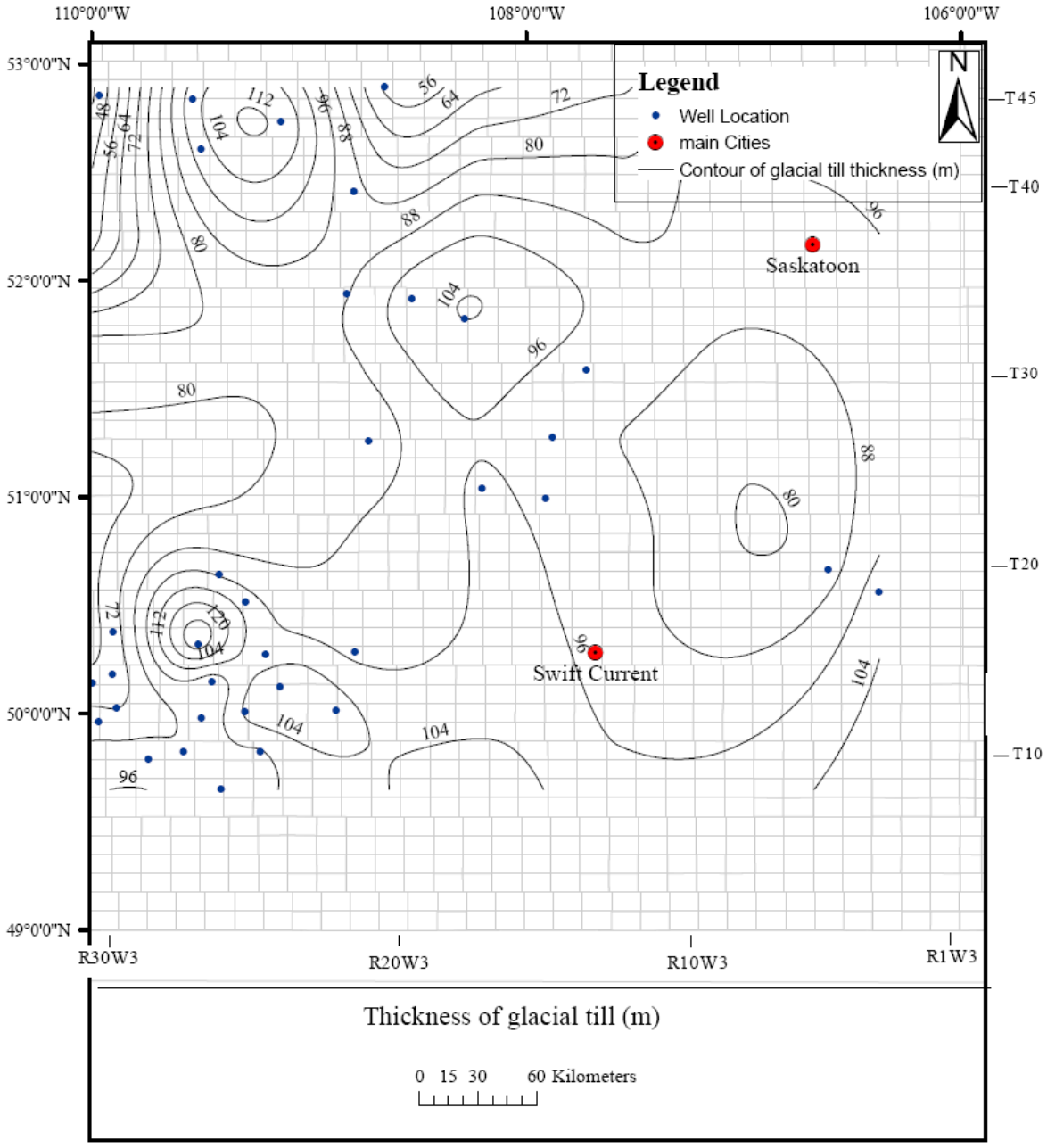

Figure A.1: Southwest Saskatchewan glacial till thickness (m).

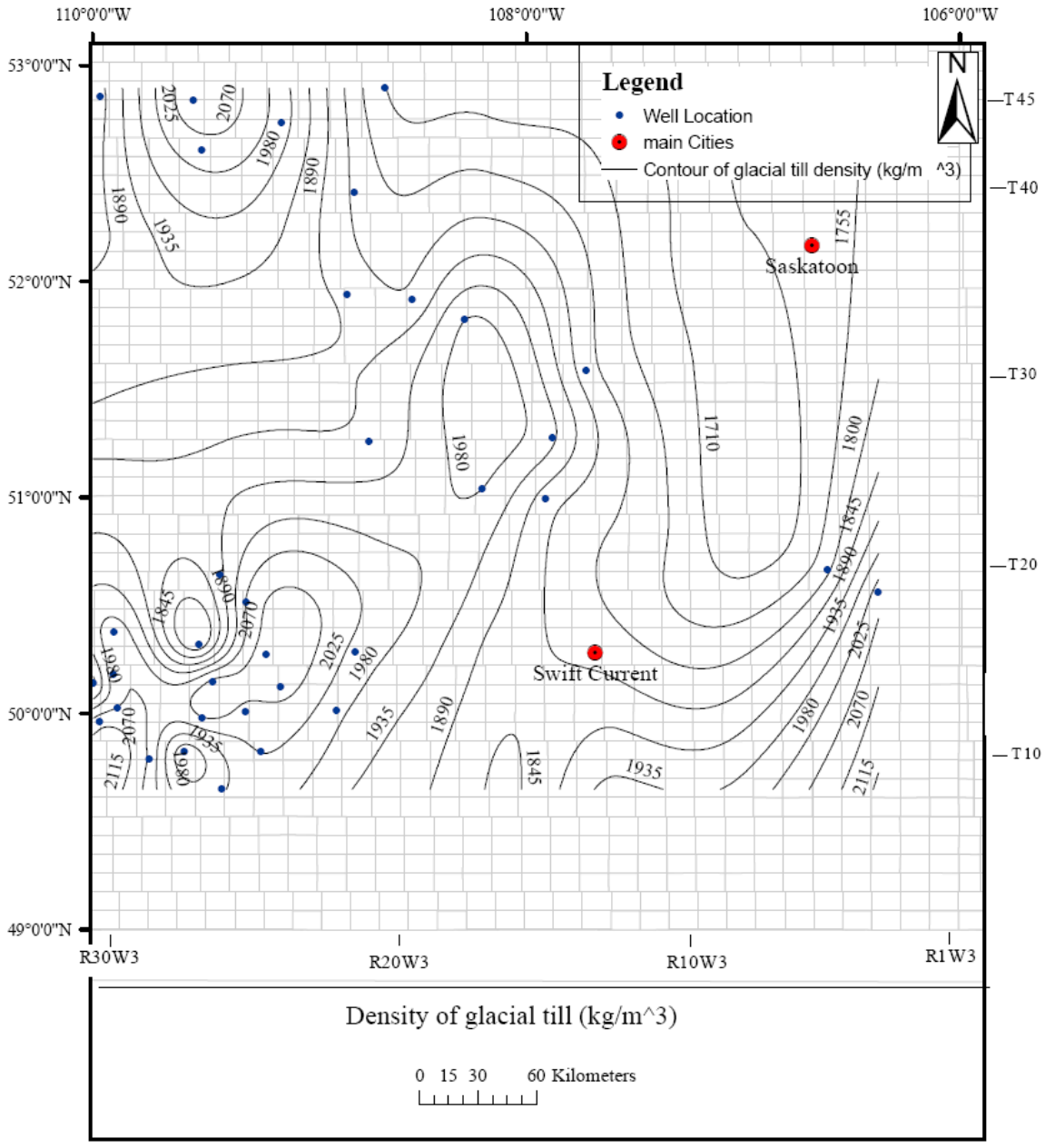

Figure A.2: Southwest Saskatchewan glacial till density (kg/m^3).

Table A.1: Well ID, glacial till bottom, till density and surface to bedrock.

UWI	Glacial till bottom (m)	Density kg/m^3	Glacial till first measurement (m)	Density kg/m^3	Surface to bed rock-Till thickness (m), Bell et al. (1994)
131-11-13-008-26W3-00	96	1973.8	92	1972	100
101-07-04-010-28W3-00	92	2060.9	86	2043	50-100
111-10-15-010-27W3-00	89	1911.8	86	1922	50-100
131-11-17-010-24W3-00	95.4	2025.81	-	-	100-150
111-07-01-012-30W3-00	84	2095.3	-	-	50-100
121-06-27-012-29W3-00	80	2072.8	-	-	50-100
1431-06-09-012-26W3-00	91	2068.2	83	2022	50-100
131-06-24-012-25W3-00	105	2055.7	95	2023	100
101-06-31-013-23W3-00	110.7	2088	84	1980	100-150
141-10-24-012-22W3-00	107	1993.4	86	1890	100-150
141-06-02-014-30W3-00	75	1929	-	-	50-100
111-06-21-014-29W3-00	75	2049	-	-	50-100
101-10-13-014-26W3-00	91.3	2084	88	2055	100
141-06-23-015-24W3-00	100	2094	-	-	100-150
101-06-26-015-21W3-00	94	2012	88	1995	100-150
121-16-27-016-29W3-00	76	2045	67	2048	50-100
111-16-04-016-26W3-00	123	1818	111	1800	100-150
111-04-33-019-25W3-00	95	1924	76	1917	50-100
141-06-29-019-24W3-00	100	2026.1	88	2004	100-150
102-10-32-018-03W3-00	100	1997	84	2035	100
101-10-03-020-05W3-00	85	1790.6	-	-	50-100
101-16-29-023-14W3-00	94	1869.9	91	1870	150
121-06-17-024-16W3-00	97	1980.4	80	1985	100
101-08-33-026-20W3-00	84	1903.9	75	1815	50-100
141-09-03-027-14W3-00	90	1942.83	75	1976	100-150
131-15-23-030-13W3-00	92	1822	75	1922	50-100
111-03-13-033-17W3-00	104	1979.7	101	1977	100-150
101-03-30-034-20W3-00	87.6	1880	-	-	50-100
131-05-17-034-18W3-00	100	1856.4	-	-	50-100
101-07-03-040-20W3-00	100	2042	83	1838	50-100
141-04-14-042-25W3-00	100	2048.9	82	2076	100
111-15-28-043-22W3-00	110	1999.5	84	1986	100-150
111-12-35-044-28W3-00	35	1877.3	20	1873	0-50
111-16-34-044-25W3-00	100	2097.6	22	1935	100-150
141-11-23-045-19W3-00	55	1757.8	-	-	50-100

Table A.2: Summary of vertical in-situ stress calculation for the study area.

UWI	Lea Park Formation			Viking Formation			Mannville Group		
	Depth (m)	σ_V (MPa)	σ_V (kPa/m)	Depth (m)	σ_V (MPa)	σ_V (kPa/m)	Depth (m)	σ_V (MPa)	σ_V (kPa/m)
100-08-28-002-01W4-00	294.1	6.36	21.63				1018	22.91	22.50
111-01-28-002-30W3-00	335.6	7.15	21.32	896.60	19.99	22.29	1031	23.13	22.42
131-11-21-002-29W3-00	371.6	7.91	21.29	902.60	19.80	21.94	1028.8	22.66	22.03
121-07-16-002-28W3-00	357.3	7.79	21.81						
121-11-33-002-26W3-00	361.8	7.62	21.06	1012.80	22.37	22.09	1132.8	25.14	22.19
121-05-34-002-25W3-00	424.3	8.66	20.41	1087.30	23.01	21.17	1204.3	25.58	21.24
141-10-30-002-24W3-00	461.6	9.74	21.09	1124.60	24.84	22.09	1232.6	27.34	22.18
131-09-25-002-21W3-00	459.3	9.89	21.53	1116.30	24.39	21.85	1194.3	26.17	21.92
101-05-24-002-20W3-00	459	9.79	21.33	1104.00	23.76	21.53	1194	25.79	21.60
101-04-11-001-18W3-00	357.1	7.47	20.93	1005.10	21.60	21.49	1098.1	23.66	21.55
141-11-10-002-15W3-00	293.4	6.14	20.91	829.89	17.69	21.32	988.4	21.28	21.53
100-07-27-005-01W4-00	420.7	9.06	21.52				1161.7	26.18	22.54
141-06-32-004-29W3-00	342.6	7.16	20.90	996.60	22.05	22.13	1107.6	24.63	22.24
101-10-13-004-28W3-00	357.1	7.34	21.08						
101-06-28-004-27W3-00	359.8	7.39	20.72	1022.80	22.21	21.72	1145.8	25.01	21.82
121-09-17-004-26W3-00	360.7	7.41	20.55	1026.70	22.35	21.76	1140.7	24.89	21.82
111-11-14-004-25W3-00	403.5	8.16	20.38	1066.50	22.65	21.23	1174.5	25.08	21.36
141-12-28-004-24W3-00	405.7	8.53	21.02						
111-06-17-003-15W3-00				899.69	19.01	21.13	989.45	20.99	21.22
141-11-33-003-15W3-00	366.9	7.56	20.60						
141-12-20-003-14W3-00				921.94	19.17	20.80	994.3	20.77	20.89
101-11-25-003-14W3-00	345	7.17	20.77						
100-11-05-006-01W4-00	452.75	9.69	21.39				1214.75	27.25	22.44
141-11-36-006-30W3-00	484.6	10.14	20.91						
101-11-18-006-29W3-00	471.59	9.96	21.11	1161.59	25.80	22.21	1299.59	29.02	22.33
141-07-33-006-28W3-00	468.3	9.94	21.22	1170.30	25.75	22.00	1290.3	28.50	22.09
101-14-15-005-27W3-00	421.76	8.78	20.81	1039.76	22.82	21.95	1156.76	25.51	22.05
121-03-03-006-26W3-00	403.5	8.47	20.99	1075.50	23.26	21.63	1192.5	25.88	21.71
141-11-26-006-25W3-00	498.8	10.50	21.05						
101-07-08-006-20W3-00	524.94	10.99	20.94	1160.94	25.18	21.69	1250.94	27.23	21.77
141-06-22-007-10W3-00	408.1	8.32	20.40	972.10	20.70	21.30	1047.1	22.37	21.36
100-06-29-009-01W4-00	430.7	8.97	20.84				1153.7	25.32	21.95
141-16-30-008-27W-00	474.8	9.86	20.76						
131-11-13-008-26W3-00	533.2	11.02	20.66						
131-06-32-008-25W3-00	656.9	13.45	20.47	1289.90	27.55	21.36	1406.9	30.18	21.45
101-04-26-008-21W3-00	646.88	13.10	20.24	1258.88	26.16	20.78	1348.88	28.20	20.90
141-02-08-008-20W3-00	482.7	10.08	20.87	1100.70	23.83	21.65	1190.7	25.87	21.73
111-09-05-008-19W3-00	492.5	9.78	19.86	1119.50	23.15	20.68	1200.5	24.95	20.79
101-14-08-009-18W3-00	534.7	10.64	19.89	1128.70	23.44	20.76	1224.7	25.56	20.87
131-01-02-008-12W3-00	460.5	9.35	20.30	979.50	20.30	20.72	1054.5	21.96	20.83
141-12-22-008-11W3-00	457.16	9.25	20.23	1003.16	21.31	21.24	1090.16	23.27	21.34
141-07-26-009-07W3-00	422.08	8.50	20.15	959.08	20.26	21.12	1022.08	21.70	21.23
141-07-10-008-04W3-00	405.5	8.29	20.44	966.50	20.65	21.36	1023.5	21.94	21.43
100-06-22-010-01W4-00	353.57	7.42	20.98						
100-09-19-010-01W4-00							1048.17	23.35	22.28
131-07-02-010-29W3-00	337	7.23	21.46						
101-07-04-010-28W3-00	350.9	7.44	21.19						
141-06-01-010-26W3-00	346.2	8.12	20.60	1036.20	22.81	22.01	1132.2	25.03	22.10
131-11-17-010-24W3-00	442.83	9.21	20.81						
101-04-36-010-20W3-00	481.6	9.58	19.89	1075.60	22.33	20.76	1150.6	23.96	20.82
121-11-03-011-19W3-00	512.4	9.68	20.19	1139.40	24.07	21.13	1208.4	25.64	21.22
141-10-07-010-18W3-00	510.23	9.99	19.59	1134.23	23.08	20.35	1215.23	24.88	20.48
111-08-07-011-16W3-00	532.9	8.82	19.77	1108.90	23.20	20.92	1180.9	24.80	21.00
100-04-18-012-01W4-00	260.81	5.60	21.46				869.81	19.44	22.36
111-07-01-012-30W3-00	274.03	5.88	21.47						
121-06-24-013-29W3-00				768.40	17.24	22.44	861.4	19.39	22.51
121-06-27-012-29W3-00	267.21	5.77	21.59						
141-11-35-012-28W3-00	282.5	6.16	21.81						
141-06-14-012-27W3-00	304.8	6.31	20.70	808.80	17.58	21.73	910.8	19.90	21.85

UWI	Lea Park Formation			Viking Formation			Mannville Group		
	Depth (m)	σ_V (MPa)	σ_V (kPa/m)	Depth (m)	σ_V (MPa)	σ_V (kPa/m)	Depth (m)	σ_V (MPa)	σ_V (kPa/m)
141-06-09-012-26W3-00	310.8	6.45	20.74						
131-06-24-012-25W3-00	330	6.95	21.07	858.00	18.93	22.07			
141-10-24-012-22W3-00	344.8	7.05	20.43						
141-10-05-013-21W3-00	423.73	8.74	20.63	904.40	19.18	21.20	982.59	20.91	21.28
101-06-22-012-20W3-00	467.4	9.69	20.74	950.40	20.47	21.54	1022.4	22.07	21.58
101-13-01-012-19W3-00	531.7	10.75	20.23	1122.70	23.33	20.78	1203.7	25.13	20.87
101-16-16-012-18W3-00	511.55	10.25	20.04	1105.55	23.28	21.05	1183.55	25.03	21.14
121-16-29-012-17W3-00	485.2	9.69	19.96	1061.20	22.14	20.86	1136.2	23.81	20.95
141-09-20-012-13W3-00	453.7	8.90	19.62						
131-10-16-013-08W3-00	437.6	8.68	19.83	947.60	19.69	20.78	1001.6	20.88	20.85
100-02-27-014-01W4-00	295.6	6.12	20.69				874.6	18.94	21.66
141-06-02-014-30W3-00	253.9	5.56	21.89						
111-06-21-014-29W3-00	248.7	5.42	21.80						
131-13-22-015-27W3-00	284.4	5.85	20.80	779.40	16.95	21.75	884.4	19.33	21.86
101-10-13-014-26W3-00	277.3	5.95	21.45						
121--07-06-014-23W3-00	291.3	6.14	21.09	801.30	17.57	21.92	888.3	19.48	21.93
141-06-21-014-22W3-00	292.1	6.17	21.12						
101-06-26-015-21W3-00	301.4	6.24	20.71						
141-01-04-014-20W3-00	315.3	6.36	20.19	885.30	18.68	21.10	987.3	21.00	21.27
131-15-10-014-19W3-00	336.4	6.67	19.82	924.17	18.66	20.19	1005.2	20.46	20.35
121-07-13-014-18W3-00	347.5	6.67	19.20	926.50	18.94	20.44	992.5	20.43	20.58
121-13-04-014-16W3-00	439.3	8.60	19.57	1009.30	20.86	20.67	1075.3	22.31	20.75
101-16-08-014-15W3-00	438.6	9.03	20.59	1002.60	21.12	21.06	1062.6	22.47	21.15
100-10-22-017-01W4-00	257.8	5.53	21.47				872.8	19.82	22.71
121-16-27-016-29W3-00	247.3	5.27	21.31						
101-11-02-016-28W3-00	259.6	5.39	20.76	805.60	17.65	21.91	904.6	19.92	22.02
121-12-22-016-27W3-00	252.6	5.25	20.79	801.60	17.79	22.20	904	20.15	22.29
111-16-04-016-26W3-00	264.73	5.33	20.15	801.73	17.48	21.80	909.73	19.98	21.96
101-07-34-016-23W3-00	258.5	5.57	21.53						
121-06-35-016-22W3-00	260.6	5.45	20.91	767.60	16.74	21.80			
101-09-25-016-20W3-00	270.6	5.32	20.32	843.60	18.14	21.50	915.6	19.80	21.62
101-02-27-016-19W3-00	273	5.52	20.22	837.00	17.94	21.44	900	19.37	21.52
141-06-20-016-18W3-00	294.6	6.00	20.35	816.60	17.23	21.10	909.6	19.29	21.21
121-02-27-016-16W3-00	300.6	6.10	20.29	846.60	18.05	21.31	909.6	19.48	21.41
111-07-30-016-15W3-00	317.1	6.41	20.22	857.10	18.26	21.30	917.1	19.65	21.43
141-14-33-016-12W3-00	380.4	7.45	19.59						
100-03-04-018-01W4-00	222.68	4.75	21.33				859.71	19.19	22.32
141-05-03-019-29W3-00	229.2	4.72	20.59	766.20	16.23	21.18	859.2	18.24	21.23
131-08-30-018-28W3-00	225.3	4.80	21.30	780.30	17.42	22.32	870.3	19.48	22.39
101-07-33-019-27W3-00	233.2	4.93	21.15	782.20	17.37	22.21	872.2	19.41	22.25
111-04-33-019-25W3-00	216.84	4.51	20.79						
141-06-29-019-24W3-00	232.4	4.85	20.88	721.40	15.86	21.98			
131-06-04-018-21W3-00	235.2	4.78	20.30	796.20	17.12	21.50	874.2	18.88	21.59
131-11-07-018-17W3-00	267	5.36	20.08	780.00	16.57	21.24	867	18.56	21.41
111-10-11-018-16W3-00	335.7	6.76	20.14	845.70	17.83	21.08	917.7	19.44	21.18
141-06-08-018-14W3-00	341.23	6.92	20.27						
102-10-32-018-03W3-00	414	8.36	20.16						
100-12-02-020-01W4-00	210.3	4.44	21.11				828.3	18.39	22.20
111-06-05-021-29W3-00	221.3	4.57	20.67	749.30	15.90	21.22	836.3	17.77	21.25
121-11-01-021-28W3-00	226.1	4.68	20.69	748.10	16.14	21.58	835.1	18.11	21.68
101-07-36-021-26W3-00	204.4	4.22	20.65	708.40	15.27	21.55	819.4	17.79	21.71
141-11-28-021-20W3-00	212.4	4.34	20.45	590.40	12.76	21.61	668.4	14.52	21.72
101-08-23-020-19W3-00	204.4	4.23	20.71	618.40	13.13	21.23	699.4	14.85	21.24
121-06-35-020-17W3-00	220.49	4.48	20.32						
141-06-26-020-16W3-00	244.71	4.94	20.20						
141-14-31-021-14W3-00	263.2	5.36	20.36						
101-14-06-021-13W3-00	274.43	5.64	20.57						
101-10-03-020-05W3-00	405.9	7.93	19.53						
100-06-09-22-01W4-00							864.9	18.82	21.75
101-07-09-023-25W3-00	185.6	3.78	20.39	704.60	15.47	21.95	779.61	17.14	21.99

UWI	Lea Park Formation			Viking Formation			Mannville Group		
	Depth (m)	σ_V (MPa)	σ_V (kPa/m)	Depth (m)	σ_V (MPa)	σ_V (kPa/m)	Depth (m)	σ_V (MPa)	σ_V (kPa/m)
101-10-03-023-24W3-00	184	3.81	20.69				757	16.45	21.80
141-13-28-022-20W3-00	201.84	4.15	20.57	630.39	13.44	21.32	696.99	14.94	21.43
111-04-15-022-19W3-00	199.4	4.14	20.47	631.40	13.35	21.14	700.4	14.85	21.20
101-07-13-022-17W3-00	207	4.26	20.59	660.00	14.47	21.93			
101-16-29-023-14W3-00	232	4.80	20.67	769.00	16.69	21.70	787	17.10	21.73
101-09-10-023-13W3-00	294	5.63	20.63	759.00	16.33	21.51	816	17.61	21.58
101-06-26-023-08W3-00	300.19	5.86	19.53	806.92	16.94	21.00	835.25	17.99	21.09
111-06-08-022-06W3-00	394.1	7.68	19.48	845.78	17.54	20.74	903.7	18.85	20.86
100-16-11-025-01W4-00							867.3	18.75	21.62
111-09-08-025-28W3-00	193.3	3.99	20.65	746.34	16.09	21.56	827.4	17.92	21.66
191-10-20-025-27W3-00	191.3	3.88	20.26	671.30	14.63	21.79	755.3	16.55	21.91
141-10-10-024-26W3-00	185.2	3.89	20.65	668.20	14.40	21.55	743.2	16.07	21.62
111-13-20-024-24W3-00	184	3.67	19.97	709.00	14.86	20.96	784	16.48	21.02
121-16-10-025-23W3-00	184.9	3.73	20.19	691.90	14.97	21.63	757.9	16.45	21.70
121-06-17-024-16W3-00	196.3	4.03	20.52	664.30	14.34	21.59	745.3	16.16	21.69
101-10-16-024-13W3-00	247.8	4.89	19.71	726.00	15.17	21.01	760.8	16.04	21.09
131-13-21-024-12W3-00	278.7	5.57	19.98	701.70	14.76	21.04			
100-07-31-027-01W4-00	176.31	3.60	20.43				806.31	17.51	21.72
131-05-14-026-29W3-00	176.71	3.66	20.70	752.93	16.33	21.69	828.21	18.04	21.78
141-08-17-026-28W3-00	189.61	3.90	20.55	812.16	17.66	21.74	890.34	19.42	21.82
111-12-17-026-27W3-00	187.47	3.81	20.32	705.78	15.12	21.43	792.65	17.08	21.55
131-13-19-027-26W3-00	188.48	3.77	20.64	727.06	15.70	21.59	877.63	17.40	21.69
101-04-19-026-25W3-00	177.8	3.66	20.60	750.80	16.47	21.93	813.8	17.91	22.01
101-10-31-027-22W3-00	189.6	3.49	18.41	720.60	15.39	21.35	780.6	16.77	21.48
101-08-33-026-20W3-00	201.2	3.94	19.57	717.20	15.48	21.59	750.2	16.24	21.65
101-06-29-026-19W3-00	201.4	3.95	19.63	696.40	14.96	21.48	753.4	16.24	21.56
101-11-09-027-18W3-00	184.7	3.52	19.05	670.70	13.49	20.12	706.7	14.23	20.14
101-02-13-027-16W3-00	171	3.44	20.12	639.00	13.77	21.55	672	14.52	21.61
141-09-03-027-14W3-00	156	3.14	20.12	609.10	12.99	21.32	645	13.79	21.38
100-15-35-028-01W4-00							784.5	16.78	21.39
111-14-11-028-29W3-00	145.48	2.95	20.29	724.60	15.92	21.97	791.19	17.44	22.04
101-13-01-028-28W3-00	128.2	2.58	20.16	707.20	15.45	21.84	773.2	16.93	21.90
101-03-14-028-27W3-00	163.4	3.24	19.81	739.40	15.67	21.20	802.4	17.08	21.29
101-07-34-028-25W3-00	191.19	3.92	20.48	729.77	15.78	21.62	784.78	17.00	21.67
101-06-07-028-23W3-00	136.5	3.75	20.11	682.50	14.76	21.63	742.5	16.15	21.75
111-08-33-029-22W3-00	186.3	3.77	20.21	724.30	15.47	21.36	762.3	16.27	21.34
111-16-14-028-20W3-00	198.1	3.85	19.45	708.10	14.66	20.70	762.1	15.88	20.84
101-10-25-028-19W3-00	192.3	3.75	19.51	714.30	15.41	21.57	720.3	15.55	21.58
131-16-25-029-17W3-00	184.2	3.57	19.37	652.20	13.87	21.26	694.2	14.83	21.36
100-11-18-031-01W4-00	242.31	5.10	21.03				743.31	16.13	21.70
121-02-13-031-29W3-00	191.9	3.87	20.15	704.90	15.58	22.10	761.9	16.92	22.21
131-13-12-031-28W3-00	185.1	3.72	20.07	746.10	16.06	21.53	788.1	17.00	21.58
141-14-06-031-26W3-00	186.9	3.75	20.05	735.90	15.93	21.64	789.9	17.15	21.71
131-01-27-031-25W3-00	183	3.54	19.36	678.00	13.80	20.35	726	14.76	20.33
111-15-08-031-24W3-00	183.6	3.60	19.60	660.60	13.89	21.03	714.6	15.08	21.11
131-11-04-030-22W3-00	194.6	3.86	19.82	713.60	15.07	21.11	764.6	16.18	21.16
101-09-19-030-19W3-00	199.1	3.83	19.22	730.10	15.35	21.02	772.1	16.30	21.11
101-06-16-031-18W3-00	194.4	3.72	19.14	704.40	14.92	21.18	746.4	15.87	21.26
131-15-23-030-13W3-00	150.4	2.86	19.05	576.40	12.03	20.86			
101-08-13-030-12W3-00	147	2.80	19.04	587.00	12.57	21.42			
100-06-24-033-01W4-00	172.41	3.51	20.33				766.41	16.58	21.64
111-06-12-032-29W3-00	161.3	3.32	20.58	728.30	15.75	21.63	758.3	16.42	21.65
191-08-02-032-28W3-00	166.1	3.37	20.27	700.10	14.87	21.24	763.1	16.26	21.30
111-06-01-032-27W3-00	189.4	3.85	20.33	730.40	15.75	21.56	783.4	16.91	21.58
121-16-36-032-25W3-00	198.3	3.94	19.85	708.30	14.96	21.12	759.3	16.08	21.18
111-04-33-032-24W3-00	198.9	3.95	19.88	693.90	14.86	21.41	750.9	16.14	21.49
101-12-12-032-23W3-00	175.3	3.51	20.04	667.30	14.35	21.51	724.3	15.64	21.59
111-09-30-032-21W3-00	182.5	3.61	19.78	659.50	14.24	21.59	704.5	15.27	21.67
111-03-13-033-17W3-00	161	3.02	18.74	707.00	14.89	21.06	740	15.64	21.14

UWI	Lea Park Formation			Viking Formation			Mannville Group		
	Depth (m)	σ_V (MPa)	σ_V (kPa/m)	Depth (m)	σ_V (MPa)	σ_V (kPa/m)	Depth (m)	σ_V (MPa)	σ_V (kPa/m)
111-05-27-032-16W3-00	167	3.13	18.72	704.00	14.86	21.10	743	15.73	21.17
131-04-10-033-01W3-00							528	11.08	20.98
100-07-14-035-01W4-00	237	4.91	20.73				756	16.62	21.99
101-08-20-035-28W3-00	229.6	4.67	20.34	745.60	16.20	21.73	799.6	17.44	21.81
111-13-09-034-26W3-00	219.3	4.45	20.29	720.30	15.45	21.45	771.3	16.61	21.54
101-12-18-034-25W3-00	207.3	4.18	20.16	693.30	14.91	21.51	738.3	15.92	21.57
131-08-10-034-24W3-00	187.2	3.78	20.20	679.20	14.55	21.42	736.2	15.84	21.52
111-08-10-034-23W3-00	176.7	3.39	19.20	692.70	14.64	21.14	737.7	15.65	21.22
111-02-29-034-22W3-00	174.4	3.47	19.89	624.40	13.54	21.69	675.4	14.71	21.78
101-03-30-034-20W3-00	184.4	3.62	19.62	664.40	14.23	21.42	712.4	15.33	21.52
101-08-07-034-19W3-00	200	3.97	19.83	596.00	12.54	21.04	638	13.49	21.15
104-05-17-037-01W4-00	202.9	4.14	20.41				709.9	15.46	21.77
101-07-15-036-28W3-00	179	3.60	20.09	689.00	14.81	21.50	734	15.83	21.57
111-05-06-036-27W3-00	201.23	3.99	19.81	707.96	14.58	20.60	760.08	15.73	20.69
111-10-12-036-26W3-00	184.9	3.72	20.11	637.90	13.67	21.42	679.9	14.62	21.50
111-08-08-036-25W3-00	169.37	3.31	19.53	647.15	13.61	21.03	690.58	14.58	21.11
111-07-34-037-24W3-00				616.52	13.23	21.46	659.59	14.20	21.52
101-10-20-037-23W3-00	205.8	4.09	19.85	619.80	13.09	21.12	661.8	14.06	21.25
101-07-19-036-21W3-00	142.4	2.70	18.99	622.40	12.86	20.66	670.4	13.88	20.70
101-03-28-036-19W3-00	151.4	2.81	18.59	595.40	12.47	20.95	634.4	13.35	21.04
101-10-18-036-17W3-00	157	3.06	19.46	589.00	12.63	21.44	637	13.72	21.53
121-13-14-036-03W3-00							499.2	10.58	21.19
100-08-17-038-01W4-00	203.2	4.35	21.40				707.2	15.83	22.38
111-09-11-038-27W3-00	201.23	3.72	20.23	681.70	14.63	21.46	760.08	15.64	21.53
111-05-11-038-25W3-00	167.4	3.40	20.34	626.40	13.49	21.54	668.4	14.44	21.60
111-06-26-038-24W3-00	125.3	2.50	19.99	590.30	12.63	21.39	641.3	13.78	21.49
111-14-24-038-22W3-00				545.40	11.63	21.33	593.4	12.72	21.43
101-02-28-039-21W3-00	129.6	2.50	19.25	570.60	12.26	21.49	612.6	13.22	21.58
101-07-30-039-20W3-00	119.6	2.25	18.80	578.60	12.07	20.86	626.6	13.14	20.98
101-13-19-039-18W3-00	120	2.17	18.10	561.00	11.62	20.72	606	12.62	20.82
100-15-07-040-01W4-00	175	3.48	19.86				670	14.56	21.73
111-14-20-040-28W3-00				587.90	12.69	21.58	638.9	13.86	21.69
131-07-015-040-26W3-00	140.6	2.76	19.65	602.60	13.01	21.59	653.6	14.17	21.68
111-13-14-040-25W3-00	137.7	2.72	19.73	599.70	12.93	21.56	653.7	14.16	21.67
111-06-05-040-23W3-00	135.7	2.68	19.76	588.70	12.38	21.03	633.7	13.31	21.00
101-15-33-040-21W3-00	134.94	2.59	19.20	569.28	12.00	21.08	612.72	12.99	21.19
101-07-03-040-20W3-00	133.6	2.52	18.83	565.60	11.62	20.55	607.6	12.53	20.63
111-04-12-040-19W3-00	128.6	2.33	18.11	563.60	11.42	20.27	599.6	12.22	20.38
121-01-19-041-16W3-00				565.00	11.40	20.17	586	11.86	20.23
100-12-25-043-01W4-00							713.5	15.51	21.74
111-12-12-042-28W3-00	167.1	3.31	19.83	563.10	12.05	21.40	608.1	13.06	21.48
101-10-09-042-27W3-00	159	3.16	19.84	552.00	11.75	21.29	603	12.90	21.39
141-04-14-042-25W3-00	139	2.77	19.95	493.00	10.45	21.19	547	11.66	21.31
131-07-22-042-24W3-00	159.6	2.50	19.74	546.60	11.79	21.58	585.6	12.68	21.66
141-13-18-042-23W3-00	161.7	2.59	19.19	542.70	11.66	21.49	584.7	12.62	21.58
111-15-28-043-22W3-00	159.11	2.87	19.45	512.37	10.75	20.98	552.91	11.65	21.08
101-13-34-042-20W3-00				499.30	10.21	20.45	538.3	11.05	20.53
111-03-13-042-19W3-00				540.68	10.92	20.20	576.3	11.68	20.27
131-07-30-042-17W3-00				425.52	8.69	20.41	488.2	9.41	20.54
100-14-10-045-01W4-00							509.41	10.97	21.54
111-12-35-044-28W3-00				485.00	10.28	21.20	533	11.36	21.32
111-01-30-044-27W3-00	136.3	2.70	19.79	502.30	10.87	21.50	553.3	11.96	21.62
191-13-18-044-26W3-00				484.45	10.39	21.44	532.45	11.43	21.48
111-16-34-044-25W3-00	121.1	2.50	20.68	538.10	11.44	21.26	583.1	12.45	21.34
111-13-14-045-24W3-00	122.4	2.44	19.91	431.40	9.45	21.89	473.4	10.44	22.05
101-10-04-045-23W3-00				502.23	10.73	21.37	542.76	11.64	21.44
131-05-09-045-22W3-00	127.7	2.48	19.42	484.70	10.39	21.43	520.7	11.20	21.51
121-06-18-045-21W3-00	123.1	2.34	18.99	453.10	9.35	20.63	489.1	10.15	20.76
141-11-23-045-19W3-00	73.8	1.37	18.55	391.80	8.36	21.33	427.8	9.18	21.45
141-15-04-044-18W3-00				431.93	8.99	20.81	469.57	9.82	20.90
161-04-11-045-16W3-00				424.52	8.74	20.44	441.89	9.03	20.44

Table A.3: Assumed data, average density corrections and average caliper/drill bit ratio used for vertical in-situ stress calculations.

UWI	Assumed data for Lea Park Formation (%)	Assumed data forViking Formation (%)	Assumed data for Mannville Group (%)	Average Density Correction (%)	Average Caliper/Bit
111-01-28-002-30W3-00	59.59	22.31	19.40		
131-11-21-002-29W3-00	27.72	11.41	10.00		
121-07-16-002-28W3-00	26.95				
121-11-33-002-26W3-00	49.20	17.58	16.80	2.60	1.06
121-05-34-002-25W3-00	17.70	6.90	6.20	1.90	1.1
141-10-30-002-24W3-00	49.40	20.27	18.50	2.40	1.11
131-09-25-002-21W3-00	34.00	13.97	13.10		
101-05-24-002-20W3-00	33.80	14.04	13.00		
101-04-11-001-18W3-00	39.50	14.04	12.80	5.20	1.05
141-11-10-002-15W3-00	35.61	12.59	11.30	2.90	0.99
100-07-27-005-01W4-00	50.80		18.40		1.03
141-06-32-004-29W3-00	41.20	14.15	12.70	2.90	1.05
101-10-13-004-28W3-00	43.40				
101-06-28-004-27W3-00	46.70	16.41	14.60		
121-09-17-004-26W3-00	39.30	13.80	12.40		
111-11-14-004-25W3-00	41.60	15.75	14.30		
141-12-28-004-24W3-00	23.17				
111-06-17-003-15W3-00		28.87	26.30		
141-11-33-003-15W3-00	29.68			3.10	
141-12-20-003-14W3-00		29.01	26.90	1.20	1.19
101-11-25-003-14W3-00	27.68			3.60	1.03
100-11-05-006-01W4-00	41.70		15.50	4.32	1.11
141-11-36-006-30W3-00	23.85				
101-11-18-006-29W3-00	33.21	13.48	12.05	4.54	1.12
141-07-33-006-28W3-00	30.11	12.05	10.93		
101-14-15-005-27W3-00	34.56	14.02	12.60	3.70	1.08
121-03-03-006-26W3-00	18.70	7.02	6.33		
141-11-26-006-25W3-00	17.00				
101-07-08-006-20W3-00	28.56	12.92	12.00	3.70	1.19
141-06-22-007-10W3-00	51.10	21.61	20.10		
100-06-29-009-01W4-00	14.83		5.54	3.70	0.89
141-16-30-008-27W-00	24.81			1.40	1.08
131-11-13-008-26W3-00	17.30				
131-06-32-008-25W3-00	27.40	13.95	12.80		
101-04-26-008-21W3-00	24.90	12.78	11.90	3.40	1.17
141-02-08-008-20W3-00	35.99	15.78	14.60	3.90	0.99
111-09-05-008-19W3-00	31.20	13.71	12.80	3.30	1.09
101-14-08-009-18W3-00	26.50	12.55	11.60	3.60	1.13
131-01-02-008-12W3-00	45.28	21.29	19.80		
141-12-22-008-11W3-00	44.88	20.45	18.80		
141-07-26-009-07W3-00	48.82	21.49	20.20		
141-07-10-008-04W3-00	50.40	21.16	20.00		
100-06-22-010-01W4-00	52.32			3.87	1.24
100-09-19-010-01W4-00			17.65	1.57	1.12
131-07-02-010-29W3-00	25.22			4.50	1.05
101-07-04-010-28W3-00	24.76			4.20	1.01
141-06-01-010-26W3-00	41.10	13.72	12.60	4.10	1.03
131-11-17-010-24W3-00	21.54			3.20	1.03
101-04-36-010-20W3-00	30.90	13.82	12.90	2.00	1.02
121-11-03-011-19W3-00	27.40	12.32	11.60		
141-10-07-010-18W3-00	37.50	17.48	16.30	5.85	1.05
111-08-07-011-16W3-00	30.80	14.78	13.90	4.00	1.1
100-04-18-012-01W4-00	68.94		20.70	1.40	1.05
111-07-01-012-30W3-00	31.31			2.20	0.97
121-06-24-013-29W3-00		13.07	11.70	4.51	1.03
121-06-27-012-29W3-00	30.65			2.50	
141-11-35-012-28W3-00	41.59			4.00	1.04

UWI	Assumed data for Lea Park Formation (%)	Assumed data forViking Formation (%)	Assumed data for Mannville Group (%)	Average Density Correction (%)	Average Caliper/Bit
141-06-14-012-27W3-00	37.99	14.32	12.70		
141-06-09-012-26W3-00	23.75			3.88	1.03
131-06-24-012-25W3-00	29.09	11.19		4.90	1.05
141-10-24-012-22W3-00	25.20			2.81	1.08
141-10-05-013-21W3-00	37.13	17.40	16.00	2.90	1.05
101-06-22-012-20W3-00	26.83	13.19	12.30		
101-13-01-012-19W3-00	27.80	13.16	12.30	3.30	1.1
101-16-16-012-18W3-00	41.94	19.41	18.13	3.88	1.1
121-16-29-012-17W3-00	28.90	13.21	12.30	5.35	1.02
141-09-20-012-13W3-00	25.90			5.48	1.14
131-10-16-013-08W3-00	45.20	20.85	19.70		
100-02-27-014-01W4-00	64.48		21.80	3.83	1.29
141-06-02-014-30W3-00	29.11				
111-06-21-014-29W3-00	30.04			4.50	1.03
131-13-22-015-27W3-00	39.87	14.55	12.82	2.40	1.05
101-10-13-014-26W3-00	31.84			4.60	1.1
121--07-06-014-23W3-00	36.15	13.14	11.90	4.35	1.14
141-06-21-014-22W3-00	27.08			4.10	
101-06-26-015-21W3-00	29.33			5.00	1.04
141-01-04-014-20W3-00	45.77	16.30	14.62	4.40	1.18
131-15-10-014-19W3-00	44.00	16.03	14.70	2.20	1.08
121-07-13-014-18W3-00	58.60	21.96	20.50		
121-13-04-014-16W3-00	46.70	20.34	19.10	4.30	1.02
101-16-08-014-15W3-00	28.90	12.63	11.91	5.71	1.07
100-10-22-017-01W4-00	54.62		16.13	2.60	1.01
121-16-27-016-29W3-00	27.21				
101-11-02-016-28W3-00	43.37	13.98	12.45	2.30	1.04
121-12-22-016-27W3-00	45.37	14.30	12.68	2.20	1.03
111-16-04-016-26W3-00	42.21	13.94	12.30	2.20	1.08
101-07-34-016-23W3-00	40.81			2.80	1.01
121-06-35-016-22W3-00	44.74	15.19		2.70	1.05
101-09-25-016-20W3-00	72.30	23.19	21.52		
101-02-27-016-19W3-00	51.65	16.85	15.70	2.20	1.03
141-06-20-016-18W3-00	48.07	17.34	15.57	3.60	1.1
121-02-27-016-16W3-00	45.10	16.02	14.90	1.90	1.02
111-07-30-016-15W3-00	65.00	24.05	22.50		
141-14-33-016-12W3-00	32.26			4.20	1.04
100-03-04-018-01W4-00	85.14		22.05	2.20	1.06
141-05-03-019-29W3-00	48.95	14.64	13.10		
131-08-30-018-28W3-00	78.70	22.72	20.40		
101-07-33-019-27W3-00	54.97	16.39	14.70	2.90	1.04
111-04-33-019-25W3-00	35.06			1.10	1.03
141-06-29-019-24W3-00	38.04	12.25		3.00	1.08
131-06-04-018-21W3-00	71.90	21.25	19.40	1.70	1.03
131-11-07-018-17W3-00	41.57	14.23	12.80	5.20	1.02
111-10-11-018-16W3-00	49.10	19.47	17.90	2.61	1.04
141-06-08-018-14W3-00	55.90			3.70	1.02
102-10-32-018-03W3-00	20.50				
100-12-02-020-01W4-00	84.31		21.41	4.61	1.06
111-06-05-021-29W3-00	68.82	20.33	18.20	4.94	1.15
121-11-01-021-28W3-00	54.89	16.59	14.90		
101-07-36-021-26W3-00	63.31	18.27	15.79	5.00	1.07
141-11-28-021-20W3-00	68.93	24.80	21.90		
101-08-23-020-19W3-00	55.97	18.50	16.40	2.20	1.07
121-06-35-020-17W3-00	39.59			5.22	
141-06-26-020-16W3-00	71.60			2.60	1.02
141-14-31-021-14W3-00	46.50			1.60	
101-14-06-021-13W3-00	44.08			1.80	1.02
101-10-03-020-05W3-00	20.90			5.80	1.02
100-06-09-22-01W4-00			24.38	1.90	1.14
101-07-09-023-25W3-00	62.82	16.55	15.00		

UWI	Assumed data for Lea Park Formation (%)	Assumed data forViking Formation (%)	Assumed data for Mannville Group (%)	Average Density Correction (%)	Average Caliper/Bit
101-10-03-023-24W3-00	83.70		20.30	4.11	1.05
141-13-28-022-20W3-00	55.53	17.78	16.10	2.50	1.03
111-04-15-022-19W3-00	68.41	21.60	19.50		
101-07-13-022-17W3-00	42.03	13.18			
101-16-29-023-14W3-00	39.22	11.83	11.56	1.60	1.05
101-09-10-023-13W3-00	32.70	12.65	11.80	2.20	1.01
101-06-26-023-08W3-00	35.30	11.72	11.10	2.40	1.03
111-06-08-022-06W3-00	28.00	13.04	12.20	2.50	1.06
100-16-11-025-01W4-00			17.70	2.10	1.03
111-09-08-025-28W3-00	94.80	21.24	19.10	0.90	1.01
191-10-20-025-27W3-00	78.04	22.24	19.80	3.20	1.22
141-10-10-024-26W3-00	95.14	26.37	23.70		
111-13-20-024-24W3-00	73.91	19.18	17.30	4.66	1.07
121-16-10-025-23W3-00	56.19	15.02	13.70	3.32	1.05
121-06-17-024-16W3-00	40.40	11.94	10.64	3.80	1.1
101-10-16-024-13W3-00	46.70	15.95	15.20		
131-13-21-024-12W3-00	37.57	14.92			
100-07-31-027-01W4-00	76.20		16.70	5.10	0.99
131-05-14-026-29W3-00	59.00	13.85	12.60	3.10	1.04
141-08-17-026-28W3-00	84.73	19.78	18.00	0.90	0.99
111-12-17-026-27W3-00	50.57	21.43	11.96	3.00	1.01
131-13-19-027-26W3-00	55.45	14.37	11.91	4.39	1.06
101-04-19-026-25W3-00	59.51	14.09	13.00		
101-10-31-027-22W3-00	57.28	15.07	13.91	4.00	1
101-08-33-026-20W3-00	37.38	10.49	10.00	3.30	1
101-06-29-026-19W3-00	55.31	16.00	14.80		
101-11-09-027-18W3-00	90.25	24.85	23.60		
101-02-13-027-16W3-00	56.10	15.02	14.30		
141-09-03-027-14W3-00	48.10	12.33	11.60		
100-15-35-028-01W4-00			23.10	4.88	1.11
111-14-11-028-29W3-00	82.10	21.97	15.10	4.00	1.04
101-13-01-028-28W3-00	81.30	14.73	13.48	4.60	
101-03-14-028-27W3-00	65.10	14.39	13.30	3.80	1.08
101-07-34-028-25W3-00	60.60	15.88	14.80	2.20	1.09
101-06-07-028-23W3-00	59.25	16.19	14.88	4.70	0.99
111-08-33-029-22W3-00	55.98	14.40	13.70	4.40	1
111-16-14-028-20W3-00	53.05	14.84	13.80		
101-10-25-028-19W3-00	59.44	16.00	15.87	4.60	0.99
131-16-25-029-17W3-00	57.70	16.28	15.30		
100-11-18-031-01W4-00	54.19		17.70	0.60	1.03
121-02-13-031-29W3-00	66.00	14.03	12.98	2.20	1.05
131-13-12-031-28W3-00	54.62	13.55	12.83	3.10	1.01
141-14-06-031-26W3-00	50.24	12.76	11.90	3.35	
131-01-27-031-25W3-00	91.80	24.78	23.10	1.30	1.09
111-15-08-031-24W3-00	57.52	15.99	14.80	5.60	1.11
131-11-04-030-22W3-00	53.80	14.66	13.70	2.00	1.04
101-09-19-030-19W3-00	48.77	13.30	12.58	2.90	1.03
101-06-16-031-18W3-00	41.40	13.54	12.80		
131-15-23-030-13W3-00	50.13	13.08			
101-08-13-030-12W3-00	65.31	16.35			
100-06-24-033-01W4-00	75.64		17.00	4.60	1.06
111-06-12-032-29W3-00	64.66	14.32	13.75	5.50	1.05
191-08-02-032-28W3-00	51.23	12.16	11.15	3.70	1.12
111-06-01-032-27W3-00	58.82	14.16	14.22	1.20	1.02
121-16-36-032-25W3-00	53.10	14.87	13.90	3.30	1.03
111-04-33-032-24W3-00	45.70	13.10	12.11	3.78	1.01
101-12-12-032-23W3-00	55.50	14.58	13.43	1.70	1.04
111-09-30-032-21W3-00	45.80	12.66	11.90	6.20	1.02
111-03-13-033-17W3-00	62.73	14.29	13.60		
111-05-27-032-16W3-00	64.07	15.20	14.40		
131-04-10-033-01W3-00			29.50		

APPENDIX B: MINIMUM HORIZONTAL STRESS DATA

Table B.1: Magnitude of minimum horizontal stress at the perforated zone- Viking Formation (estimated as 0.90× ISIP).

UWI	Top Perf (m)	ISIP BHP MPa	FC kPa/m	Minimum Horizontal Stress MPa	σ_h Grad kPa/m
111/02-32-045-23W3/0	414.5	9.68	23.35	8.71	21.02
131/15-09-044-23W3/0	517	11.5	22.24	10.35	20.02
131/08-34-042-23W3/0	541	11.88	21.96	10.69	19.77
131/03-20-042-22W3/0	570	13.15	23.07	11.83	20.76
141/04-30-041-23W3/0	531.5	11.25	21.16	10.12	19.05
141/10-14-041-22W3/0	578	11.68	20.21	10.51	18.19
131/06-04-041-21W3/0	575	10.81	18.8	9.73	16.92
141/15-22-040-25W3/0	615	13.05	21.22	11.75	19.1
141/10-32-040-22W3/0	559	12.13	21.7	10.92	19.53
101/10-16-040-21W3/0	573	13.52	23.6	12.17	21.24
121/11-29-039-25W3/0	608.3	12.97	21.32	11.67	19.19
131/11-23-039-23W3/0	497	12.67	25.48	11.4	22.94
101/10-22-039-22W3/0	559.5	12.09	21.61	10.88	19.45
111/07-07-038-24W3/0	614	13.2	21.5	11.88	19.35
141/14-09-037-27W3/0	694.5	13.96	20.1	12.56	18.09
101/14-05-037-26W3/0	649	11.67	17.98	10.5	16.18
121/12-01-036-28W3/0	691	13.1	18.96	11.79	17.06
101/06-25-036-27W3/0	648.5	11.93	18.4	10.74	16.56
141/14-06-036-26W3/0	652.5	12.2	18.7	10.98	16.83
111/03-17-036-25W3/0	636	12.5	19.65	11.25	17.69
111/10-33-035-28W3/0	727.2	14.1	19.39	12.69	17.45
141/14-24-035-27W3/0	711.5	12.8	17.99	11.52	16.19
111/05-06-035-25W3/0	707	12.6	17.82	11.34	16.04
111/15-25-034-27W3/0	707	12.9	18.25	11.61	16.42
112/15-33-034-26W3/0	716.5	13.9	19.4	12.51	17.46
101/12-33-034-25W3/0	699.5	14.32	20.47	12.89	18.42
121/06-24-033-29W3/0	725	15.01	20.71	13.51	18.64
111/04-27-033-28W3/0	742	15.76	21.24	14.18	19.12
101/09-16-033-25W3/0	721	14.82	20.55	13.34	18.5
121/02-26-033-24W3/0	690	13.09	18.97	11.78	17.08
131/01-09-033-23W3/0	650	13.88	21.35	12.49	19.21
101/04-12-033-22W3-0	650	13.88	21.35	12.49	19.21
101/04-10-033-20W3-0	629	15.03	23.9	13.53	21.51
141/10-13-032-29W3/0	731	15.62	21.37	14.06	19.23
131/15-17-032-28W3/0	727	14.92	20.52	13.43	18.47
101/16-36-032-26W3/0	714.5	14.3	20.01	12.87	18.01
101/03-30-032-25W3/0	726	13.87	19.1	12.48	17.19
131/06-33-032-23W3-0	717.5	14.92	20.79	13.43	18.71
131/11-25-032-22W3/0	666	14.53	21.82	13.08	19.64
141/07-12-032-20W3/0	625	13.13	21.01	11.82	18.91
131/01-23-032-19W3/0	610	12.98	21.29	11.69	19.16
101/16-15-032-18W3/0	620	13.17	21.23	11.85	19.11
141/10-17-032-17W3/0	610.5	13.29	21.77	11.96	19.59
102/15-12-031-29W3/0	704	15.86	22.53	14.28	20.28
111/16-28-031-26W3/0	756	14.89	19.7	13.4	17.73
121/04-03-031-23W3/0	730	14.89	20.4	13.4	18.36
101/13-01-031-21W3/0	666	13.48	20.24	12.13	18.22
121/12-11-031-20W3/0	683.5	13.37	19.56	12.03	17.6

UWI	Top Perf (m)	ISIP BHP MPa	FC kPa/m	Minimum Horizontal Stress MPa	σ_h Grad kPa/m
100/15-31-031-17w3/0	609	13.37	21.96	12.04	19.76
121/08-31-031-17W3/0	615.5	12.05	19.58	10.85	17.62
111/04-23-030-28W3/0	714.5	15.21	21.29	13.69	19.16
111/10-25-030-26W3/0	746	14.1	18.9	12.69	17.01
100/06-31-030-25W3/0	709.5	13.19	18.6	11.88	16.74
141/08-30-030-23W3/0	700	14.14	20.2	12.73	18.18
131/16-31-030-21W3/0	669	13.3	19.89	11.97	17.9
121/09-32-030-20W3/0	690	11.94	17.3	10.75	15.57
131/15-23-030-13W3/0	586.5	10.5	17.9	9.45	16.11
101/11-14-029-29W3/0	745	16.02	21.5	14.42	19.35
111/03-27-029-28W3/0	677.5	16.95	25.02	15.26	22.52
111/16-35-029-27W3/0	720	13.82	19.19	12.44	17.28
111/11-17-029-26W3/0	734	14.5	19.76	13.05	17.78
121/06-24-029-24W3/0	705	14.69	20.83	13.22	18.75
111/04-29-029-23W3/0	692	14.24	20.58	12.82	18.52
121/06-12-029-20W3/0	738	15.44	20.92	13.9	18.83
141/10-02-029-18W3/0	699.5	15.46	22.11	13.92	19.9
131/06-14-029-17W3/0	694	15.31	22.06	13.78	19.85
102/10-07-028-28W3/0	692	13.21	19.09	11.89	17.18
131/01-28-028-27W3/0	699	12.42	17.77	11.18	15.99
101/11-24-028-25W3/0	718	14.72	20.5	13.25	18.45
101/08-22-028-24W3/0	691.5	14.59	21.1	13.13	18.99
101/02-24-028-23W3/0	721	14.67	20.35	13.21	18.32
131/08-18-028-22W3/0	740	13.76	18.59	12.38	16.74
111/15-17-028-18W3/0	683	15.94	23.33	14.34	21
141/10-02-028-17W3/0	724	14.31	19.77	12.88	17.79
111/13-31-027-23W3/0	676.8	14.21	21	12.79	18.9
101/10-21-027-22W3/0	712	15.53	21.81	13.97	19.63
101/02-12-027-20W3/0	720	14.09	19.56	12.68	17.61
100/03-06-027-19W3/0	715.5	13.38	18.7	12.04	16.83
101/13-35-026-20W3/0	703.5	15.27	21.71	13.74	19.54
101/04-29-026-19W3/0	710	14.06	19.8	12.65	17.82
131/10-06-026-17W3/0	672.5	13.1	19.48	11.79	17.53
101/06-19-026-15W3/0	624	13.75	22.04	12.38	19.83
121/06-04-026-14W3/0	604	12.71	21.05	11.44	18.95
101/06-29-025-18W3/0	670	13.67	20.4	12.3	18.36
101/12-07-025-17W3/0	643.4	14.31	22.24	12.88	20.02
101/01-33-025-15W3/0	634	14.19	22.38	12.77	20.14
101/13-05-025-14W3/0	718	16.12	22.45	14.51	20.21
141/06-02-024-17W3/0	626	10.6	16.93	9.54	15.24
131/11-10-024-16W3/0	609	13.4	22	12.06	19.8
121/16-20-024-14W3/0	667	13.54	20.3	12.19	18.27
101/10-16-024-13W3/0	725	14.57	20.1	13.11	18.09
101/02-20-024-13W3/0	726.4	15.91	21.9	14.32	19.71
111/01-22-019-29W3/0	769.5	14.45	18.78	13	16.9
121/12-35-013-25W3/0	797	16.42	20.6	14.78	18.54
141/08-28-013-13W3/0	869	15.95	18.35	14.36	16.52

Table B.2: Magnitudes and gradients of minimum horizontal stress and pore pressure at the top of the Mannville Group. σ_{Hmin} was estimated by a simple gradient model, using relevant Viking Formation data.

UWI	Depth (m)	Minimum Horizontal Stress MPa	Minimum horizontal stress gradient kPa/m	Pore pressure MPa
111/02-32-045-23W3/0	473	9.94	21.02	
131/15-09-044-23W3/0	559	11.19	20.02	6.94
131/08-34-042-23W3/0	575	11.37	19.77	12.29
131/03-20-042-22W3/0	614	12.75	20.76	8.25
141/04-30-041-23W3/0	570	10.86	19.05	8.85
141/10-14-041-22W3/0	616	11.2	18.19	11.56
131/06-04-041-21W3/0	595	10.07	16.92	9.06
141/15-22-040-25W3/0	662	12.64	19.1	9.93
141/10-32-040-22W3/0	598	11.68	19.53	8.68
101/10-16-040-21W3/0	616	13.08	21.24	9.42
121/11-29-039-25W3/0	639	12.26	19.19	9
131/11-23-039-23W3/0	633	14.52	22.94	9.06
101/10-22-039-22W3/0	598	11.63	19.45	9.67
111/07-07-038-24W3/0	656	12.7	19.35	9.02
141/14-09-037-27W3/0	736	13.31	18.09	9.18
101/14-05-037-26W3/0	693	11.21	16.18	8.91
121/12-01-036-28W3/0	735	12.54	17.06	9.36
101/06-25-036-27W3/0	695	11.51	16.56	9.08
141/14-06-036-26W3/0	680	11.44	16.83	8.51
111/03-17-036-25W3/0	680	12.03	17.69	9.44
111/10-33-035-28W3/0	770	13.44	17.45	8.89
111/05-06-035-25W3/0	754	12.09	16.04	7.43
111/15-25-034-27W3/0	731	12	16.42	8.65
112/15-33-034-26W3/0	760	13.27	17.46	9.54
101/12-33-034-25W3/0	747	13.76	18.42	8.51
121/06-24-033-29W3/0	750	13.98	18.64	8.68
111/04-27-033-28W3/0	787	15.04	19.12	8.37
101/09-16-033-25W3/0	755	13.97	18.5	8.88
121/02-26-033-24W3/0	734	12.53	17.08	8.18
131/01-09-033-23W3/0	720	13.83	19.21	9.57
101/04-12-033-22W3-0	680	13.07	19.21	9.62
101/04-10-033-20W3-0	650	13.98	21.51	9.57
141/10-13-032-29W3/0	770	14.81	19.23	9.02
131/15-17-032-28W3/0	768	14.18	18.47	8.33
101/16-36-032-26W3/0	758	13.65	18.01	8.92
101/03-30-032-25W3/0	750	12.9	17.19	9.27
131/06-33-032-23W3-0	724	13.55	18.71	10.57
131/11-25-032-22W3/0	710	13.94	19.64	9.25
131/01-23-032-19W3/0	624	11.95	19.16	9.43
102/15-12-031-29W3/0	571	11.58	20.28	9.65
111/16-28-031-26W3/0	811	14.38	17.73	9.08
121/04-03-031-23W3/0	805	14.78	18.36	8.99
121/12-11-031-20W3/0	745	13.11	17.6	9.07
100/15-31-031-17w3/0	720	14.23	19.76	9.05
111/04-23-030-28W3/0	767	14.69	19.16	8.61
111/10-25-030-26W3/0	780	13.27	17.01	9.2
141/08-30-030-23W3/0	760	13.82	18.18	9.3

UWI	Depth (m)	Minimum Horizontal Stress MPa	Minimum horizontal stress gradient kPa/m	Pore pressure MPa
101/11-14-029-29W3/0	795	15.39	19.35	7.92
111/11-17-029-26W3/0	783	13.92	17.78	8.94
121/06-24-029-24W3/0	759	14.23	18.75	7.41
141/10-02-029-18W3/0	730	14.52	19.9	7.4
131/06-14-029-17W3/0	715	14.19	19.85	8.45
102/10-07-028-28W3/0	754	12.95	17.18	6.36
131/01-28-028-27W3/0	802	14.6	18.2	7.34
101/11-24-028-25W3/0	768	14.17	18.45	7.75
101/02-24-028-23W3/0	771	14.12	18.32	8.91
131/08-18-028-22W3/0	760	12.72	16.74	6.29
141/10-02-028-17W3/0	750	13.34	17.79	5.8
111/13-31-027-23W3/0	726	13.72	18.9	6.47
101/10-21-027-22W3/0	780	15.31	19.63	7.11
101/13-35-026-20W3/0	750	14.65	19.54	8.83
101/04-29-026-19W3/0	753	13.42	17.82	6.54
101/06-19-026-15W3/0	663	13.15	19.83	6.58
121/06-04-026-14W3/0	640	12.12	18.95	6.67
101/13-05-025-14W3/0	752	15.2	20.21	6.11
141/06-02-024-17W3/0	690	10.52	15.24	6.39
131/11-10-024-16W3/0	680	13.47	19.8	7.37
121/16-20-024-14W3/0	692	12.64	18.27	7.4
101/10-16-024-13W3/0	765	13.84	18.09	5.93
111/01-22-019-29W3/0	861	14.55	16.9	5.5
111/12-19-032-24W3/0	758.5	13.63	17.97	6.02
100/13-25-031-25W3/0	724	12.96	17.9	5.81
07-20-013-19W3-00	1076	17.73	16.48	6.8
06-13-031-20W3-00	745	11.88	15.95	6.15
16-34-030-20W3-00	773	13.41	17.35	5.59
9-06-031-19W3-00	742	13.86	18.68	6.01
02-20-032-25W3-00	711	13.32	18.73	6.38
101/12-24-027-26W3/0	899.5	14.6	16.24	6.26
101/09-30-032-25W3/0	712	11.21	15.75	6.72
191/16-21-017-08W3/0	1009	16.96	16.81	5.31
111/14-01-032-27W3/0	858	13.67	15.93	5.24
111/06-01-032-27W3/0	834	13.89	16.65	5.89
08-24-001-29W3-00	1041	20.61	19.8	5.79
06-30-002-25W3-00	1204	19.65	16.32	4.01
08-26-004-25W3-00	1174	16.19	13.79	4.17
07-20-004-27W3-00	1145	17.02	14.86	4.68
11-29-005-14W3-00	1031.7	16.53	16.02	4.73
16-21-005-18W3-00	1264	18.31	14.49	4.31
11-05-005-27W3-00	1145	16.61	14.51	4.97
08-04-006-19W3-00	1290	20.33	15.76	5.78
10-17-006-27W3-00	1277	17.62	13.8	4.69
08-33-006-30W3-00	1300	16.53	12.72	4.53
11-18-010-28W3-00	1082	19.25	17.79	4.56

APPENDIX C: A LITERATURE REVIEW OF COAL MECHANICAL PROPERTIES

The mechanical properties of coal can be used for various well-design and reservoir engineering applications such as borehole stability assessment, cavity completions, hydraulic fracturing, and reservoir simulation. Determination of field representative strength properties of coal by direct measurement is difficult due to the cleated nature of coal seams. Coal strength parameters express as: Mohr-Coulomb friction angle and cohesion, Hoek and Brown parameters, and static dynamic moduli including Young's modulus and Poisson's ratio.

Peak and residual strength are commonly represented using Mohr-Coulomb or Hoek and Brown criteria, obtained from laboratory tests on cores:

Mohr-Coulomb criterion

$$\tau = c + \sigma'_n \tan\phi$$

Where:

τ = shear strength

σ_n' = Effective normal stress, and

ϕ = Friction angle

c = rock cohesion

Hoek & Brown failure criterion

$$\sigma'_1 = \sigma'_3 + \sqrt{m\sigma_c\sigma'_3 + s\sigma_c^{\,2}} \qquad (2.2)$$

Where:

σ_1' = major principal effective stress at failure

σ_3' = minor principal effective stress or confining stress

σ_c = uniaxial compressive strength (UCS)

m and s are constants which depend upon the properties of the rock

Dynamic elastic mechanical properties of coal are usually estimated from wireline log data, such as density, and shear sonic logs.

No strength data are currently available for Belly River Formation or Mannville Group coals in the study area. The mechanical properties of coal available in the public domain are summarized the following paragraphs.

Figure C.1 shows the relationship between Young's modulus and Poisson's ratio for different coal seams: Cretaceous and Pennsylvanian coal data compiled from Jones et al. (1988); and Western Canadian coal parameters compiled from Kaiser and Maloney (1982). Young's modulus value ranges from 1.4 GPa to 6.14 GPa, and Poisson's ratio ranges from 0.2 to 0.43

Foroughi, et al., 1999 showed that the coal strength depends on the angle of weakness plane inclination, (β), roughness of the fracture surface and width-to height (W/H) or diameter to length (D/L) ratio. Data from Foroughi, et al., were compiled and analyzed using Rocdata 4 (Rocscience 2006).

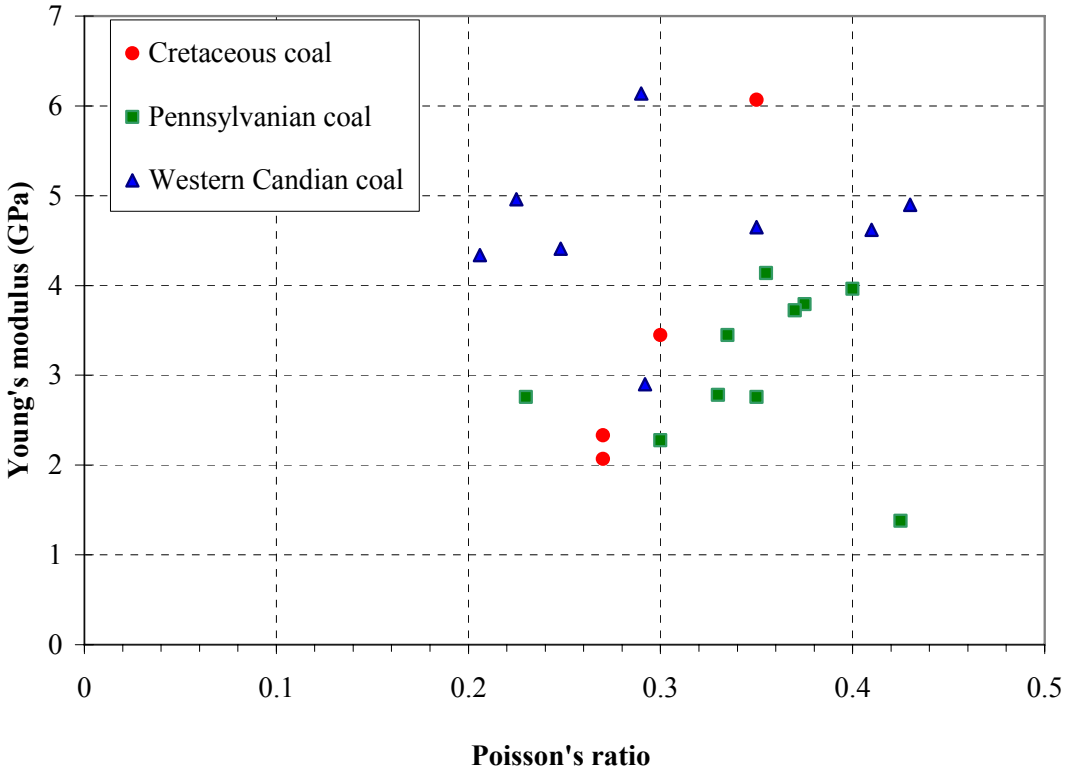

Figure C.1: Relationship between Young's modulus and Poisson's ratio for coal: (data for Cretaceous and Pennsylvanian coal from Jones, et al. 1988, Western Canadian coal parameters from Kaiser and Maloney 1982).

Figure C.2 shows a linear Mohr-Coulomb failure envelope fit to the peak strength data from multi-stage triaxial test on coal sample for a weakness plane inclination angle, (β), equal zero, the peak friction angle, (ϕ), and the peak cohesion were found to be 32° and 5.72 MPa respectively

Figure C.3 shows a non linear Hoek and Brown failure envelope fit to the peak strength data from multi-stage triaxial test on coal sample for a weakness plane inclination angle, (β), equal zero, the value of Hoek and Brown criterion were found to be m_b =8.4 MPa, s=0.72 and UCS= 17.6 MPa.

Figure C.4 shows the relationship between the angle of weakness plane inclination (β) and unconfined compressive strength (UCS). Figure C.5 shows the effect of the angle of weakness plane inclination (β) on the peak cohesion (C_P). Foroughi et al. (op. cit.) concluded that the minimum strength of coals occurs when the weakness plane inclination is 30° to 45° and that the maximum strength occurs in the direction perpendicular to the weakness plane.

Zipf (2006) measured mechanical properties of American coal in the laboratory. He found UCS ranging from 3.6 MPa to 17 MPa, friction angle from 29º to 32º, cohesion ranging from 0.6 MPa to 2.7 MPa, tensile strength from 0.17 MPa to 0.85 MPa, dilation angle of 10º, and Young's modulus of 2.5 GPa.

Table C.1 shows Hoek-Brown parameters for Moura DU coal. These values are based on a UCS of 32.7 MPa.

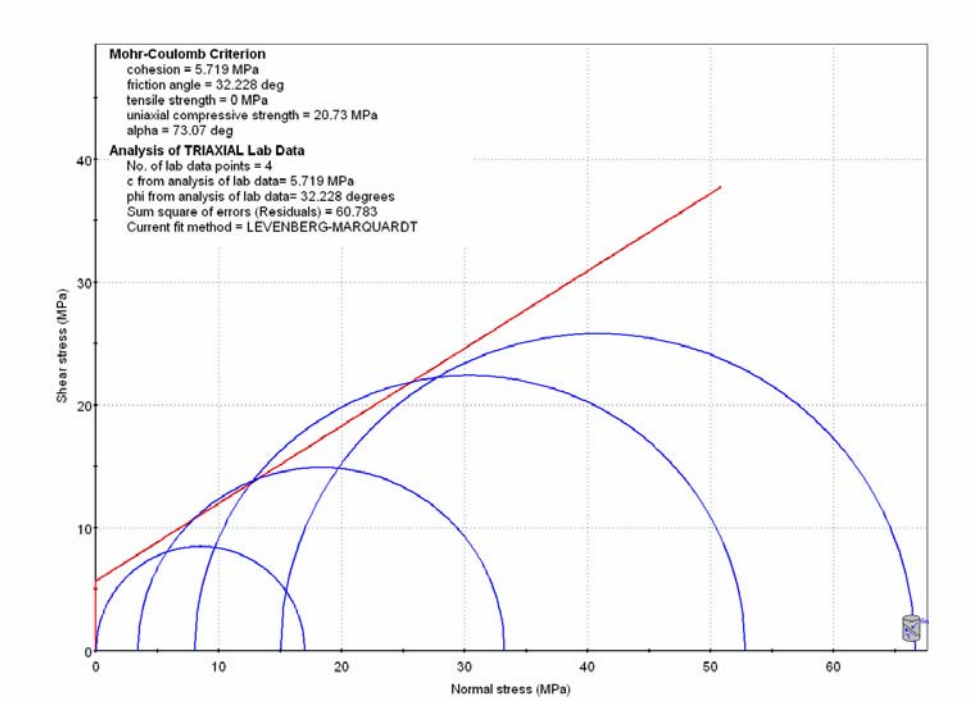

Figure C.2: Mohr-Coulomb failure envelope fit to peak multistage triaxial strength test for coal (data complied from Foroughi, et. al. 1999).

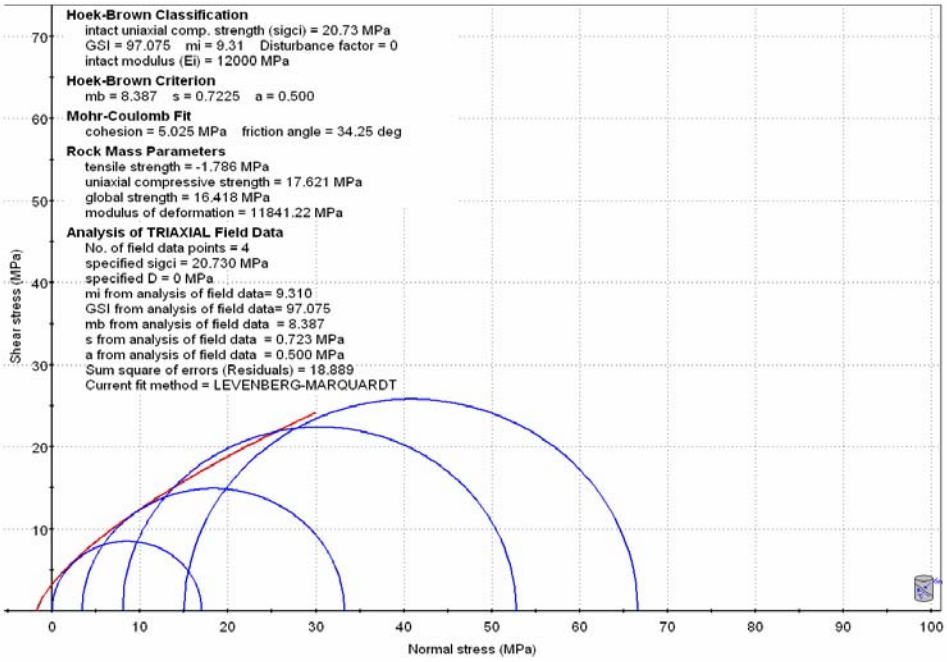

Figure C.3: Hoek-Brown failure envelope fit to peak multistage triaxial strength test for coal (data complied from Foroughi, et. al. 1999).

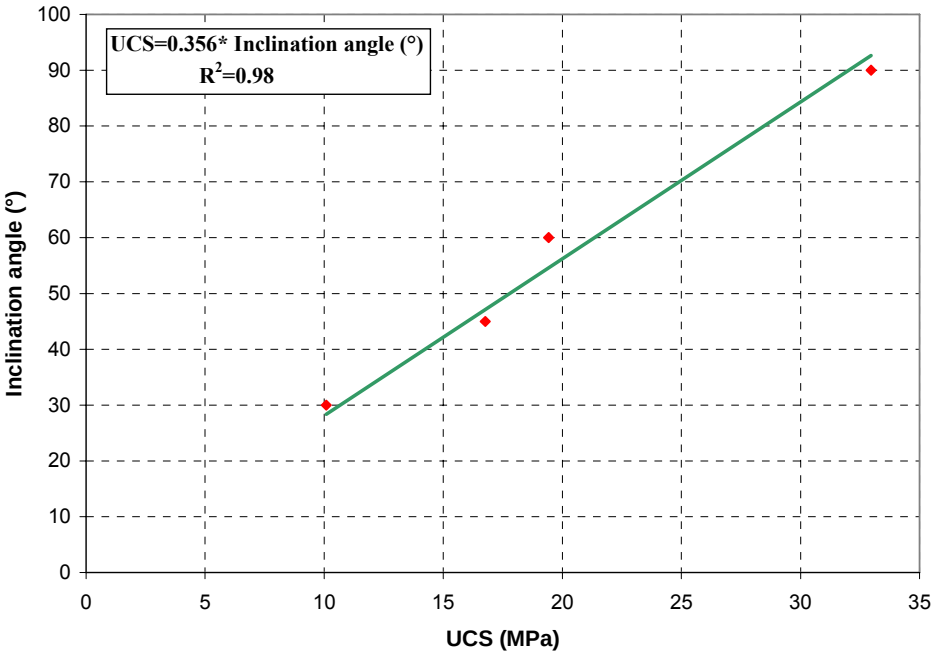

Figure C.4: Effect of angle of weakness plane inclination (β °) on unconfined compressive strength (UCS) (data complied from Foroughi, et. al. 1999).

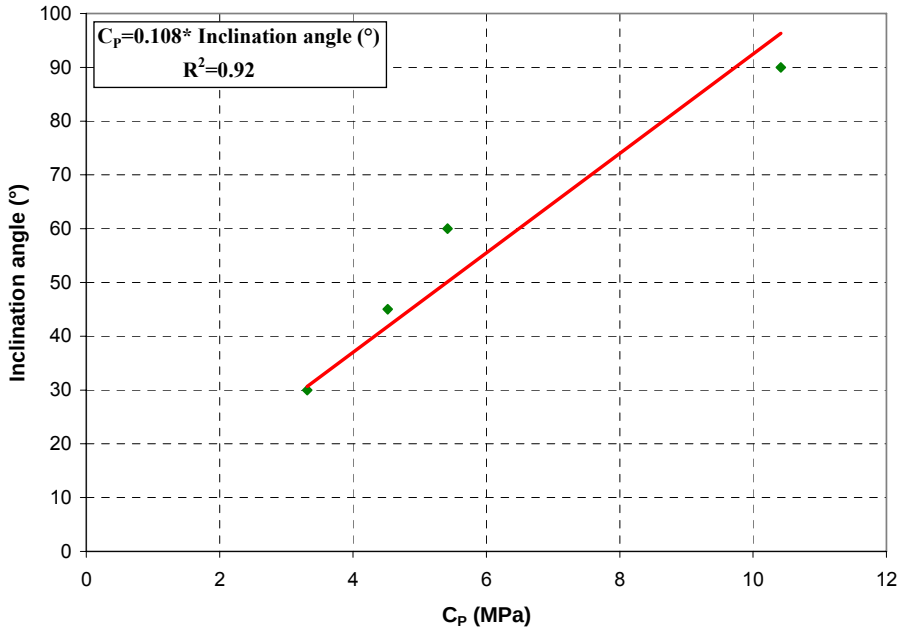

Figure C.5: Effect of angle of weakness plane inclination (β °) on peak cohesion (C_P) (data complied from Foroughi, et. al. 1999).

Table C.1: Hoek-Brown parameters for Moura DU coal.

Diameter mm	m_b	S	a
61	19.4	1	0.5
101	13.3	0.555	0.5
146	10	0.236	0.5
300	5.7	0.184	0.6
Rock mass	2.6	0.051	0.65

APPENDIX D: BOREHOLE STABILITY ANALYSES FOR BELLY RIVER COALS

Given that the Belly River coals exist as numerous thin seams, these coals will likely be developed using vertical wells, with hydraulic fracturing used to stimulate production in most of the seams. This development strategy has proven effective for Horseshoe Canyon coals in the Alberta Basin. The main objective of the borehole stability analyses conducted in this Appendix was to investigate the minimum borehole pressure (i.e., drilling fluid density) required to prevent severe borehole collapse while drilling vertical wells in Belly River coals. It is important to answer this question for wells in weak rocks such as coals, in which instability problems may easily become unmanageable if bottomhole pressures are too low.

Representative rock mechanical properties were obtained by back-analyzing borehole enlargement in Belly River coals, as measured by caliper logs in well TEXACO EDGELL 1-4-10-22W3 (which are shown in Figure D.1). Conditions at this well were considered to be representative for much of the deeper Belly River coal deposits that are likely to be developed in the study area, for which borehole instability risks are greatest. [Note: This being the case, the fact that the calipers are only enlarged to diameters roughly 35% greater than the drill bit size bodes well for hole stability in these coals.] Rock mechanical properties were adjusted until model-predicted yielded zone size matched the enlarged hole size measured with calipers. The values for these properties were constrained using mechanical properties compiled for various coals from various countries, including Canada (see Appendix C; and Hawkes, 2003). As such, the values obtained from back-analysis are realistic. However, it is important to understand that more accurate predictions of borehole stability in these coals would require the measurement of rock mechanical properties on core samples. Large-diameter samples would be best, in order to capture the effects of small-scale discontinuities such as cleats on strength.

The input parameters used for base case modelling are summarized in Table D.1. The extent of borehole yielding predicted for this base case is shown in Figure D.2. The normalized yielded zone area (NYZA) for this base case is 0.35.

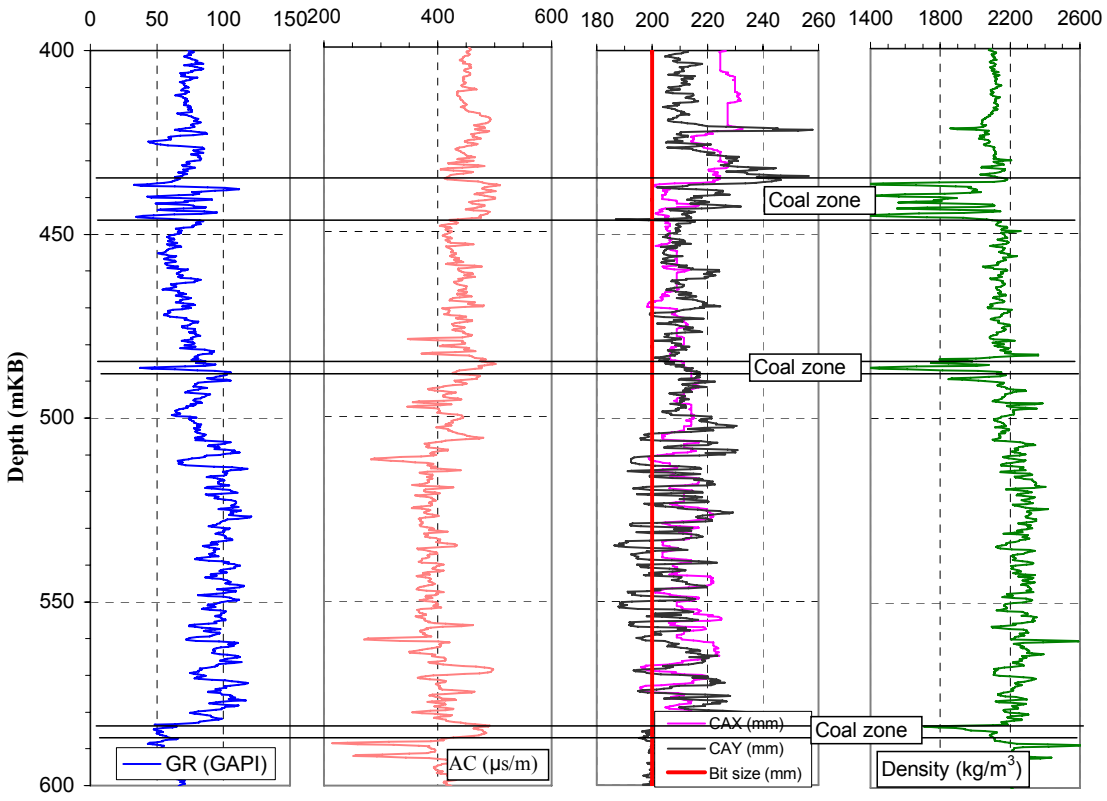

Figure D.1: Gamma ray (GR), sonic transit time (AC), dual-arm caliper (CAX, CAY), and density log readings through Belly River coals and adjacent strata, TEXACO EDGELL 1-4-10-22W3.

Table D.1: Input parameters for borehole stability modelling - Belly River coal.

Well name: TEXACO EDGELL 1-4-10-22	
Depth	426 m
Vertical stress gradient	21.7 kPa/m
Maximum horizontal stress gradient	23.5 kPa/m
Minimum horizontal stress gradient	17.0 kPa/m
Minimum horizontal stress orientation	340°
Well trajectory	Vertical
Formation pressure gradient	8.56 kPa/m
Equivalent circulating mud density	1160 kg/m^3
UCS	4.2 MPa
m_{peak}	4
S_{peak}	1
Young's modulus	1.7 GPa
Poisson's ratio	0.35
$m_{residual}$	2
$S_{residual}$	0.5

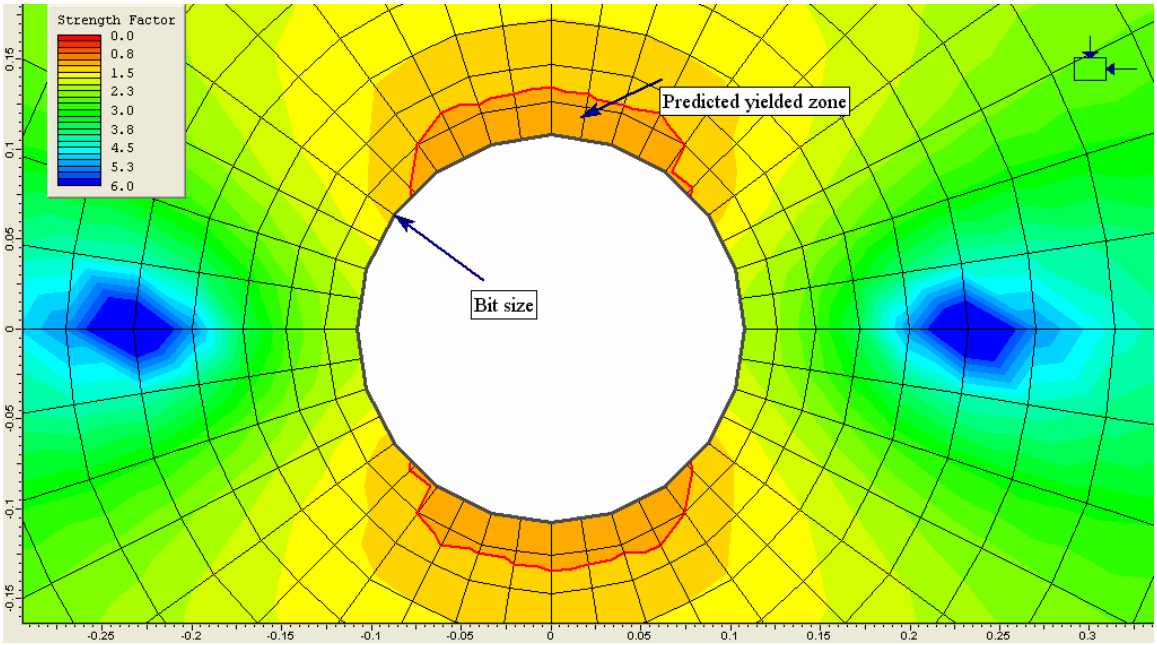

Figure D.2: Cross-sectional view of rock yielding around a vertical well for base-case conditions in Belly River coal, predicted using Phase2.

Given the uncertainty in rock mechanical properties, a sensitivity analysis was run using unconfined compressive strengths 25% greater than and less than the base case value. The results, shown in Figure D.3, indicate that NYZA values are less than 1.0 for all cases considered, for all weighted mud systems (i.e., density > 1000 kg/m^3). Similarly, given uncertainty in the maximum horizontal stress magnitude (σ_{Hmax}), a sensitivity analysis was run using values 10% greater than and less than the base case value. The results, shown in Figure D.4, indicate that NYZA values are less than 0.9 for all cases considered, for all weighted mud systems.

As a rough guideline, NYZA values greater than 1 are often regarded as indicators of unacceptable borehole instability (e.g., McLellan and Hawkes, 2001). Given that the NYZA's predicted in this study were all less than 1, this suggests that vertical drilling of the Belly River coals should be feasible, without the need for weighted mud systems. As such, it seems reasonable to expect that the drilling risks for vertical wells passing through these thin, weak coal zones should be manageable. However, additional analyses using rock mechanical properties measured on large-diameter core samples would be required to confirm this.

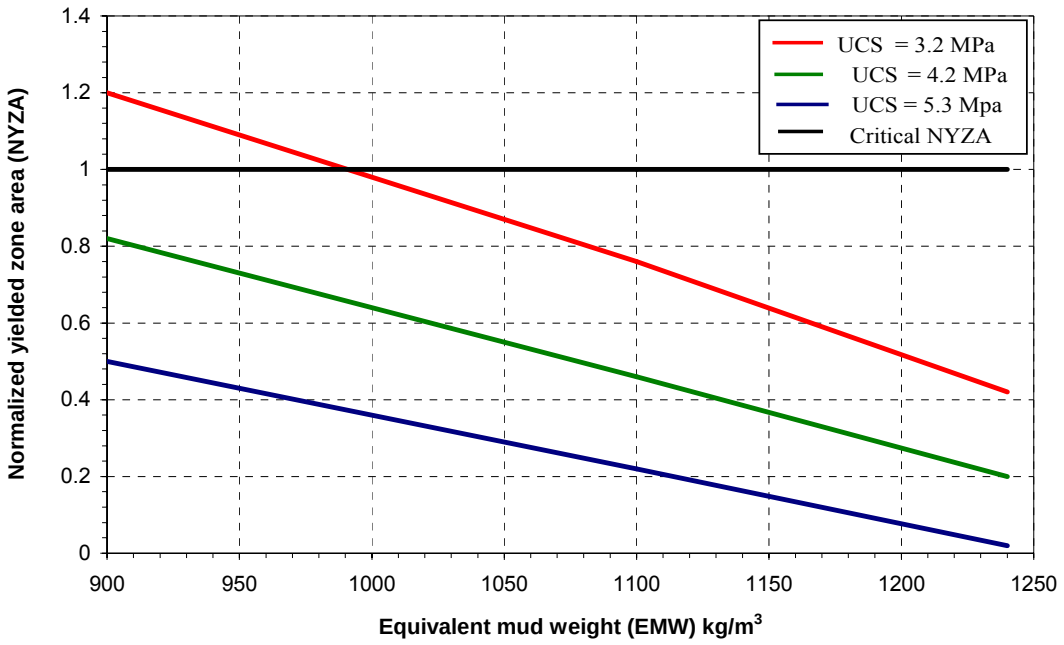

Figure D.3: Sensitivity of borehole yielding to UCS for a vertical well in Belly River coal at a vertical depth of 436 m. UCS for the base case is 4.2 MPa.

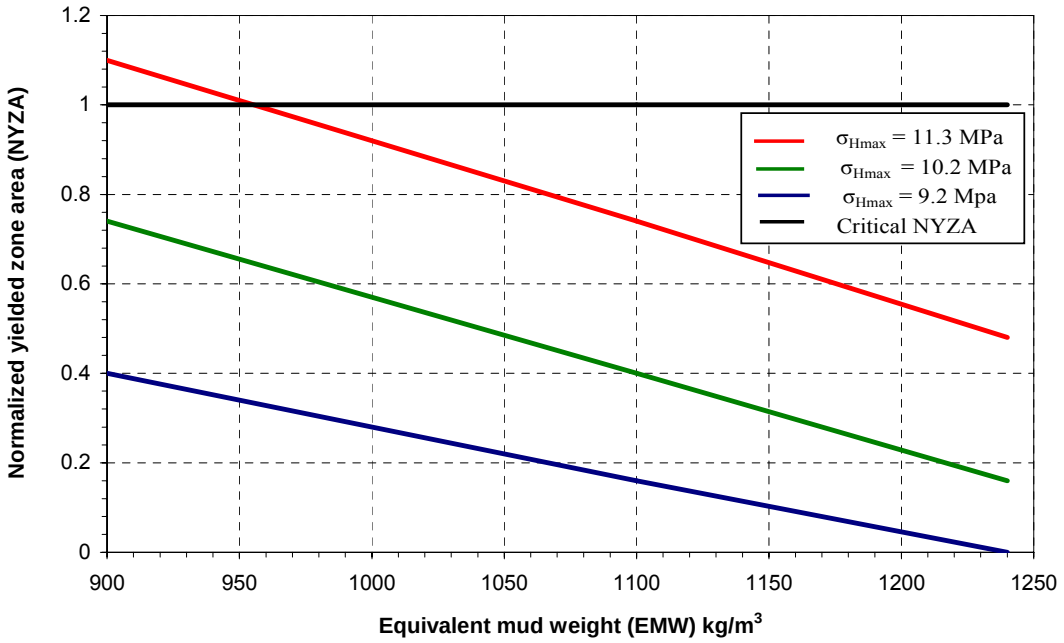

Figure D.4: Sensitivity of borehole yielding to maximum horizontal stress (σ_{Hmax}) magnitude for a vertical well in Belly River coal at a vertical depth of 436 m. σ_{Hmax} for the base case is 10.2 MPa.